

POLYTECHNIC UNIVERSITY OF TURIN

Master's Degree in Aerospace Engineering



Master's Degree Thesis

Dynamic modelling of the electrical system of a hybrid-powered aircraft

Supervisors

Prof. Marco FIORITI

Eng. Luigi ZUTTA

Candidate

Barbara TURSO

April 2025

Summary

The aim of this thesis work is to analyse the dynamic modelling of the electrical system of a hybrid-electric propulsion aircraft. The European HERA project, which envisages the construction of a regional transport aircraft with hybrid-electric propulsion by mid-2030, serves as a reference for this project. For the modelling of the system, the AMESim Simcenter simulation software was used.

In the first part of the work, an analysis was conducted of the state-of-the-art demonstrators and technologies currently available for hybrid-electric propulsion aircraft. Subsequently, an in-depth study of the electrical system architecture of the reference aircraft was conducted, a crucial step in the development of the models in Amesim.

Before proceeding with the modelling of the real loads, simulations were conducted to test the selected AC generator model, varying the value of the loads to assess the impact of these variations on the electrical quantities of the generator and to verify that the transients met the regulatory requirements.

Once the verification was complete, the modelling of the AC and DC generation system was proceeded with, connecting the actual loads of the reference aircraft. The two systems were modelled separately.

In view of the hybrid-electric propulsion system, the alternating current generation system was connected to a battery to assess the impact of the charging process on the generation system.

In conclusion, the results of the simulations were reviewed in the final chapter, where the conclusions of the study were drawn and future developments discussed.

Acknowledgements

Alla mia famiglia

Table of Contents

List of Tables	VII
List of Figures	VIII
Acronyms	XII
1 Introduction	1
2 State of the art	6
2.1 Electrification in aviation industry	6
2.2 Hybrid Electric Aircraft	8
2.2.1 Architecture of propulsion system	9
2.2.2 Advantages and disadvantages of HE propulsion	10
2.2.3 Demonstrators	11
2.3 Current technology and projections	13
2.3.1 Electric machines	13
2.3.2 Power electronics	15
2.3.3 Power system efficiency	15
2.3.4 Batteries	16
2.3.5 Fuel cells	18
2.3.6 Supercapacitors	19
3 Electrical Power System	21
3.1 Consequences of electrification on EPS	22
3.2 EPS architectures	25
3.2.1 More electric	25
3.2.2 Hybrid-Electric	27
3.2.3 NASA N3-X power system design	28
4 Reference aircraft	30
4.1 ATR72 electrical system	34

4.1.1	DC power generation	36
4.1.2	AC power generation	38
5	Dynamic modeling of EPS	42
5.1	Modelling levels	42
5.2	Modelling software: AMESim Simcenter	44
5.3	AC generation modelling on AMESim	45
5.3.1	General aircraft AC generation	45
5.3.2	AC generation	53
5.4	DC generation modelling on AMESim	59
6	Battery charge	67
7	Conclusions	83
A	MIL-STD-704 F	86
	Bibliography	87

List of Tables

3.1	MEA standardized voltage levels [30]	22
4.1	Inverter design characteristics [37]	38
4.2	Generator characteristics	40
5.1	Mechanical and electrical disturbances	46
5.2	Resistance profile for set 1, set 2 and set 3	49
5.3	Voltage values at $t = 2s$	50
5.4	AC Loads	54
5.5	First inductive load inputs	55
5.6	Resistive load inputs	55
5.7	Second inductive load inputs	55
5.8	DC Loads	61
5.9	First induction load inputs	61
5.10	Second inductive load inputs	62
5.11	First resistive load inputs	62
5.12	Second resistive load inputs	62
6.1	Output values transformer and TRU	74

List of Figures

1.1	CO_2 emissions from the aviation sector and its impact on global warming	2
1.2	Environmental objectives [7]	3
1.3	Hera objective [9]	4
1.4	USCs concept trade-off and possible concept configuration [8]	5
1.5	Use Case A propulsive architecture [9]	5
2.1	On the left the difference between the traditional APU (a) and the electric APU (b). On the right ECS with bleed air (a) and electric ECS (b)	7
2.2	Electrical propulsion architectures [10]	8
2.3	Hybrid propulsion architectures [16]	9
2.4	Series-parallel architecture [17]	10
2.5	PEGASUS propulsor configuration and locations	11
2.6	On the left ATR EVO, on the right RTX demonstrator	12
2.7	State of the Art of aircraft generators actually in the market and future prospects [25]	13
2.8	(A) Current State of the Art of motor and generator, (B) Stated Research Goals for Some Current Research Programs, and (C) the Committee's 20-Year Projection of the Performance of motor and generator configured for aircraft applications [25]	14
2.9	Efficiency drop in a turboelectric aircraft	16
2.10	Electrical system component performance requirements for Parallel Hybrid, All-Electric, and Turboelectric Propulsion Systems	17
2.11	Schematic diagram of the PEMFC and SOFC operation	18
2.12	Ragone plot [29]	20
3.1	Power distribution for DC system (a), AC system (b), DC and AC system (c) [12]	21
3.2	Centralized versus remote distribution [31]	23
3.3	Paschen's Law	24

3.4	Potential EPS architecture with electric propulsion system	26
3.5	Potential EPS architecture for hybrid-electric aircraft	27
3.6	Proposed EP architecture for NASA N3-X [34]	28
4.1	Aircraft dimensions	30
4.2	PW127 characteristics	31
4.3	Climb gradient	31
4.4	CO_2 emissions and noise levels	32
4.5	Liters of fuel per passengers per 100 Km and cash operating cost per trip on 250 Nm	33
4.6	ATR72 electrical system [37]	34
4.7	DC power system [37]	36
4.8	DC essential bus power - normal supply [38]	37
4.9	115V and 26V distribution	38
4.10	115V and 26V network	39
4.11	AC wild network [38]	41
5.1	SAE AIR 6326 modelling levels [39]	43
5.2	AMEsim libraries [40]	44
5.3	Simcenter Amesim model of an Aircraft AC Generation	45
5.4	EMDWRSM01 - Wound Rotor Synchronous Machine (WRSM)	46
5.5	Electrical outputs	47
5.6	Electrical transient on network	47
5.7	Electromagnetic torque	48
5.8	Torque transients	48
5.9	Voltage outputs	49
5.10	Voltage transients	51
5.11	Envelope of normal 400 Hz and variable frequency AC voltage transient [42]	52
5.12	AC modelling	53
5.13	Loads modelling	54
5.14	Voltage trend	55
5.15	Current trend	56
5.16	Power trend	57
5.17	Voltage transients	58
5.18	DC generation	59
5.19	DC motor	60
5.20	DC loads modelling	60
5.21	DC voltage trend	62
5.22	DC voltage peaks	63
5.23	Envelope of normal voltage transients for 28 volts DC system [42]	63

5.24	DC current trend	64
5.25	DC current peaks	65
5.26	DC power trend	65
5.27	DC power peaks	66
6.1	Battery pack characteristic requirement	67
6.2	Battery modelling	68
6.3	Output voltage GCU	69
6.4	Output current GCU	70
6.5	Output power GCU	70
6.6	Input voltage transformer	71
6.7	Output voltage transformer	71
6.8	Output power transformer	72
6.9	Input and output current transformer	72
6.10	Output DC voltage	73
6.11	Output DC current	73
6.12	Output DC power	74
6.13	Input voltage battery	75
6.14	Input current battery	75
6.15	Output voltage GCU (t=8s)	76
6.16	Battery state of charge	76
6.17	Battery state of charge	77
6.18	Voltage GCU (SOC=95%)	77
6.19	Voltage GCU (battery capacity = 2 kWh)	78
6.20	Voltage GCU (battery capacity = 3 kWh)	79
6.21	Modelling with current limitation	80
6.22	Input current battery	81
6.23	Power GCU	81
6.24	Voltage GCU	82
6.25	Battery SOC	82
A.1	AC normal operation characteristics - 400Hz [42]	86
A.2	DC normal operation characteristics [42]	86

Acronyms

MEA

More Electric Aircraft

MEA

All Electric Aircraft

HEA

Hybrid-Electric Aircraft

HEP

Hybrid-Electric Propulsion

ICE

Internal Combustion Engine

UAM

Urban Air Mobility

UAV

Unmanned Aerial Vehicle

EPS

Electrical Power System

SOC

State Of Charge

Chapter 1

Introduction

Since the beginning of the 21st century, the aviation sector has grown rapidly, contributing significantly to the global economy. However, the increase in air traffic has led to a heavy reliance on fossil energy, resulting in increased greenhouse gas emissions. In this context, the concept of sustainable aviation is not just desirable, it is imperative. In 2019, the aviation sector emitted approximately 918 million tonnes of CO_2 , representing a 29% increase compared to 2013. On a global scale, this sector contributes 2% of total emissions, with the transportation sector accounting for 12% of these emissions. However, this percentage is projected to rise in line with the increasing economisation of transportation, which is driving an expansion in air traffic [1]. In the absence of intervention, Kreimeier et al. [2] report that these emissions could rise at an annual rate of approximately 4–5%. The atmospheric lifetime of CO_2 released by aircraft has been estimated to be 100 years, due to the absence of re-absorption by vegetation, which consequently amplifies its impact by a factor of four relative to CO_2 emissions from the ground [3].

In order to address this issue of environmental sustainability, several organisations such as ICAO and companies in the sector are working on the development of technologies to reduce emissions. It is notable that Council Regulation (EU) No 558/2014 of 6 May 2014 has established a programme named Clean Aviation with the objective of integrating new technologies capable of reducing CO_2 levels and validating them in order to achieve a reduction in emissions by a minimum of 20-30% [4]. In July 2021, the European Commission adopted proposals for an intermediate target of at least 55% GHG emissions reduction by 2030 with the aim of achieving climate neutrality by 2050 [5].

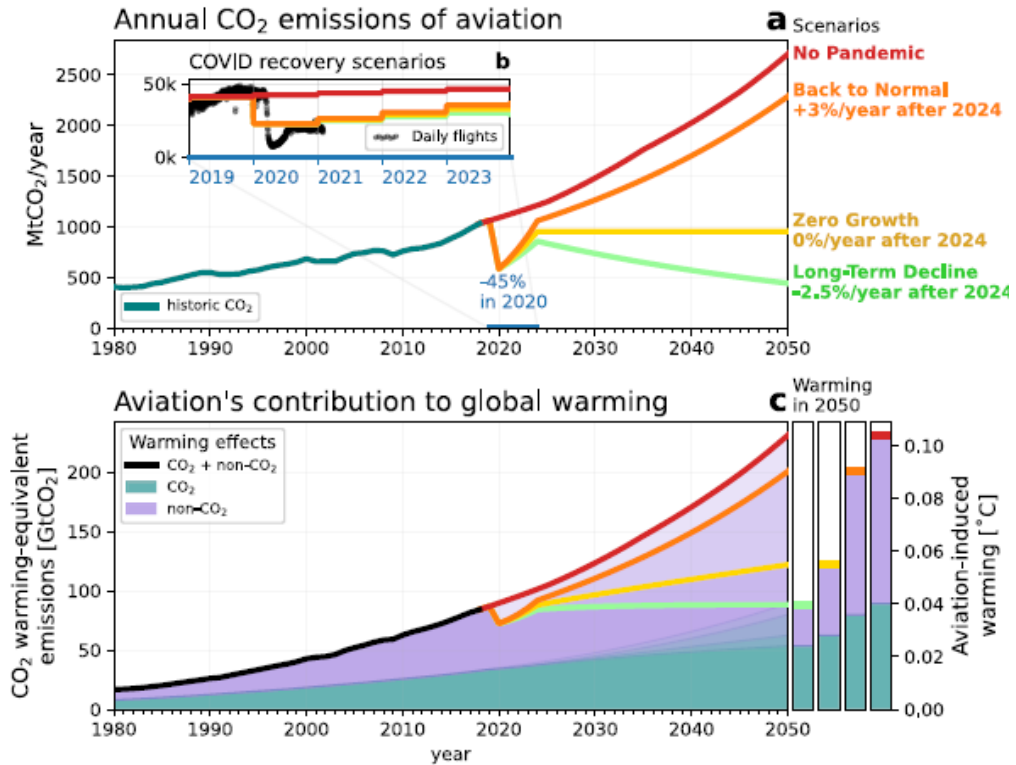


Figure 1.1: CO_2 emissions from the aviation sector and its impact on global warming

The figure 1.1 illustrates the trajectory of CO_2 emissions from the aviation sector and its impact on global warming. The top graph illustrates the projected annual CO_2 emissions from 1980 to 2050 under various post-Covid-19 recovery scenarios. The projections are presented in four scenarios: No Pandemic (in red, continuous growth projection as if the pandemic had not occurred), Back to Normal (in orange, growth of 3% per year after 2024), Zero Growth (in yellow, no growth in emissions after 2024) and Long-Term Decline (in green, decline of 2.5% per year after 2024). The bottom graph illustrates the contribution of aviation emissions to global warming, distinguishing between the impact of CO_2 alone and the combined effects of CO_2 and other non- CO_2 factors, including water vapour and nitrogen oxides. The colours highlight the various contributions to CO_2 equivalent warming and demonstrate how, in the absence of intervention, aviation-induced global warming could increase significantly by 2050 [6].

In the European context, the European Union's Clean Aviation research and innovation programme includes the HERA project, to which this thesis refers. The project, co-ordinated by Leonardo S.p.A., aims to realise regional turboprop

transport aircraft configurations with a capacity of 50-100 passengers, with entry into service scheduled for 2035. The HERA aircraft integrates applicable solutions to comply with certification and interact with the ground infrastructure. Recent research on regional hybrid turboprop architectures has focused efforts on the use of batteries to power electric motors. However, HERA proposes an alternative approach, based on on-board power generation using hydrogen fuel cells, with a high-voltage distribution system to power the electric motors. The aircraft will be equipped with a hybrid-electric propulsion system assisted by 100% per cent drop-in or hydrogen fuels, whether fuel cells or H₂ combustion for the thermal energy source, in order to achieve up to 90% per cent emission reduction in compliance with ICAO noise regulations [7].

HIGH LEVEL OBJECTIVE AT SYSTEM LEVEL	QUANTIFICATION AT SYSTEM LEVEL (%)
Fuel Reduction	50%
CO ₂ Reduction	90% (SAF included)
Noise reduction	65%

Figure 1.2: Environmental objectives [7]

The Figure 1.3 shows the CO₂ emissions per aircraft segment and range in 2018, with a specific focus on the area covered by HERA, determined on the basis of a consolidated assessment of the capacities of alternative energy sources and their impact to 2035. Currently, the use of batteries and hydrogen cells is rather limited, as their capacity does not yet guarantee adequate flexibility. The limited scope of optimal application of new low greenhouse gas emission technologies affects the implementation of HERA in terms of aircraft configuration to be studied. Consequently, for a regional aircraft, given its size, range and mission, a hybrid-electric propulsion system with a heat engine burning 100% SAF and possibly hydrogen, coupled with an electric propulsion system based on fuel cells and/or batteries, could be used. The final choice will depend on several factors, including weight, power density and volume of the energy source, safety considerations, effects on aircraft performance, flexibility of use, productivity index and sustainability. In addition, the distribution of power between batteries, fuel cells and thermal engines will depend on the size of the aircraft and its typical mission: the larger the size and the longer the flight, the greater the prevalence of hydrogen; the smaller the size and the shorter the flight, the greater the use of electrical energy sources [8].

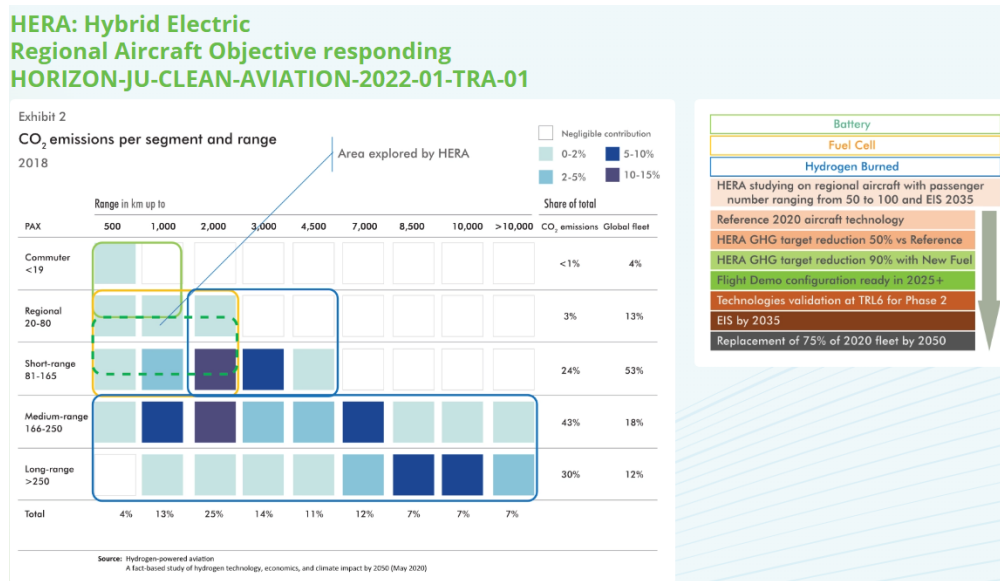


Figure 1.3: Hera objective [9]

The globally shared goal is that through the use of electric devices of a few MW, capable of fulfilling severe aviation functions and ensuring safety, a significant share of propulsive power can be provided from electric sources, thus reducing the size of the heat engine. The electrification of critical functions such as propulsion for regional aircraft can also be applied to larger aircraft, as they have some fundamental aspects in common:

- have similar safety criteria and certifications, which allows for easier technology transfer
- they face the same operational issues (such as maintenance, air traffic management, etc.)
- the infrastructures in which they operate are similar.

This allows the electrification developed for regional aircraft to be adapted to larger aircraft as well, without the need for significant modifications.

In the context of the project under consideration, two use cases were developed, which can be distinguished according to the type of propulsion adopted. The second use case (USC_B), in particular, employs distributed propulsion.

Figure 1.5 illustrates the structure of the propulsion scheme, which includes the combined use of a battery, a fuel cell and a liquid hydrogen tank for power. Further components include electric motors (EM) coupled to gearboxes (GM), which in turn drive the propellers. Finally, the system is completed by combustion engines using Jet A1.



Figure 1.4: USCs concept trade-off and possible concept configuration [8]

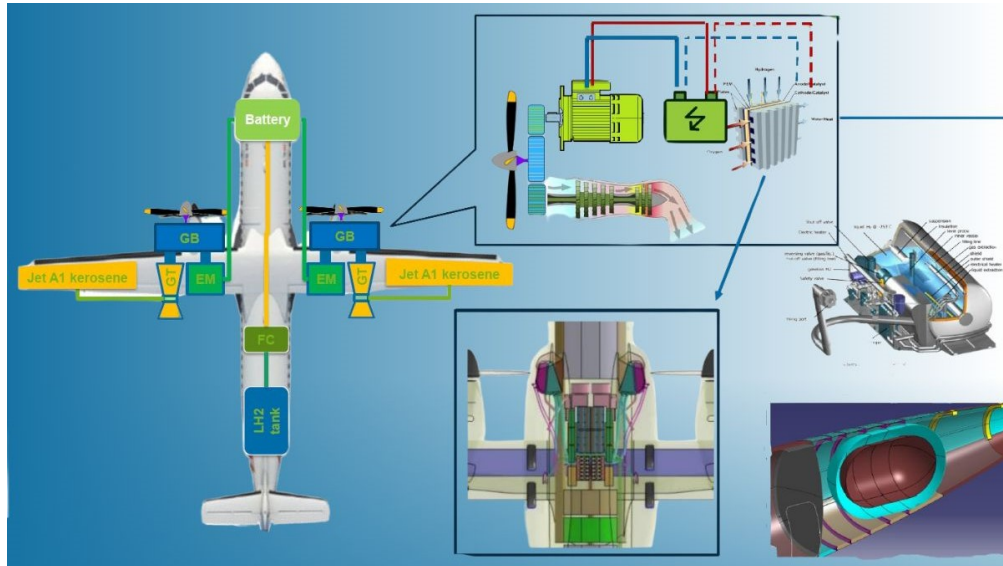


Figure 1.5: Use Case A propulsive architecture [9]

Chapter 2

State of the art

2.1 Electrification in aviation industry

In order to attain the goals set forth by international organisations regarding prospective aircraft emissions, the potential of electrification was duly considered. For an aircraft, the aerospace industry has adopted two approaches to electrification: the More Electric Aircraft, which involves reducing the reliance on conventional power systems through a transition to electric alternatives, and Electric Propulsion, which utilises electric motors in place of thermal-combustion engines [10].

In a conventional aircraft, approximately 95% of the power generated by the engine is allocated to thrust, while the remainder feeds the following onboard systems:

- hydraulic system, that supplies power to flight controls, landing gear extension and retraction, nose-wheel steering, braking, and thrust reversing;
- pneumatic system, that supplies power for cabin pressurization, anti-icing and de-icing, and for engine starting;
- electrical system, which provides power for lightning, avionics and galleys;
- mechanical system, that provides power for fuel and oil pumps.

The primary objective of the MEA concept is to diminish reliance on conventional power systems by transitioning to electric alternatives that offer advantages in fuel and weight consumption reduction. An example of More Electric Aircraft is the B787, where the pneumatic system was eliminated and a set of electrical compressors were introduced to regulate the temperature and pressure in the cabin [11]. The removal of the pneumatic system eliminates the necessity for a bleed air system on the gas turbine, which markedly enhances the efficiency of the turbine

and reduces the fuel consumption by a factor of 1 – 2% [12]. Since the elimination of the pneumatic system, main engine generators through electrical wires supply the necessary power to achieve the main engine start. With the electric starting of the engine and de-icing, it is possible to eliminate the pneumatic and hydraulic function of APU, as shown on the right in Figure 2.1.

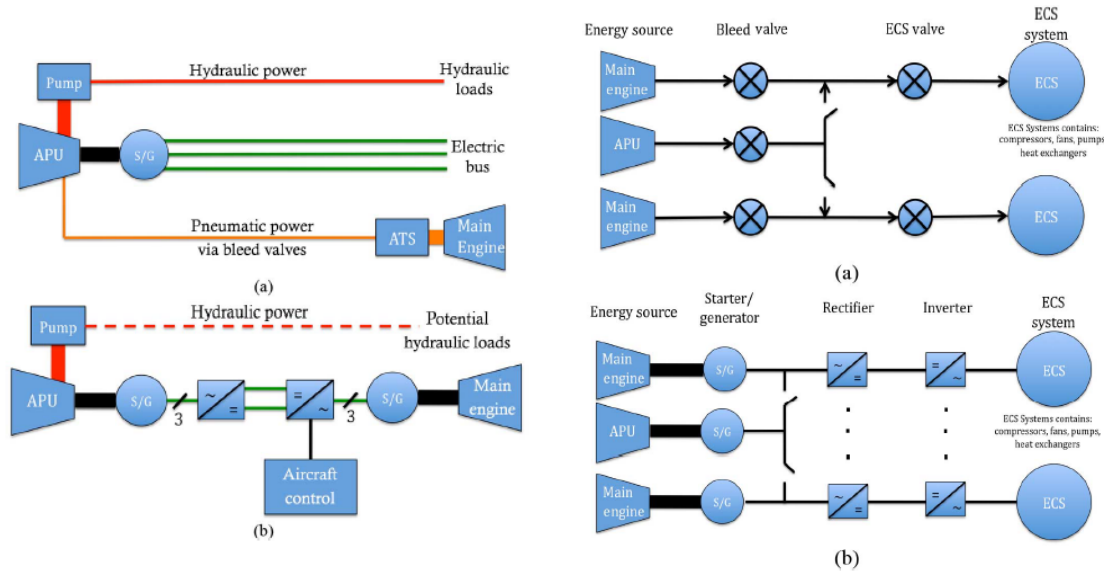


Figure 2.1: On the left the difference between the traditional APU (a) and the electric APU (b). On the right ECS with bleed air (a) and electric ECS (b)

While the electrification of systems has resulted in enhanced reliability, lower weight and maintenance costs, and improved efficiency, electrical systems do present certain challenges. These include the necessity for advances in power electronics to manage the growing loads and the requirement to dissipate the excess heat generated by losses within the electrical power chain [10]. In light of the inadequacy of the modifications introduced by the MEA concept to attain the necessary reduction in emissions for future decades, the potential of electric propulsion is being explored [13].

In the context of electrical propulsion, aircraft designers have three main options in terms of aircraft architecture [10]:

- hybrid-electric architecture (parallel or series);
- turbo-electric architecture, where the mechanical energy from the turbo-shaft is converted into electrical energy used to power distributed electric motor-driven fans;

- all-electric propulsion, where the only source of energy for the motor is a battery.

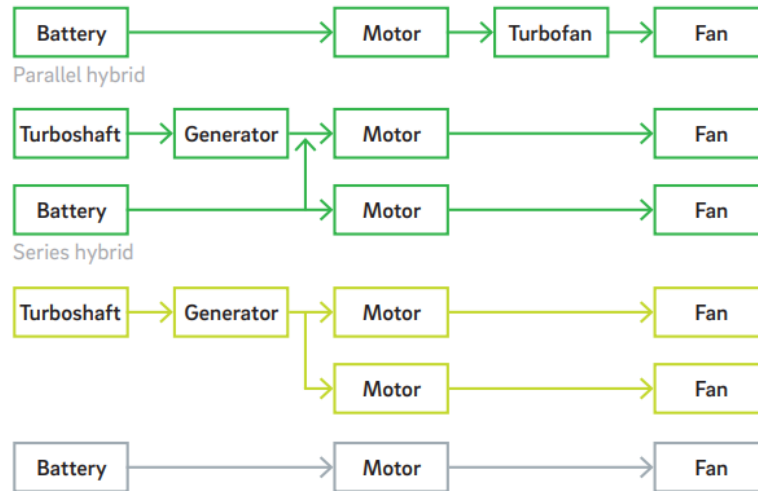


Figure 2.2: Electrical propulsion architectures [10]

2.2 Hybrid Electric Aircraft

In consideration of the current limitations of battery energy storage technology and the advancement of the associated components essential for energy distribution on aircraft, the feasibility of an all-electric aircraft concept remains challenging to achieve at this time. Consequently, further alternatives have been investigated, and one solution that has gained prominence is the hybrid-electric aircraft concept, which involves a combination of electric propulsion with internal combustion propulsion systems. In order to meet the trend of reducing emissions, greener fuel types such as hydrogen or SAFs should be used [12] [14]. Most major aerospace companies, such as Boeing or Airbus, believe that hybrid electric propulsion represents a possible trade-off solution for general aviation aircraft, whereby emissions and fuel consumption can be mitigated while ensuring adequate range and endurance performance [15].

2.2.1 Architecture of propulsion system

There are two different tipologies of HEP architectures:

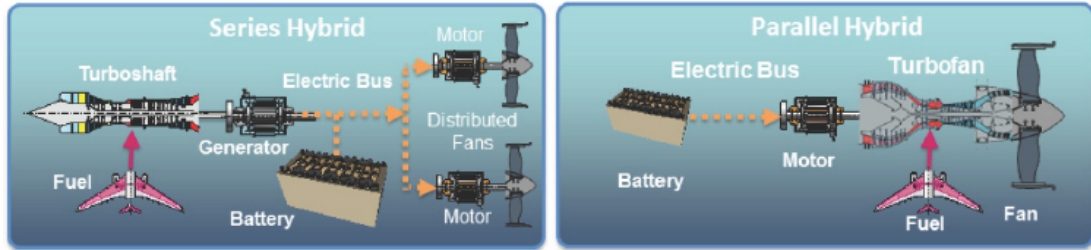


Figure 2.3: Hybrid propulsion architectures [16]

- Series hybrid architecture: combustion engine power is converted into electrical energy via a generator, which can be used to power the EM that drives the propeller, or stored in the battery.
- Parallel hybrid architecture: both combustion engine and electric motor contributes directly to the propulsion of the aircraft

Series architecture is more efficient for short flights and phases requiring low power, such as taxiing; in contrast, parallel architecture is better suited to longer flights and scenarios requiring more flexible power management. Therefore, series systems are preferred for use in urban and short-range transport aircraft, including unmanned aerial vehicles (UAVs) and electric urban air mobility (UAM) aircraft. In contrast, parallel hybrid systems are more suitable for use in medium-sized commercial aircraft, which require increased autonomy and power during take-off and cruise phases. Although series architecture is less complex and potentially more cost-effective, it is limited over long distances, where parallel architecture offers superior performance and flexibility despite the increased complexity [15]. Furthermore, the existing literature also documents the possibility of mixed systems (Figure 2.4) which combine both serial and parallel architectures. Such mixed systems are more complex, but they also exhibit enhanced functionality due to the exploitation of both serial and parallel architecture advantages. Typically, the mixed system is even heavier than both serial and parallel architectures, which prevents this architecture from being used in aviation; however, in the automotive sector it is commonly found [17].

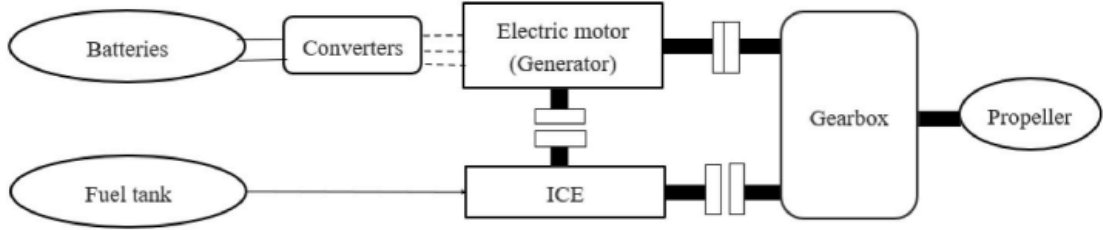


Figure 2.4: Series-parallel architecture [17]

2.2.2 Advantages and disadvantages of HE propulsion

This section will investigate the advantages and disadvantages of hybrid propulsion, considering its capacity to advance the transition to sustainable aviation and the obstacles that persist regarding its implementation [17].

From a mechanical standpoint, a thermal engine can operate at consistent parameters throughout the entirety of a flight, thereby enhancing overall efficiency. Furthermore, the ICE can be downsized due to the presence of batteries, which provide supplementary energy during the most energy-intensive phases, such as take-off and climbing. The utilisation of electric motors mitigates the damage caused to gas turbines during flight phases in proximity to the ground, which may be caused by sand or other particles. A disadvantage of hybrid architectures is that they require a large number of components, which results in an increase in empty weight, due to the fixed mass of the batteries during flight, reducing the payload and the number of passengers. In addition, the presence of a greater quantity of components leads to an increase in energy loss.

In the event of an engine failure, the batteries can provide the necessary power to ensure a safe emergency landing. Therefore, the redundancy of energy sources, comprising a thermal engine and an electric motor, contributes to enhanced operational safety and improved reliability. This is due to the fact that the electric motor is much more reliable and easier to maintain than a thermal one, due to its simple structure. It should be taken into consideration that the incorporation of novel components into the propulsion system of a hybrid electric aircraft may present challenges with regard to their certification. Hybrid propulsion systems must comply with current safety standards and provide the requisite reliability, which can prove challenging in the presence of devices such as batteries, which are susceptible to self-ignition.

The utilisation of electric motors has the effect of reducing fuel consumption, which in turn has an impact on operating costs, given that fuel represents 51% of the total costs borne by the owner. A further advantage is that the simple structure of electric motors results in lower maintenance costs. Despite these economic

advantages, Siemens predicted that a hybrid electric aircraft would cost between 10% and 30% more to purchase than a conventional aircraft. In addition, the use of this new type of aircraft would require a significant economic investment to make the airport infrastructure suitable for charging and changing batteries [18].

2.2.3 Demonstrators

Within the domain of hybrid-electric propulsion, an important research and development activity has been carried out, and many demonstrators have been developed. The demonstrators are essential in the functional testing and verification of the most critical elements of the new propulsion systems.

NASA developed a regional aircraft concept called PEGASUS (Parallel Electric-Gas Architecture with Synergistic Utilization Scheme) with a capacity of 48 passengers [19]. This concept was developed on the basis of the ATR 42-500, with some modifications to the engines and propulsion power. Compared to the ATR, this aircraft will have a total of five engines of three different categories:

- two parallel hybrid electric wingtip propulsors which provide most of the cruise thrust reducing drag;
- two inboard all-electric propulsors are employed to augment thrust during take-off and climb. During cruise, however, these are folded in order to reduce drag;
- one aft all-electric propulsor using boundary layer ingestion in order to decrease the propulsive power and increase aerodynamic efficiency.

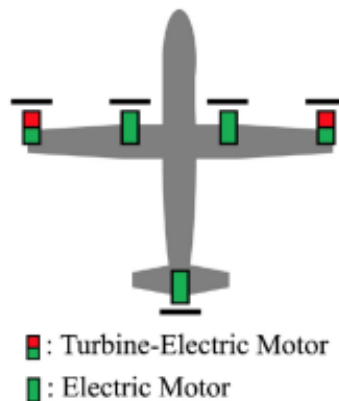


Figure 2.5: PEGASUS propulsor configuration and locations

Pegasus concept was design to fly a 200 nautical mile mission with all-electric propulsion and a 400 nautical mile mission with hybrid-electric propulsion.

In May 2022 ATR announced the 'EVO' concept, a two-engine turboprop that integrate hybrid-electric capabilities and is designed to run on 100% SAF, significantly reducing carbon emissions with an entry into service targeted by 2030. When operating on kerosene, it will emit over 20% less CO₂ than comparable in-service aircraft powered by PW127M engines matching the current aircraft's 72-passenger load and optimum 200 nm range, and using SAF could bring emissions close to zero. So, the aircraft promises a 20% improvement in fuel efficiency and maintaince costs, due to the use of lighter materials and optimized systems. Another upgrades is the new eco-design which includes new propellers, improved systems and cabin using bio-sourced materials which aim to improve performance while enhancing passenger comfort. A hybrid hydrogen system would likely result in a reduction in passenger capacity to below 60, accompanied by a 40% decrease in emissions per passenger. In this conceptual framework, the parallel hybrid architecture incorporates two battery packs that deliver a power output ranging from 300 to 500 kW. These packs serve as the source of power for electric motors that are coupled mechanically with propeller gearboxes. In conditions of elevated temperature and pressure, electric power will support the turboprop engine during take-off and during the climb, contributing approximately 10% of the total power. In typical operating scenarios, electrical energy could supply up to 20% of the power needed during the top-of-climb phase and the beginning of cruise. The batteries are designed to be recharged later in the cruise phase, during descent and on the ground between flights, with the assistance of the thermal engines [20] [21].



Figure 2.6: On the left ATR EVO, on the right RTX demonstrator

Pratt&Whitney and Collins Aerospace are well-placed to drive the advancement of integrated hybrid-electric propulsion technologies through the STEP-Tech Demonstrator programme, which is designed to facilitate the creation of scalable and adaptable technologies for advanced air mobility and regional aircraft. In the latter category of aircraft, collaboration has been established with De Havilland Canada for the development of a regional hybrid electric flight demonstrator based on the modified De Havilland Canada Dash 8-100 [22] [23]. One of the two PW120-class turboprops is substituted with a parallel hybrid-electric powertrain comprising 2 Collins Aerospace MW electric motor generators positioned on the high and low spool of the geared turbofan engine [24]. This configuration of electric and thermal engines may result in a 30% improvement in fuel efficiency compared to traditional engines. A ground demonstration of the propulsion system was successfully executed on 2022, while a flight demonstration is scheduled for the end of 2024.

2.3 Current technology and projections

2.3.1 Electric machines

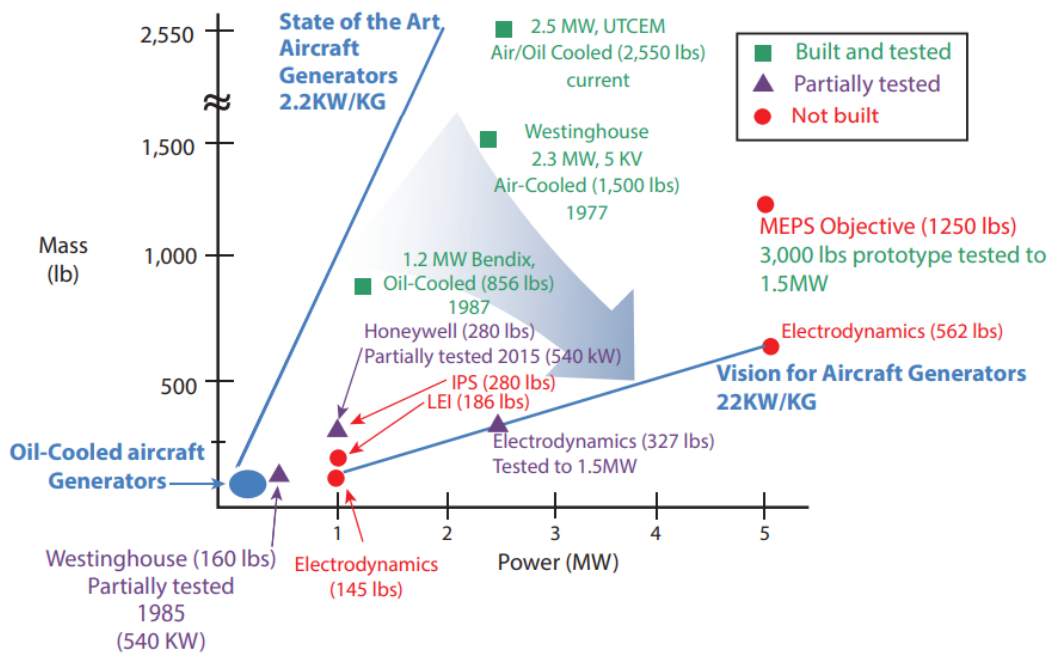


Figure 2.7: State of the Art of aircraft generators actually in the market and future prospects [25]

The function of a generator is to generate electrical power and deliver torque to start the engine. Once the engines are operational and burning fuel, generators become the primary sources of secondary electrical power (non-propulsive). In Figure 2.7 the relationship between the power and mass of various aircraft generators, both current and under development or design, including wound-field synchronous, permanent magnet, and wire-wound superconducting synchronous machines is shown [25]. As evidenced by the image, contemporary aircraft generators are characterised by models that attain a power-to-mass ratio of approximately 2.2 kW/kg. Prominent examples include UTCEM’s 2.5 MW generator and Bendix’s 1.2 MW generator, both of which have been constructed and subjected to rigorous testing. These systems exemplify the most advanced technologies currently available, optimised to combine high power with relatively low mass. The future direction for aircraft generators is the significant increase in efficiency. This objective is outlined in the ‘Vision for Aircraft Generators’, which aims to achieve a ratio of 22 kW/kg. This objective signifies a landmark transformation in the realm of aircraft generator design, marking a substantial enhancement in performance metrics concerning weight and power. The adoption of innovative technologies, new materials, and advanced cooling systems will be key to achieving these ambitious goals, as suggested by the proposed developments of the MEPS generator and other solutions not yet built but in the design phase.

	Motor and Generator	
	Power Capability (MW)	Specific Power (kW/kg) ^b
A. Current state of the art		
Noncryogenic ^c	0.25	2.2
Cryogenic power ^d	1.5	0.2
B. Research goals ^e		
NASA 10-year goals ^f	1-3	13
NASA 15-year goals	5-10	16
U.S. Air Force 20-year goals ^g	1	5
Ohio State Univ. 3-year goals	0.3	15
Ohio State Univ. 5-year goals	2	15
Airbus 15-year goal		10-15
McLaren automotive projection ^h		
C. Committee’s projection of the state of the art in 20 years (noncryogenic) ⁱ		
	~1-3	~9

Figure 2.8: (A) Current State of the Art of motor and generator, (B) Stated Research Goals for Some Current Research Programs, and (C) the Committee’s 20-Year Projection of the Performance of motor and generator configured for aircraft applications [25]

As reported in Figure 2.8, it is foreseen an increase in the specific power output of motors and generators to approximately 9 kW/kg within the next two decades, with power levels ranging from 1 to 3 MW. This augmentation in power output is hypothesised to be achieved through some strategies such as an increase in the operational speed of the machines, an enhancement in the power conversion efficiency and lastly, an increase in the power generation and distribution voltage.

2.3.2 Power electronics

In the context of aircraft equipped with power supply systems operating within the MW range, it is essential to acknowledge the critical function of power electronics. Currently, power electronics systems for aircraft with power requirements in the MW range are predominantly constructed using silicon carbide (SiC), a material that has been demonstrated to exhibit superior efficiency in comparison to silicon-based systems. This advancement in silicon carbide technology has also been shown to deliver enhanced voltage performance and increased reliability.

The current specific power of power electronics systems for aircraft applications based on silicon technology is approximately 2.2 kW/kg. However, with the advent of silicon carbide (SiC), a substantial improvement in this specific power is predicted, with a projected increase to approximately 9 kW/kg within the next two decades.

In terms of circuit protection, silicon-based systems can currently manage currents of up to 25 A at 270 V DC, corresponding to a power of approximately 7 kW. However, for higher power values, the utilisation of mechanical circuit breakers is requisite, with the capacity to protect up to 500 A at 270 V DC, corresponding to a power output of approximately 135 kW. SiC-based systems are projected to facilitate the protection of circuits with electronic components capable of managing up to 200 A at ± 270 V (540 V), achieving a power output of 108 kW, and with mechanical circuit breakers up to 1,000 A at ± 270 V, resulting in a total power of 540 kW.

2.3.3 Power system efficiency

With regard to hybrid-electric systems, the current declared efficiency value is 95%; however, this figure does not take into account the power conversion systems, but rather only the machinery itself. Consequently, this declared value is not an accurate representation, as conversion systems invariably incur losses. When the electrical machine is operating below its maximum capacity, the overall efficiency of the system may decline due to inherent losses that are not load-dependent.

As demonstrated in Figure 2.9, the efficiency of the power system is calculated. For each phase of the system, an efficiency of 95% is assumed, resulting in an overall system efficiency of 80%. This value must be combined with the turbine and

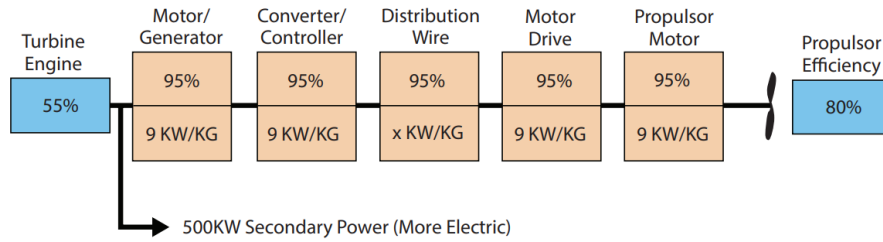


Figure 2.9: Efficiency drop in a turboelectric aircraft

propulsor efficiency to derive the final fuel-to-propulsor efficiency of 35%, which is significantly lower than the initial estimate.

In the field of hybrid-electric propulsion, various solutions have been proposed in the academic literature. In order to avoid a reduction in overall efficiency, it is suggested that the conversion and control electronics be eliminated so that the generators drive the thruster motors directly. This approach would result in the elimination of the converter control and engine drive stages. However, the applicability of this solution remains to be demonstrated [26].

2.3.4 Batteries

Batteries, as energy storage devices, play a key role in electric or hybrid-electric propulsion aircraft, as they provide electricity without direct carbon emissions. However, it is necessary to consider indirect emissions related to the power source utilised in the battery charging process. Despite the minor contribution of these emissions, batteries remain a highly promising solution within the domain of sustainable propulsion, as the mitigation of these indirect emissions is more efficiently achievable on the ground than at altitude. For a regional and single-aisle aircraft is required a battery with a specific energy greater than 800 Wh/kg to enable hybrid propulsion. This far exceeds the Committee's 20-year projection on the specific energy of batteries. As reported in [25] it is expected that in 20 years' time batteries could reach a specific energy of 400-600 Wh/kg.

Aircraft Requirements	Electric System ^a		Battery ^b
	Power Capability (MW)	Specific Power (kW/kg) ^c	Specific Energy (Wh/kg)
General aviation and commuter			
Parallel hybrid	Motor <1	>3	>250
All-electric	Motor <1	>6.5	>400
Turboelectric	Motor and generator <1	>6.5	n/a
Regional and single-aisle			
Parallel hybrid	Motor 1-6	>3	>800
All-electric ^b	Motor 1-11	>6.5	>1,800
Turboelectric	Motor 1.5-3; generator 1-11	>6.5	n/a
Twin-aisle			
Parallel hybrid	Not studied		
All-electric	Not feasible		
Turboelectric	Motor 4; generator 30	>10	n/a
APU for large aircraft	Generator 0.5-1	>3	Not studied

^a Includes power electronics.

^b Total battery system and usable energy for discharge durations that are relevant to commercial aviation flight times, nominally 1-10 hours. Values shown are for rechargeable batteries; primary (nonrechargeable) batteries are not considered relevant to commercial aviation.

^c Conversion factors: 1 kW/kg = 0.61 HP/lb; 1 kg/kW = 2.2 lb/kW = 1.64 lb/HP.

Figure 2.10: Electrical system component performance requirements for Parallel Hybrid, All-Electric, and Turboelectric Propulsion Systems

As previously referenced, the primary challenge confronting the aviation sector pertains to the necessity of enhancing the specific energy of batteries. The present market offers lithium-ion batteries. These batteries possess a power capability in over 10 MW and a specific energy of between 150 and 200 Wh/kg. Alternatively, lithium-sulfur batteries have been developed, offering a specific energy of 350 Wh/kg. A further prospect under consideration in the extant literature pertains to lithium-air batteries, a subject of investigation by numerous corporations, including NASA and Samsung [27]. The estimated specific energy for this battery type ranges from 1000-2000 Wh/kg, with a specific power of 0.4-0.67 kW/kg. However, the commercialisation of this technology is not anticipated to occur before 2030, due to the need for further research and development to address existing challenges. The primary challenge confronting Li-air batteries pertains to the rapid decomposition of the electrolyte, a phenomenon that imposes limitations on their rechargeability and consequently curtails the number of cycles they can sustain when compared to Li-ion batteries. Achieving the requisite specific energy levels for the commercial deployment of battery-powered electric and hybrid aircraft propulsion systems necessitates significant technological advancements in "beyond lithium-ion" battery systems. These advancements are crucial for these systems to make a substantial impact on reducing carbon emissions in commercial aviation.

2.3.5 Fuel cells

The functioning of these devices is based on an electrochemical reaction that allows the conversion of chemical energy from a fuel source into electricity, heat and water. At the anode, the fuel is oxidised by the release of protons and electrons that reach the cathode, where oxygen is present. An electrolyte is positioned between the anode and cathode, facilitating the selective movement of protons but impeding the passage of electrons. These electrons reach the cathode through an external circuit, thereby generating an electric current. In the event of hydrogen being utilised as the fuel source, the exhaust from fuel cells is entirely carbon-free. Using a hydrocarbon fuel results in the exhaust containing CO_2 , which is directly proportional to the amount of fuel consumed. However, in this scenario, NO_x and particulate emissions are non-existent.

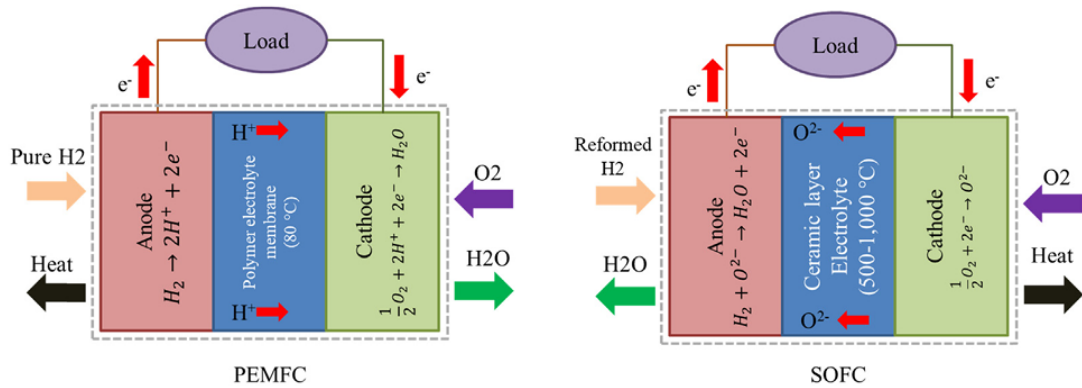


Figure 2.11: Schematic diagram of the PEMFC and SOFC operation

There are different types of fuel cells on the market, which are categorised according to the type of electrolyte and fuel used. In the aviation field, the most widely used are proton membrane exchange fuel cells (PEMFC) and solid oxide fuel cells (SOFC).

- The **PEM** fuel cells operate within a low temperature and pressure range ($80^\circ - 120^\circ$). These devices are configured to permit the exclusive utilisation of hydrogen as fuel source, with operational power ranges exceeding 100 W and efficiency levels ranging from 40% to 60%. Notable advantages include their simplicity and low weight.
- In the **SO** fuel cell a dense ceramic layer is utilize as electrolyte. The operating range of these devices allows them to operate at high temperatures ($750^\circ - 1000^\circ$) but with lower efficiencies than the previous category (25% - 50%). They have flexibility in terms of fuel choice, as hydrocarbon fuels can also

be used, in addition to hydrogen. This type of fuel cell is often used in co-generation applications since, operating at high temperatures, a significant portion of the fuel's energy is dissipated in the form of heat that can be recovered in a co-generation system. On the other hand, however, the high operating temperatures make these types of devices unsuitable for applications where frequent switching on and off is expected. SOFCs are also often used in combination with gas or steam turbines to create hybrid systems.

A study of the characteristics of these two types of fuel cells reveals that SOFCs are more efficient when used in stationary systems, as they are designed to work under stable and continuous load conditions, where heat can be recovered. However, for dynamic applications, the preference is for PEMFCs, due to their lower operating temperature, which ensures a faster and more flexible response to variations in load [25] [28].

2.3.6 Supercapacitors

Another energy storage device that has been the focus of research for use in hybrid-electric propulsion is the supercapacitor. This is because it has a high power density, which allows for rapid charging and discharging. It consists of two electrodes, on which positive and negative charges accumulate when a voltage is applied to the supercapacitor, separated by an insulating dielectric material. Energy is stored electrostatically as in a traditional capacitor. Although supercapacitors have a higher energy density than conventional capacitors, they still have a lower energy density than batteries. Other advantages include their ability to survive thousands of charge-discharge cycles, giving them a longer life than batteries. It is possible to combine supercapacitors and batteries in hybrid systems to extend battery life. Their ability to store and release large amounts of energy in a short period of time makes them ideal for applications where peak power is required. The fact that they operate over a wide range and are maintenance free is another reason why they are ideal for aviation applications.

There are currently three types of supercapacitor: electrochemical double layer capacitors, pseudocapacitors and hybrid capacitors. In the first, the storage of charge is physical, while in the pseudocapacitors the storage of energy takes place with a transfer between the electrode and the electrolyte, so it's a chemical charge. The hybrid capacitor is a combination of the other two types.

In Table ?? are reported some reference values for each type of supercapacitors.

Type	V	Power density [kW/kg]	Energy density [Wh/kg]
EDLS	2.5-3.5	1-3	5-12
Pseudocapacitor	2-3.5	1-2	10-15
Hybrid	1.5-3.3	1-2	10-15

In Figure 2.12 a logarithmic scale representation of the energy density versus the power density of different energy storage devices is reported. This graph provides an overview of the characteristics of the technologies in question. It is evident that capacitors exhibit high specific power but low specific energy values, rendering them particularly well-suited for applications requiring rapid energy release. In contrast, batteries and fuel cells are positioned at the lower and right-hand extremities of the graph, as they are characterised by higher levels of specific energy. This makes them more suitable for applications necessitating large-scale energy storage, which can be gradually released over extended periods.

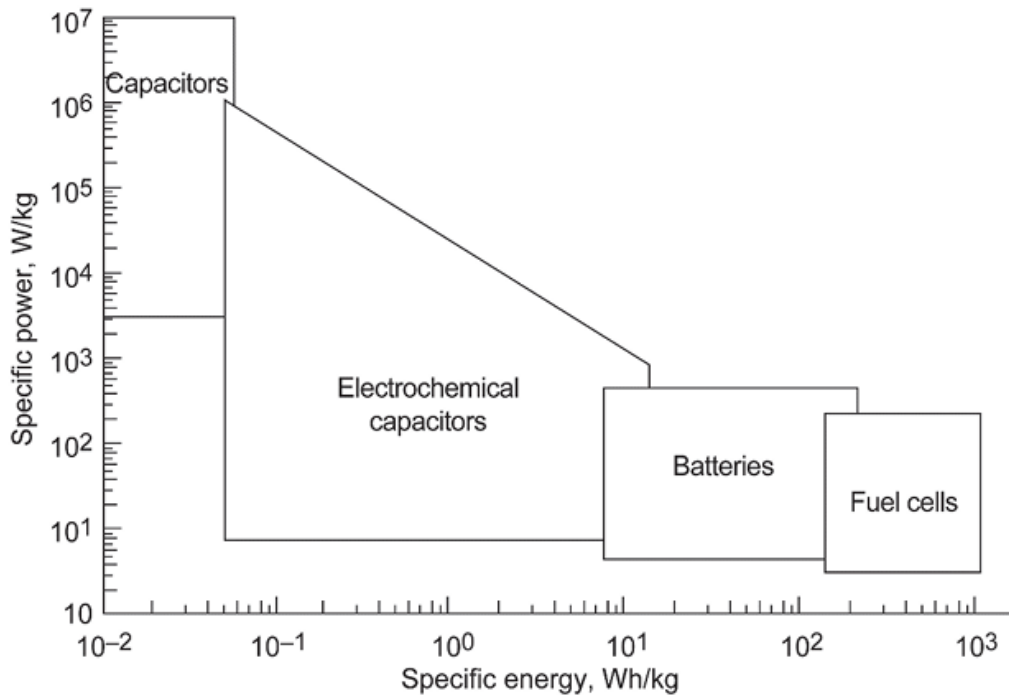


Figure 2.12: Ragone plot [29]

Chapter 3

Electrical Power System

Conventional commercial aircraft generally operate on power supply systems that use both alternating current (AC) and direct current (DC) lines. Electrical generation is mainly based on a constant voltage and frequency system (115 V AC, 400 Hz), with generators mechanically coupled to the main engines. This system powered essential loads such as avionics, lighting and auxiliary loads. However, many main functions, such as engine start-up, environmental control systems (ECS) and de-icing, were not powered electrically. In addition, a 28 V DC bus is generated via transformers and rectifiers from the 115 V AC bus, with further voltage reductions (e.g. 5 V, 3.3 V) to power electronic circuits and microprocessors. Multiple buses distribute power, ensuring redundancy and safety, while switches and control systems protect and monitor the aircraft's electrical network [11].

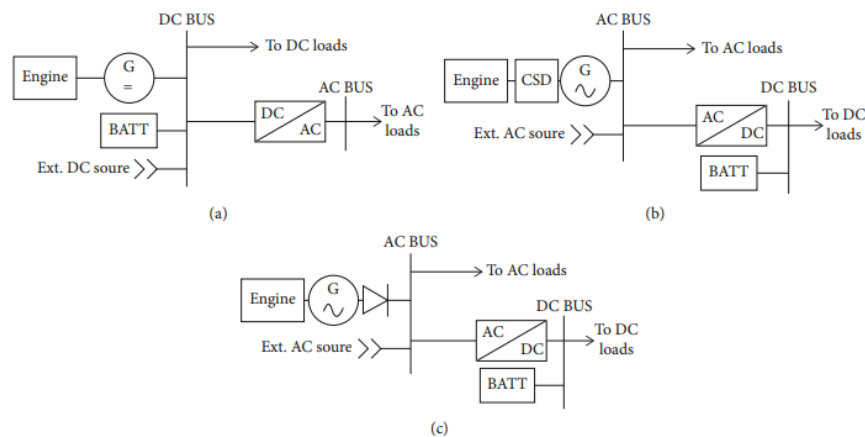


Figure 3.1: Power distribution for DC system (a), AC system (b), DC and AC system (c) [12]

3.1 Consequences of electrification on EPS

As discussed in 2.1, the concept of *More Electric Aircraft* provides an electrification of traditional systems (mechanical, hydraulic and pneumatic). This type of electrification results in a significant increase in electrical energy requirements, which must be met by the electrical power system, thereby increasing its complexity. For reference, the electrical load of the B737 was 100 kVA, whereas the B787 requires 1 MVA [12].

In this new category of aircraft, a decision was made to transition from constant to variable frequency while maintaining a constant voltage, generally 115 or 230 V AC. The bus frequency varies proportionally with engine speed and ranges from 350 to 800 Hz. The following table (3.1) provides a comprehensive overview of the MEA voltage levels that have been documented in the extant literature. With regard to the AC levels, it is important to note that these are referred to both variable and constant frequency.

DC	540 V ($\pm 270V$)	270 V ($\pm 135V$)	28 V
AC	230 V	115 V	

Table 3.1: MEA standardized voltage levels [30]

Therefore the transition to electrification led to the introduction of high voltage primary distribution, becoming AC variable frequency, and high voltage DC distribution.

A key distinction between a conventional aircraft and a MEA one concerns the method of power generation and distribution. In a traditional aircraft, power is generated in close proximity to the main engines and APU, and then directed towards the front for protection and control. In contrast, a MEA aircraft employs a remote distribution configuration, facilitated by the integration of advanced solid-state power controllers and contactors [11].

This new configuration has certain advantages:

- as the distance between generation and consumption is reduced, there is an observed decrease in line losses and an increase in efficiency
- weight and volume savings
- increase of fuel efficiency
- maintenance cost savings

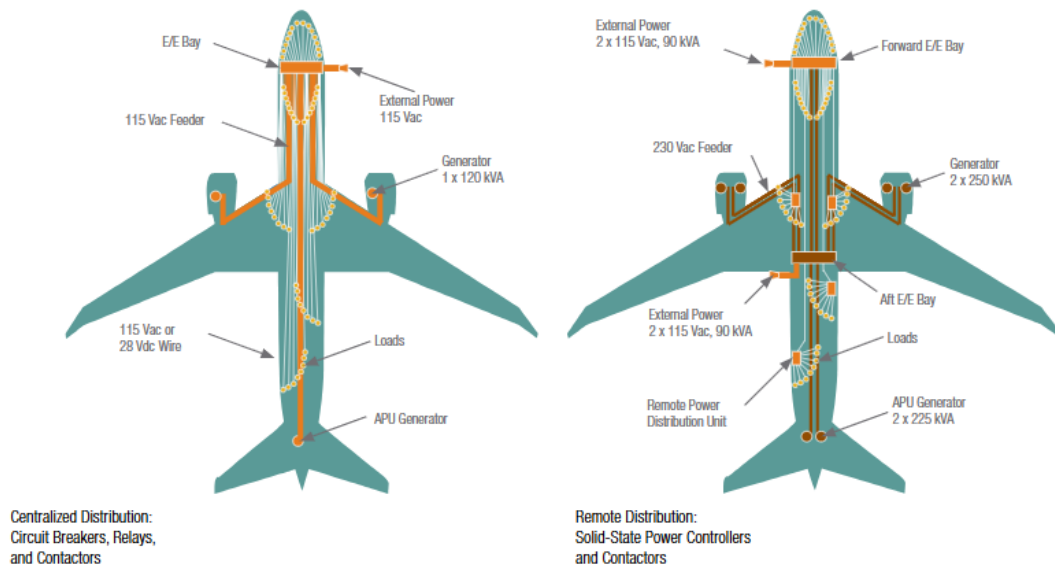


Figure 3.2: Centralized versus remote distribution [31]

In order to address the increased power demand on board electric and hybrid-electric aircraft, the utilisation of power distribution systems with voltage levels in the order of kV is proposed. Although the adoption of kV standards for power distribution is already prevalent in ground systems applications, the aerospace field operates at a significantly lower kV level. The utilisation of higher voltage levels has been observed to result in a reduction in current levels, thereby decreasing the weight of conductors. However, it should be noted that higher voltage requirements often necessitate the use of thicker insulation, which in turn contributes to an increase in cable weight [32]. In the design of aircraft electrical systems, Paschen's law must be considered when discussing voltage levels in order to prevent electrical discharges and breakdowns, particularly at high altitudes. This law delineates the behaviour of the breakdown voltage required to initiate an electrical discharge in a gas between two electrodes as a function of the gas pressure and the distance between the electrodes, considering metal plates in air under a uniform electric field. As demonstrated by the graph in the Figure 3.3, the breakdown voltage is estimated to be approximately 327 V DC. This value is not exceeded in the aeronautical field, as it is below the threshold required to prevent arcing, whether at low or high altitudes. In order to overcome the limitations imposed by Paschen's law in new aircraft with higher voltage levels, a combined approach is necessary that considers electrical system integration and the incorporation of new technologies,

alongside insulation and isolation. As discussed in [33], the integration of high-voltage systems in aircraft introduces significant challenges, primarily related to the risks of electrical discharge, partial insulation degradation, and tracking. A critical aspect is the analysis of the maximum voltage peaks and transients present in the system, and the selection of appropriate insulation materials, safety distances and optimal geometric configurations to minimise such risks. The paper further underscores the importance of derating, and the incorporation of reduction factors, to safeguard system reliability when accounting for production and operational variables. The partial discharges should not simply be controlled through the use of special materials, but should be completely prevented. Testing is another key element to ensure the safety and effectiveness of components. However, it is important to note that testing techniques commonly used for sea-level environments require specific adaptation to ensure that they are effective for equipment intended to operate at high altitudes.

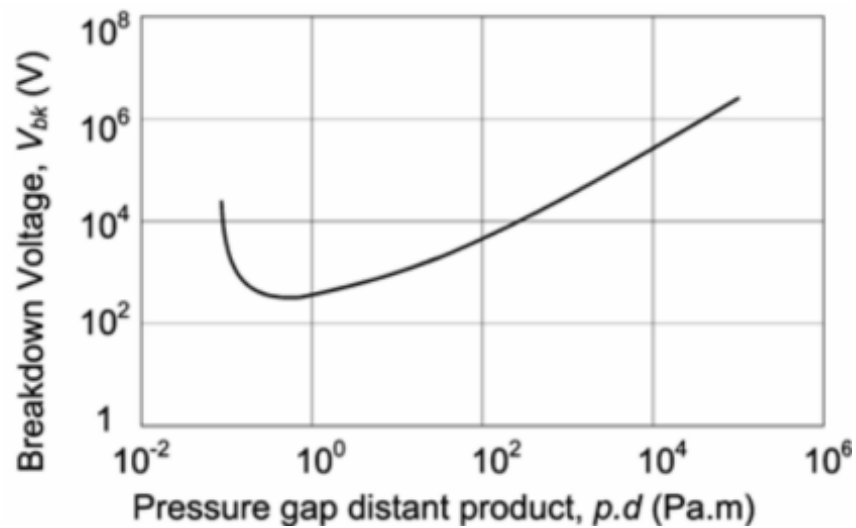


Figure 3.3: Paschen's Law

3.2 EPS architectures

3.2.1 More electric

The illustration in Figure 3.4 proposed an EPS architecture for a MEA aircraft [11]. This design is an example of a multi-tiered power supply system, which has been developed to satisfy the requirements of efficiency, reliability and redundancy.

In this architectural model, the following elements can be distinguished:

- Two generators for each main engine;
- APU which provides auxiliary energy both on the ground and under specific operating conditions;
- RAT which feeds the AC primary bus in case of emergency.

Secondary busses are directly sourced from the primary AC bus using the following PE converters:

- ATRU, an AC/DC converter that is using for systems with loads requiring a stable and reliable DC voltage;
- TRU adjusts the incoming AC voltage to the desired level and then converts it to DC. In this particular case, it fulfils the function of converting the incoming voltage from the primary AC bus to the 28 V DC bus;
- ATU converts the primary bus voltage from 230 V AC variable frequency to the secondary bus supplying 115 V AC 400 Hz constant frequency.

In consideration of the specified architecture, the presence of an electric propulsion system is assumed, directly fed from the primary AC bus, with a voltage of 2 kV AC. No particular propulsion architecture is specified, but the figure shows four fans as an example of a possible distributed propulsion system.

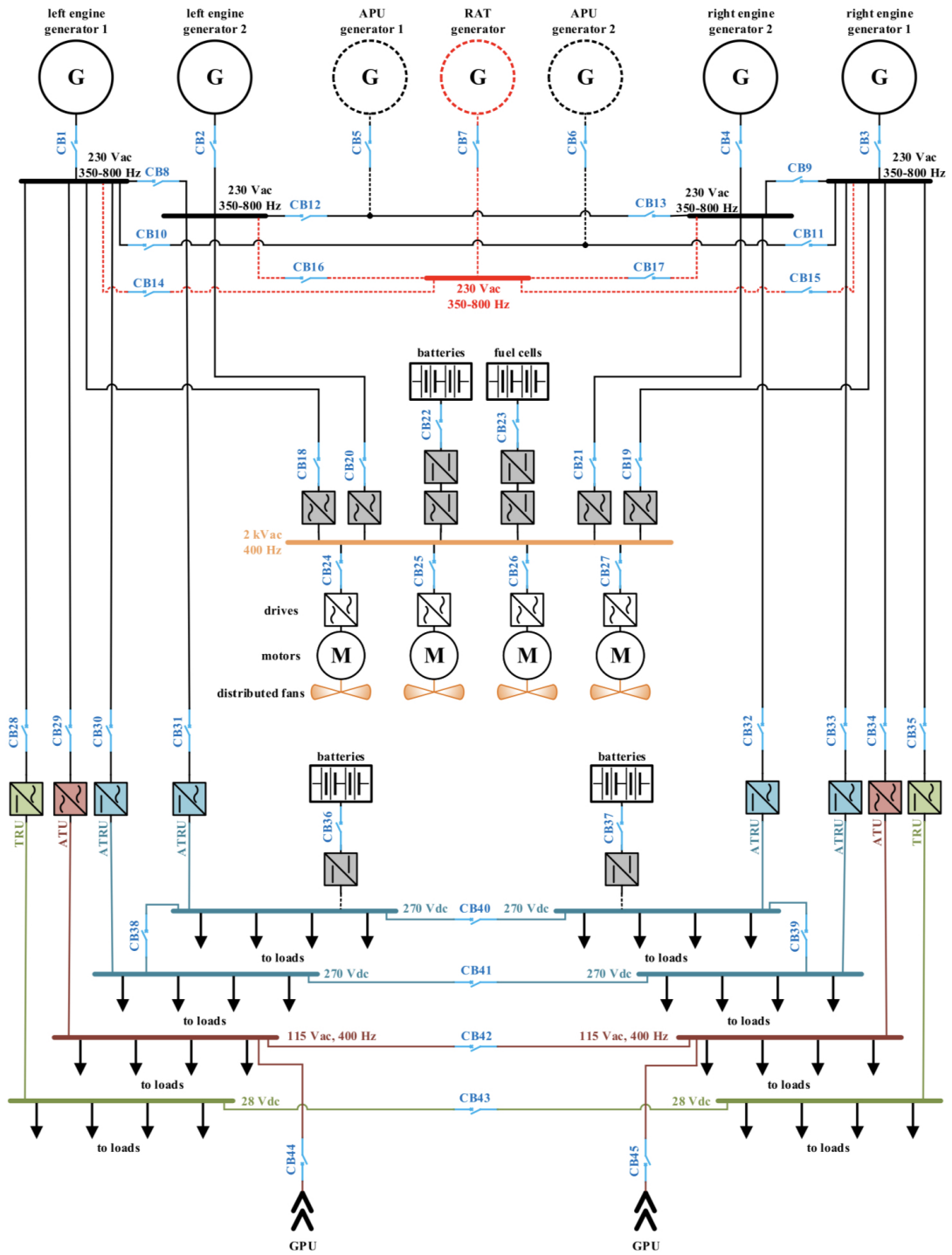


Figure 3.4: Potential EPS architecture with electric propulsion system

3.2.2 Hybrid-Electric

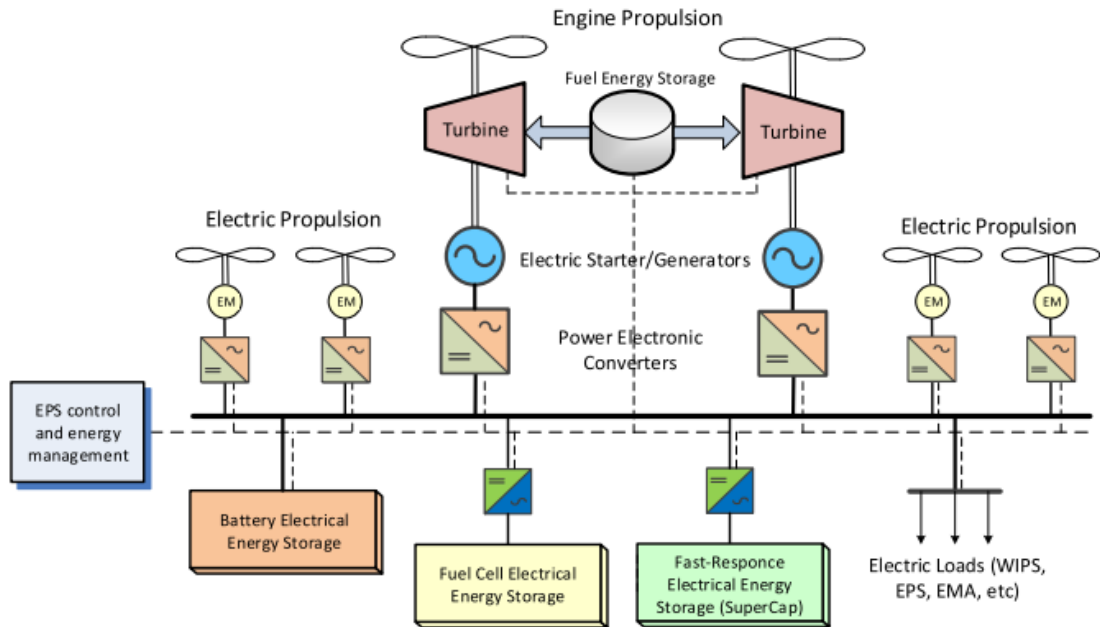


Figure 3.5: Potential EPS architecture for hybrid-electric aircraft

As illustrated in Figure 3.5, a potential architectural configuration for an electric hybrid aircraft is presented. For this particular type of propulsion system, the turbine engine is utilised not only for direct propulsion but also for the generation of electricity. Furthermore, electric motors contribute to the aircraft's propulsion by utilising the energy produced by the turbines through generators and storage systems. This configuration is designed to reduce the load on the turbines during flight, thereby enhancing their energy efficiency. The architecture in question involves the integration of three distinct energy storage systems: batteries, fuel cells and supercapacitors. This strategic design choice enables the system to meet different operational requirements, thereby enhancing its efficiency and reliability.

The complementarity of these three technologies allows for the optimisation of their respective strengths while mitigating their weaknesses:

- batteries are considered to be optimal for the provision of continuous energy; however, they are slow to sudden load changes and are subject to degradation if used intensively. They are considered to be a stable source of energy for electric propulsion and can be used to supply supercapacitors when required;
- fuel cells are a sustainable energy source, but their response time is relatively slow, which makes them unsuitable for sudden power peaks. The primary

objective of fuel cells is to ensure the sustained functioning of the system, thereby supplying both batteries and electrical loads during steady-state operation;

- supercapacitors are well suited to scenarios involving rapid intervention and power peaks and are thus used to handle sudden changes, but they are incapable of storing large amounts of energy over the long term.

3.2.3 NASA N3-X power system design

In the field of hybrid-electric propulsion, the NASA N3-X aircraft is a notable example. It is designed to use a distributed propulsion system, powered by electrochemical energy units (EEUs) and a medium-voltage direct current (MVDC) power supply system. The objectives of the N3-X are to significantly reduce greenhouse gas emissions and improve energy efficiency, representing a step toward the adoption of all-electric aircraft for long-haul commercial flights.

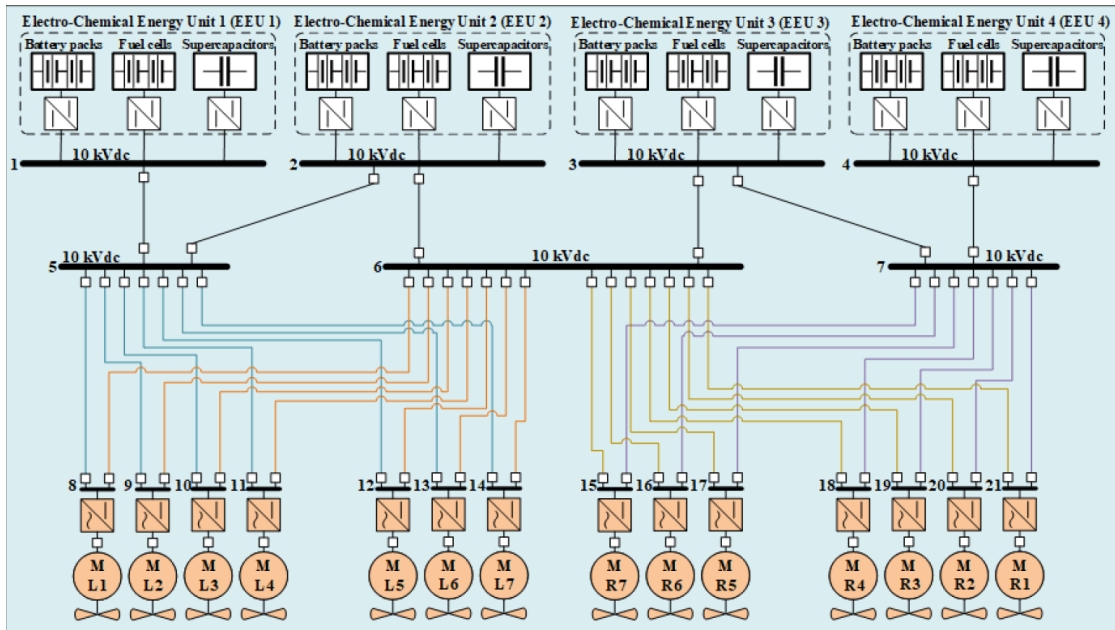


Figure 3.6: Proposed EP architecture for NASA N3-X [34]

The proposed architecture of the electrical system of the aircraft (Fig.3.6) involves an update from the original design of the NASA N3-X, which featured two superconducting electric generators connected to the two turboshaft engines, to a configuration where four electrochemical power units have been incorporated. Each of these EEU consist of battery, fuel cell and supercapacitors. Each of these

units is connected to a 10 kV DC primary bus, which in turn feeds interconnected secondary bus lines to ensure redundancy and a balanced power distribution.

The decision to adopt a medium voltage direct current (MVDC) power supply system was driven by several key advantages, not least of which is the reduction of power losses during transmission along the cables. This is made possible by the use of a higher voltage (10 kV DC), which improves the overall efficiency of the system. In addition, the MVDC system helps to reduce the overall weight of the aircraft. This is particularly significant in the field of aviation, where weight reduction directly correlates with increased energy efficiency. The cables utilised in an MVDC system are lighter than those required for an alternating current (AC) or low-voltage system, thereby enabling a more optimised configuration. Another important factor is the MVDC system's compatibility with the integration of different energy sources, such as batteries, fuel cells and supercapacitors, which inherently provide direct current (DC) power. This approach simplifies the system compared to one based on alternating current, which would require additional conversions to integrate these energy sources. Furthermore, the choice of an MVDC system offers greater reliability and flexibility due to its modular configuration, with EEUs able to be integrated so that, in the event of failure of one part of the system, the other units continue to supply energy, thus improving the operational safety of the aircraft.

Chapter 4

Reference aircraft

The reference aircraft for the HERA project is the ATR 72, recognized as the most cost-effective regional aircraft, positioning it as the industry reference. It is a twin-engine Pratt & Whitney PW127 turboprop aircraft with a maximum capacity of 78 passengers [35]. The 'Flex Operation' concept enables two levels of power for the engine to obtain a better performance with higher payload, one for standard operations (PW127F) and the other (PW127M) for 'hot & high' operations.

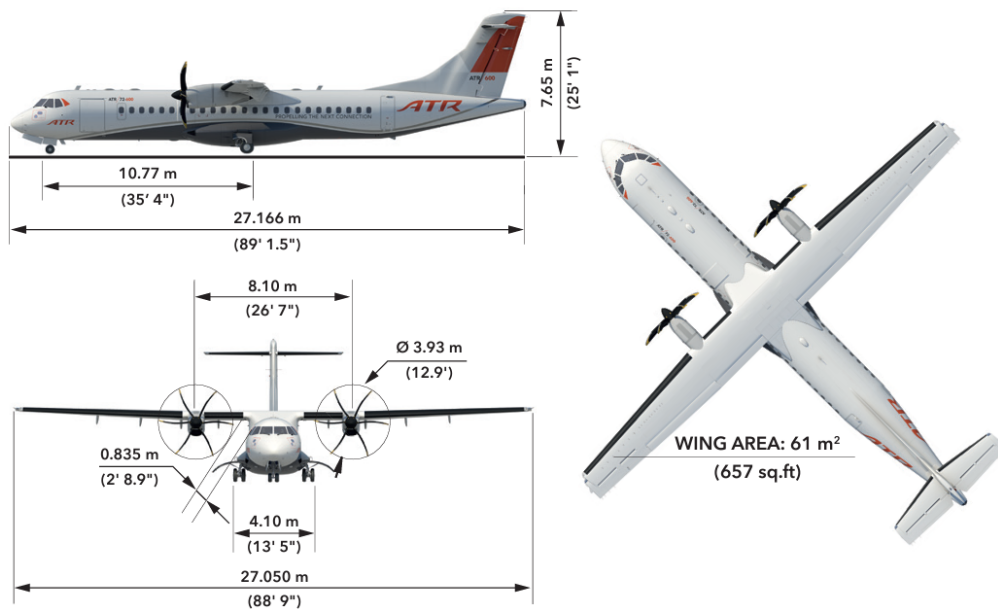


Figure 4.1: Aircraft dimensions

Engines Pratt & Whitney Canada	PW127M/N
Take-off power	2,475 SHP
Take-off power - One engine	2,750 SHP
Max continuous	2,500 SHP
Max climb	2,192 SHP
Max cruise	2,132 SHP

Figure 4.2: PW127 characteristics

The ability to have two different power levels allows an increase of climb gradient in hot and high conditions with an improve of MTOW of 500 kg. This allows it to maintain a one engine out net ceiling of 1,000 ft higher than other aircraft belonging to its category.

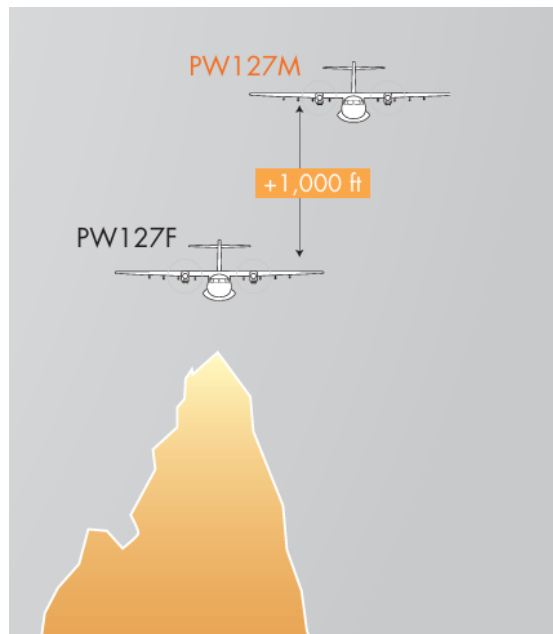


Figure 4.3: Climb gradient

Thanks to lighter structure, optimized speed and well suited engine for short sectors, the ATR 72 is more fuel efficient than any other regional aircraft, in fact it's considered as the most environmental friendly aircraft in its category (Fig.4.4) [35] [36].

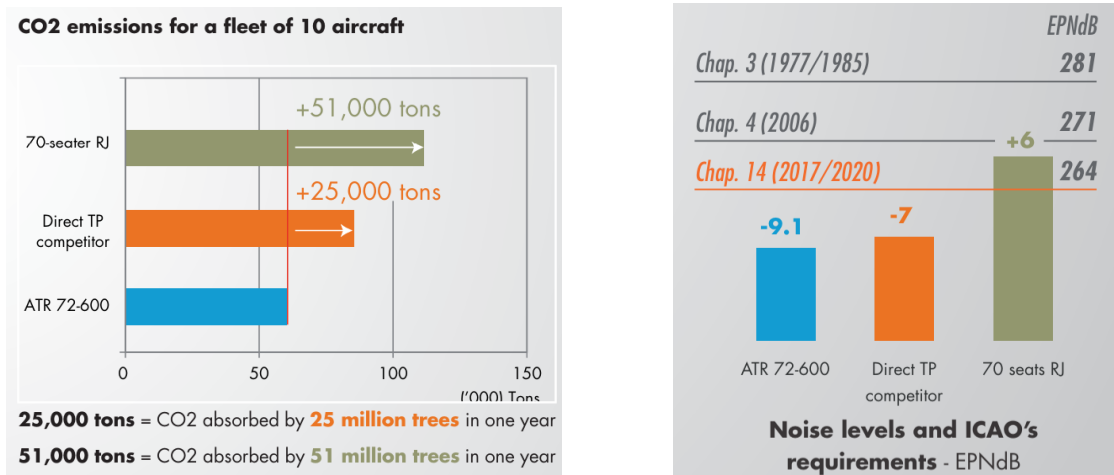


Figure 4.4: CO_2 emissions and noise levels

In Fig.4.5 the ATR72 is positioned in relation to other turboprops and regional jets of a similar size. As is demonstrated, the ATR 72 exhibits the most efficient fuel consumption, with a rate of less than 3 litres per passenger per 100 km. It is also the only aircraft in this category that adheres to the IATA's recommended practices. Furthermore, within the operating cost category, the ATR72 demonstrates a reduction in fuel bill, engine and airframe maintenance costs, and airport and navigation charges [36].

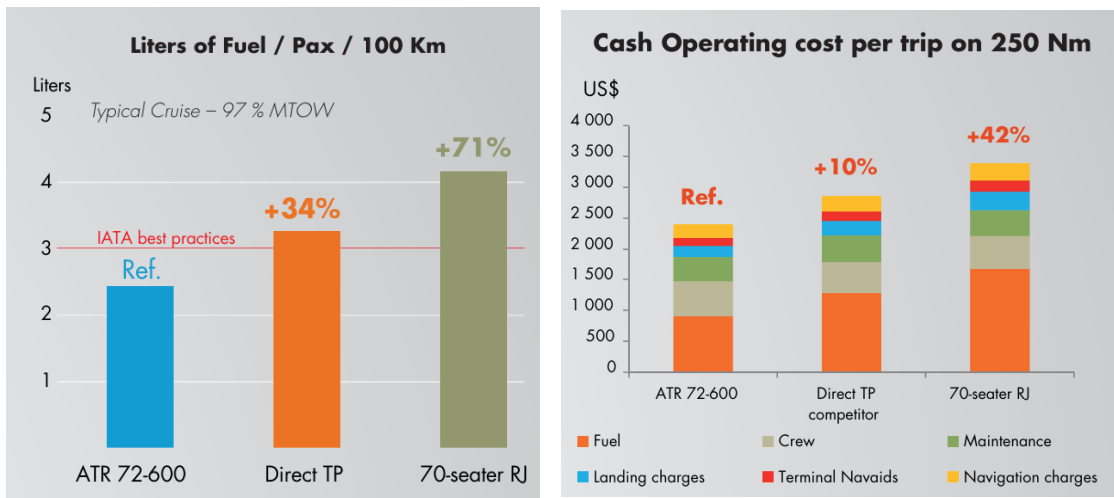


Figure 4.5: Liters of fuel per passengers per 100 Km and cash operating cost per trip on 250 Nm

4.1 ATR72 electrical system

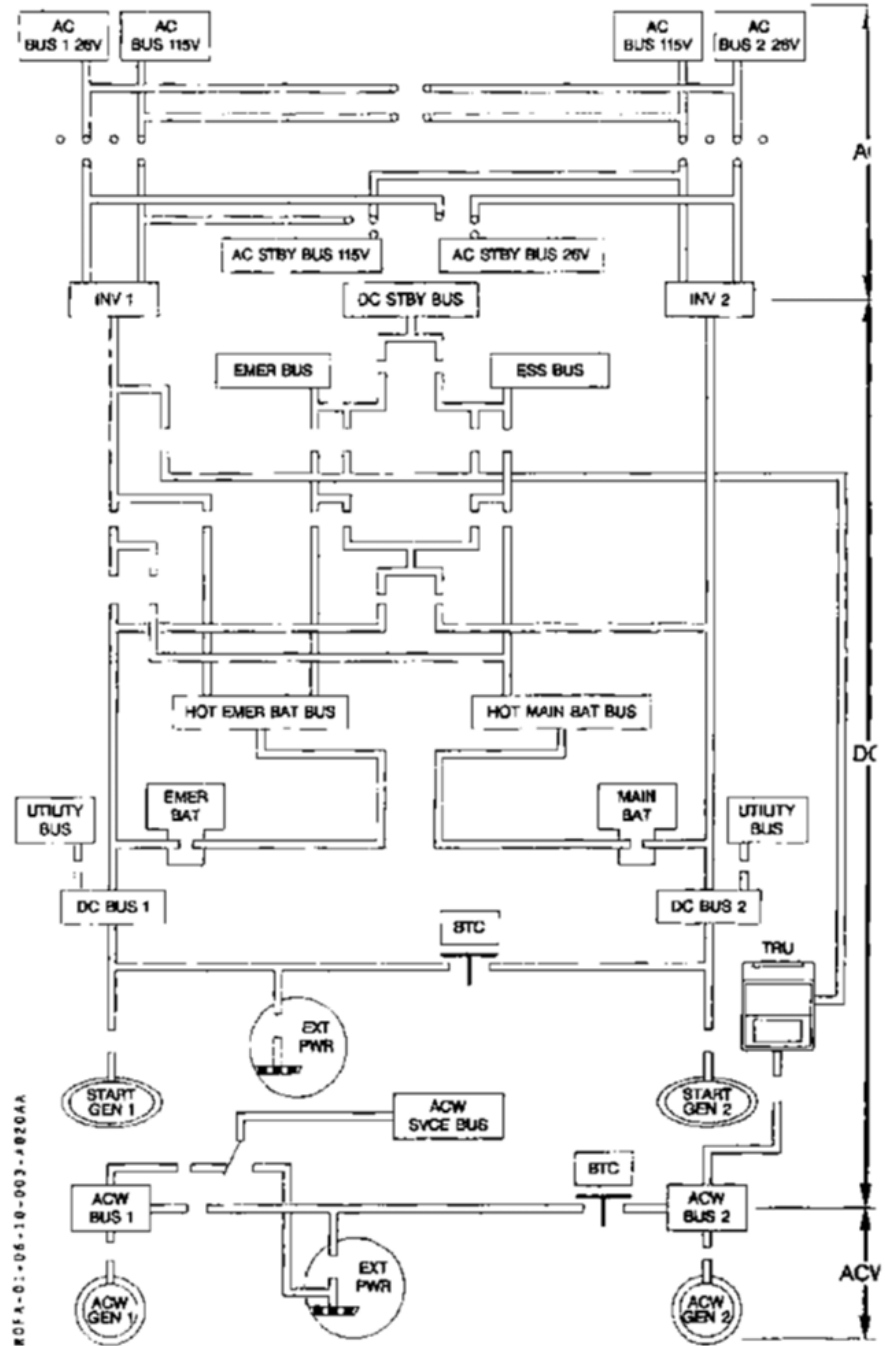


Figure 4.6: ATR72 electrical system [37]

The electrical system on the ATR72 consists of the following power generation devices:

- main and emergency batteries
- two engine driven starter-generators
- two AC variable frequency generators
- two external power units (DC and AC)

Two static inverters can convert DC power into AC power at constant frequency. On the other hand, through a Transformer Rectifier Unit (TRU) it's possible to obtain DC power from AC variable generators. The electrical system is divided into the left and right networks which they operate independently. Although, they can be connected together through bus tie contactors in the event of a failure. The logic of AC and DC systems is controlled by the Bus Power Control Unit (BPCU), one for each system. This unit controls the configuration of the electrical system by controlling various contactors.

4.1.1 DC power generation

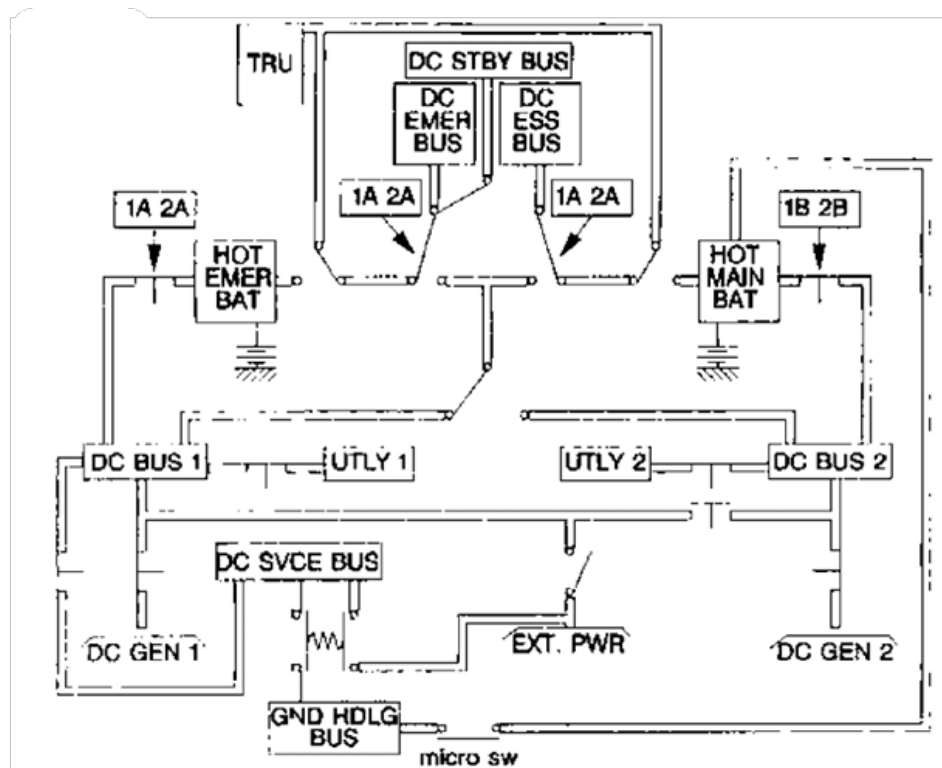


Figure 4.7: DC power system [37]

In normal condition the 28 V DC system is powered by two starter generators driven by the engine accessory gear boxes. When operating as a generator, they produce a nominal setting of 30 V (they each output a nominal 12 kW of power). In case of emergency power is provide by two batteries, main battery and emergency battery. If external power is available, and none of the engines are running, the starter generator is powered by DC external power through the external power contactor.

The DC distribution network is composed by eleven busses. The DC bus 1 and 2 are supplied respectively by the left and the right engine driven generator. When a generator is operating, the associated DC bus will be powered through the associated Generator Contactor. There's a bus tie contactor which connects one of the two bus with the opposite generator in case of engine failure. Each battery is connected to an associated Hot Battery Bus (HOT MAIN BAT BUS and HOT EMERGENCY BAT BUS), which are powered as long as the associated battery is charged. Under normal conditions, the hot battery buses are supplied by the DC buses, the emergency bus by DC bus 1 and the main bus by DC bus 2. In

case of main DC busses failure or thermal runaway of one of the two batteries, the associated hot bat bus is supplied by its respectively battery. In standard operating conditions, the DC Emergency bus and DC Standby bus are supplied from the HOT EMER BAT BUS. Meanwhile, the DC Essential Bus is supplied from the HOT MAIN BAT BUS. In the event of thermal runaway in one of the two batteries, the associated busses are transferred to DC bus 1 supply. Should DC bus 1 be non-operational, these busses are transferred to DC bus 2 supply by the main bus transfer contactor. If both DC generators are out of operation, DC EMER and ESS BUS can be supplied by the TRU which converts from AC to DC power. On the chance that the TRU does not work either these busses are supplied by their respective HOT BAT BUS. The function of the UTLY BUS 1 and 2 is to provide non-essential loads with power. The power supply to these buses is provided by the associated main DC BUS via contactors. The purpose of the contactors is to ensure that the utility bus can be automatically de-energized if the supply source becomes overloaded. In conclusion, the DC SRVC BUS is responsible for the provision of power during both flight and on the ground, while the GND HDLG BUS is de-energized during flight and provides DC power to loads when the aircraft is on the ground.

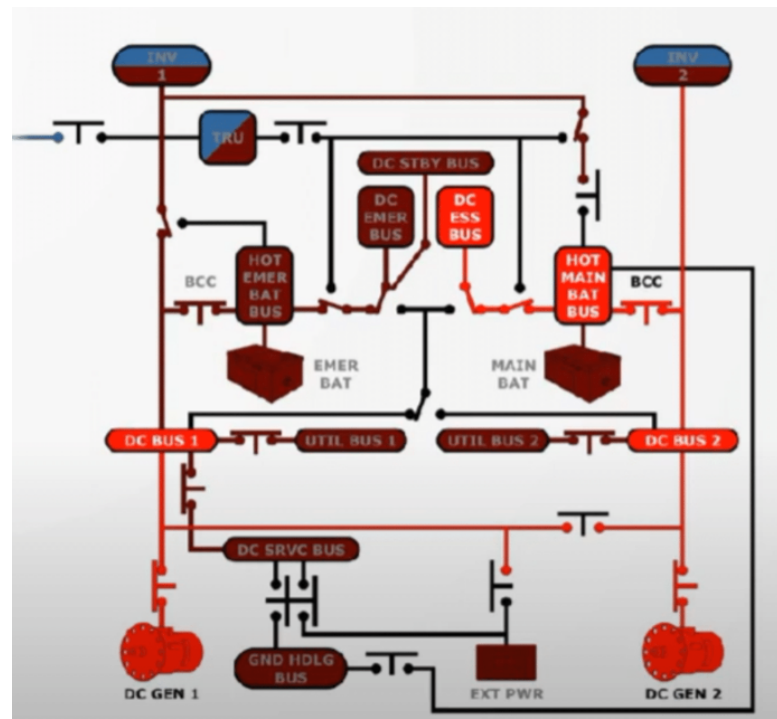


Figure 4.8: DC essential bus power - normal supply [38]

As previously referenced, the aircraft is equipped with two batteries, both of which are 24 V NiCd batteries. The main battery is rated at 43 AH and is typically utilized for the purpose of engine starting and as a source of emergency power. The emergency battery, with a rating of 15 AH, is designed to power the emergency electrical network in the event of a failure in the main battery. A secondary function of the emergency battery is to prevent power transients on critical equipment during engine starts.

4.1.2 AC power generation

AC constant frequency

AC constant frequency (400 Hz) is supplied by two single phase inverters, which are normally powered by the associated DC bus.

Power [VA]	Output voltage [V]	Frequency [Hz]
500	115±4 and 26±1	400±5

Table 4.1: Inverter design characteristics [37]

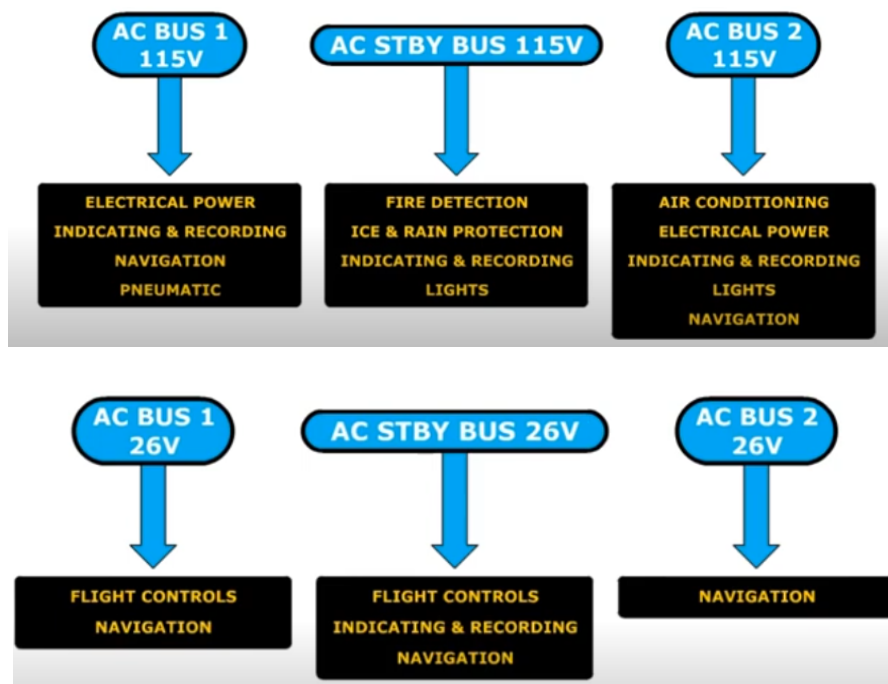


Figure 4.9: 115V and 26V distribution

In order for the inverters to operate satisfactorily, the required DC power supply must be in the range of 18 V to 31 V. The two AC buses are connected through an AC bus Tie Relay which will close automatically in the event one of the inverters fail or is not powered. The AC system consist of AC bus 1, AC bus 2 and AC standby bus.

The inverters are supplied by HOT MAIN BAT BUS or HOT EMER BAT BUS in case of DC buses loss, otherwise from the TRU if it is switched on.

The arrangement and operation of the 26 V AC system is the same as the 115 V AC system.

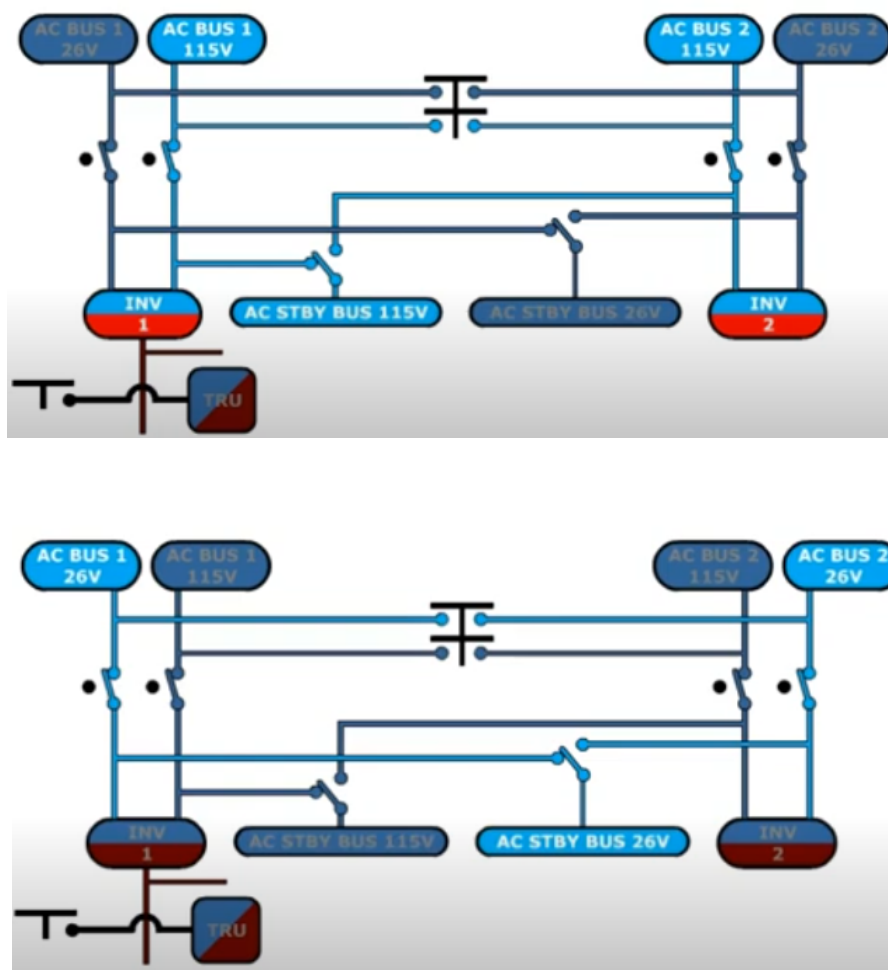


Figure 4.10: 115V and 26V network

AC wild frequency

The AC Wild system is powered by two propeller driven 3 phases generators and each generator is of the brushless, air cooled type. In this case, the frequency depends on the propeller speed.

Power [kVA]	Voltage [V]	Frequency [Hz]
20	115-200	341-488

Table 4.2: Generator characteristics

The implementation of fault protection and detection is accomplished by a GCU, which is responsible for the control of each wild generator. The GCU provides the following control and protection functions:

- overvoltage
- power and fault current limiting
- bus tie lock out
- undervoltage
- differential protection
- under frequency
- open phase
- overfrequency
- voltage regulation

The two main busses, ACW BUS 1 and ACW BUS 2, are typically supplied by the left and right generator, respectively, through a contactor. In the event of a generator failure, the associated bus will be powered by the opposing generator through the bus tie contactors. In the event of both engine generators failing, a TRU converts AC wild power into DC power, thereby supplying DC EMER BUS, DC ESS BUS, DC STBY BUS and inverter 1. Moreover, the ACW SVCE BUS is capable of supplying power during flight or when the aircraft is on the ground executing operations, with an external power source or from ACW BUS 1.

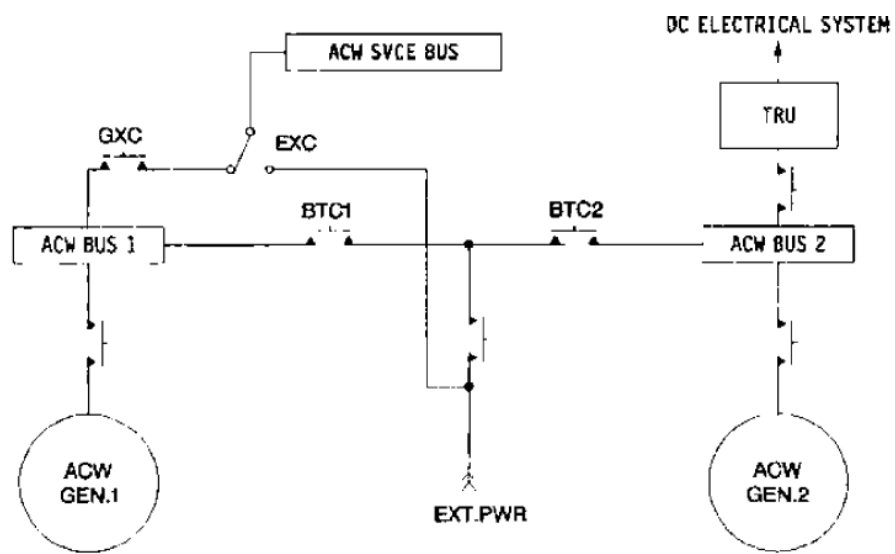


Figure 4.11: AC wild network [38]

Chapter 5

Dynamic modeling of EPS

In order to study the real behaviour of the system, a simplified and abstract representation of the system is used: the system *model*. There are various types of models:

- physical: it's a scaled representation of the system, used to experimentally analyze the system's characteristics;
- mathematical: it's a set of equations representing the behaviour of the system and which satisfying appropriate boundary conditions representing the conditions of the environment in which the system operates.

The implementation of the model is realised through the use of simulations, whereby a model is run to analyse how a system behaves over time or in specific conditions. This approach enables the observation of system evolution without the necessity for physical interaction. In the context of computerised models, the term simulation refers to the process of identifying the solution to a given mathematical model under specific conditions and subsequently visualising it [30].

The present study employs a dynamic analysis, which can be defined as a mathematical and computational approach utilised to describe the behaviour of a system that evolves over time. The purpose of this approach is to analyse how system variables change in response to internal or external factors.

5.1 Modelling levels

The SAE AIR 6326 proposes a standardized approach to modeling and simulation of EPS aircraft introducing a 4-levels paradigm [39]:

- The architecture level represents the lowest level of detail and complexity. It is the most abstract level, with a focus on the overall design and the

functional integrity of the EPS architecture. This level allows for the study of stationary power flows, control logics and simulations of events such as fault and bus reconfiguration. Utilising Boolean logic or simplified equations, this level is characterised by its computational efficiency. This level facilitates the estimation of the dimensions of various components of the electrical system, including generators, in accordance with flight scenarios;

- functional level studies the transient behavior of components and systems at low frequencies, down to about 100-150 Hz which correspond one third of base grid frequency for a typical EPS aircraft. The main focus of this level includes studies on system stability, low frequency power quality, energy and load management. This level of modelling can be used to analyse the dynamic behaviour from generator to load in a complete system;
- behavioral level models components and systems that have a frequency in the kHz range. These models generate signals that are representative of real hardware waveforms, thus rendering them suitable for harmonic analysis studies, active/passive filtering and electromagnetic compatibility (EMC) phenomena. This level is the most detailed used in EPS-level studies;
- component level is the most detailed and complex level, with a focus on the physical characteristics of the individual components. Modelling at this level enables analysis of electromagnetic, thermal and mechanical behaviour. This level is characterised by its complexity and significant computational demands, necessitating the use of short time steps.

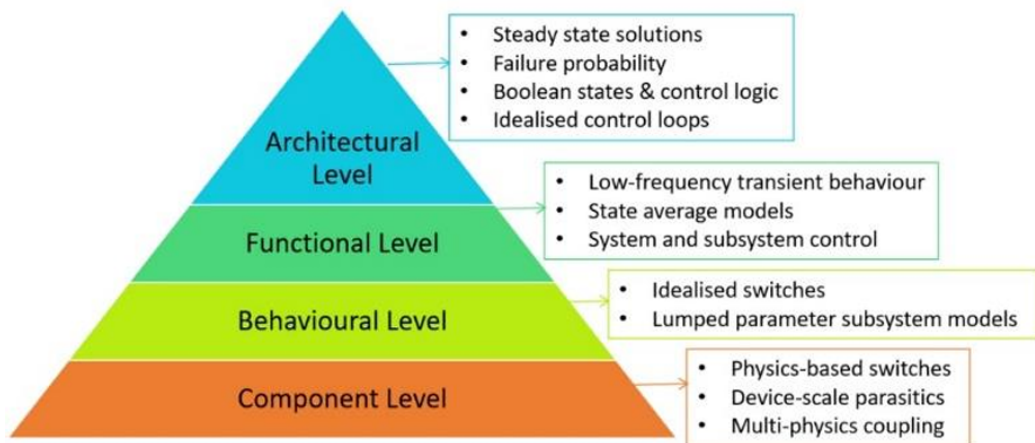


Figure 5.1: SAE AIR 6326 modelling levels [39]

5.2 Modelling software: AMESim Simcenter

For modelling and simulation within this thesis, the Simcenter Amesim system simulation platform was used, which enables the modelling of multidisciplinary systems through a predefined and customisable physical component approach. It incorporates a range of tools designed to model, analyse and studies the dynamic interactions between mechanical, electrical, hydraulic, thermal and aerodynamic subsystems. Simcenter Amesim can be combined with leading CAE, CAD and control software, as well as other Simcenter and Teamcenter solutions.



Figure 5.2: AMESim libraries [40]

In the field of engineering, AMESim refers to the set of equations that delineate the dynamic behaviour of the engineering system. The implementation of these equations is then expressed in the form of computer code, thereby constituting a model of the system. The model comprises the equations and the corresponding code for each component of the system, which are referred to as submodels [40].

For the porpouse of this study particular reference was made to Aircraft electrics library which provides various models for the electrical system based on the multi-level modeling as reported in Paragraph 5.1 [41].

5.3 AC generation modelling on AMESim

5.3.1 General aircraft AC generation

The initial step in this project was to initiate a demonstration that represented a generic AC generation scheme on board a commercial aircraft.

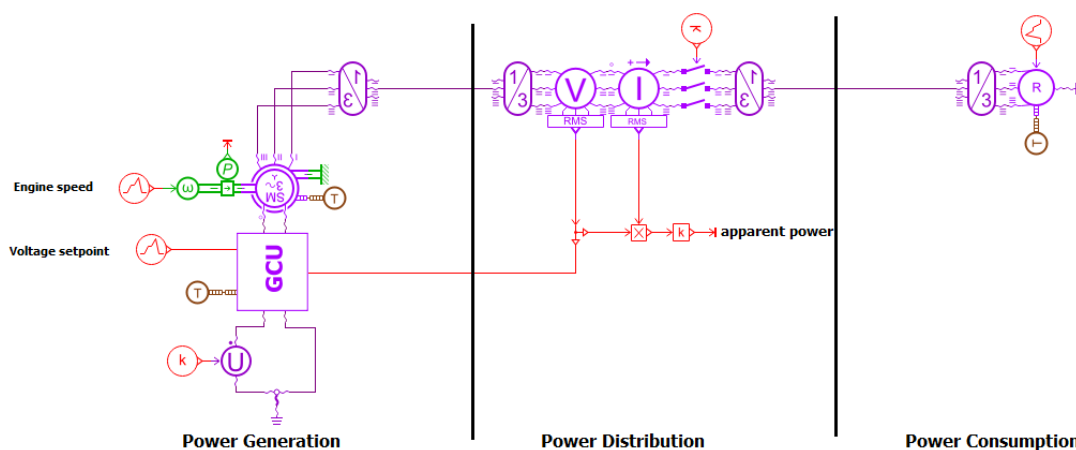


Figure 5.3: Simcenter Amesim model of an Aircraft AC Generation

The purpose of this example is to demonstrate the utilisation of the software for conducting an electrical/mechanical transient stability study on AC power generation systems. A significant aspect of the design of power generation on board aircraft is the restoration of a power system that has been subjected to disturbances. The system must be designed and operated in such a way that a certain number of credible contingencies (e.g. sudden changes in load or generator speed) do not cause mechanical parts to fail or compromise the continuity of sufficient power supply to the loads.

The model presented in Figure 5.3 to assess such analysis is a functional level variable frequency synchronous generator, which is connected to a resistive load through a generator line contactor and a busbar. The AC generator is modelling by using the component EMDWRSM01 on Amesim which represents a wound rotor synchronous machine driven directly by engine speed. A Generator Control Unit (GCU) is used to control the RMS voltage on the network by applying to the generator the voltage needed to fulfill the power demand from the consumers.

The generation of power is measured in terms of voltage and current RMS. The apparent power, which incorporates both active and reactive power, is calculated using these measures.

The distributed power is provide to a resistive load, which represents the devices that use the electrical energy generated, such as avionics systems and other on-board

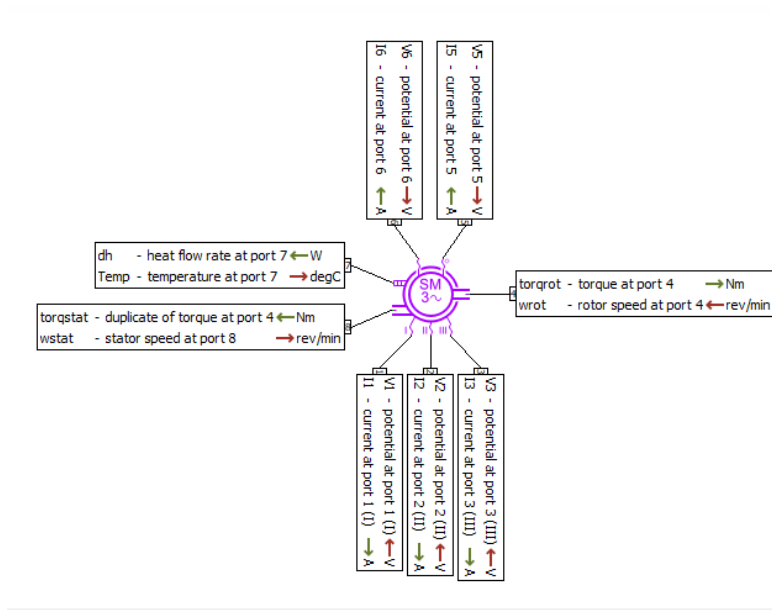


Figure 5.4: EMDWRSM01 - Wound Rotor Synchronous Machine (WRSM)

consumers.

To introduce electrical and mechanical disturbances, both the motor speed and the resistance value were varied, in the following way:

time [s]	engine speed [Rev/min]	time [s]	resistance [Ohm]
0-5	12000	0-1	1
5-end	8000	1-2	1.25
		2-3	0.75
		3-end	1

Table 5.1: Mechanical and electrical disturbances

The engine rotates the generator at 12000 RPM for 5 s and then, at $t = 5$ s the speed decreases suddenly to 8000 RPM, to remain there until the end of the simulation. The resistance at its turn varies like this: 1 Ohm from 0 to 1 s, 1.2 Ohm from 1 to 2 s, 0.75 Ohm from 2 s to 3 s and it returns to 1 Ohm until the end of the simulation (10 s). Based on these disturbances, the GCU task is to maintain the voltage at 115 VAC. The aim of the simulation is to check after each disturbance, whether, first of all, the controller is sufficiently reactive to bring the network voltage back to 115 VAC, and secondly to monitor the electrical data (current, voltage) and mechanical data (shaft torque). The values proposed in the Amesim demo were retained for this model.

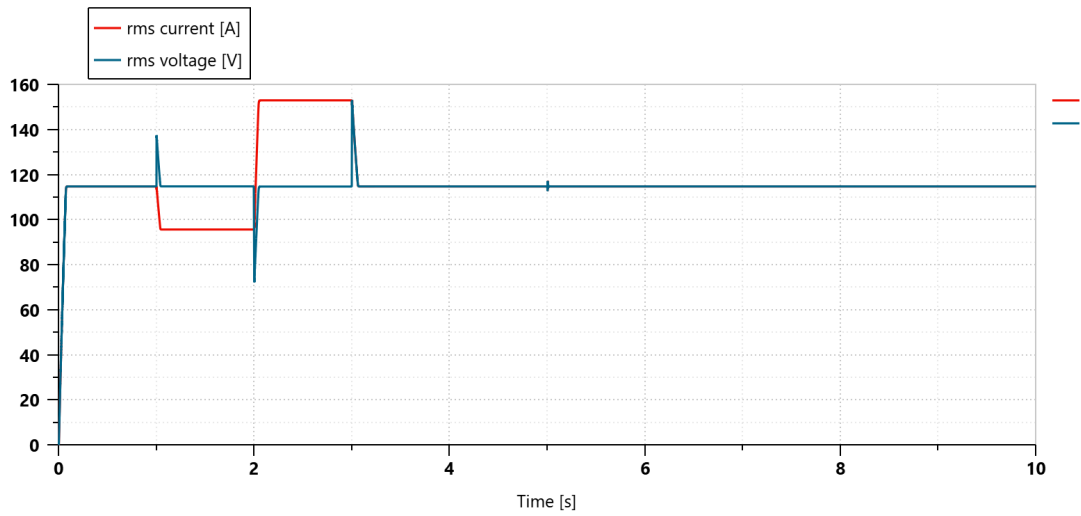


Figure 5.5: Eletrical outputs

In Figure 5.5 the voltage and current trends are reported. It is evident that fluctuations in resistance can result in corresponding variations in voltage, with an increase in resistance leading to an increase in voltage and a decrease in resistance resulting in a decrease in voltage. Once the transient is over, the controller reports the voltage to its nominal value.

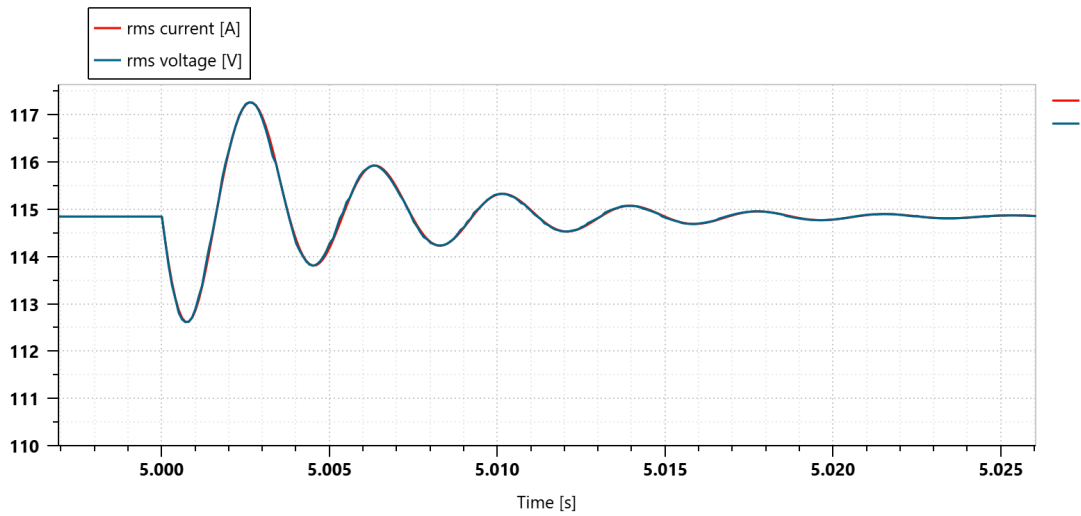


Figure 5.6: Eletrical transient on network

After 5 seconds the RPM decreases and oscillations occur on the voltage and the current (Fig.5.6). The system is seeking a new equilibrium as a result of the change in engine speed, and the oscillations represent its transition to stability.

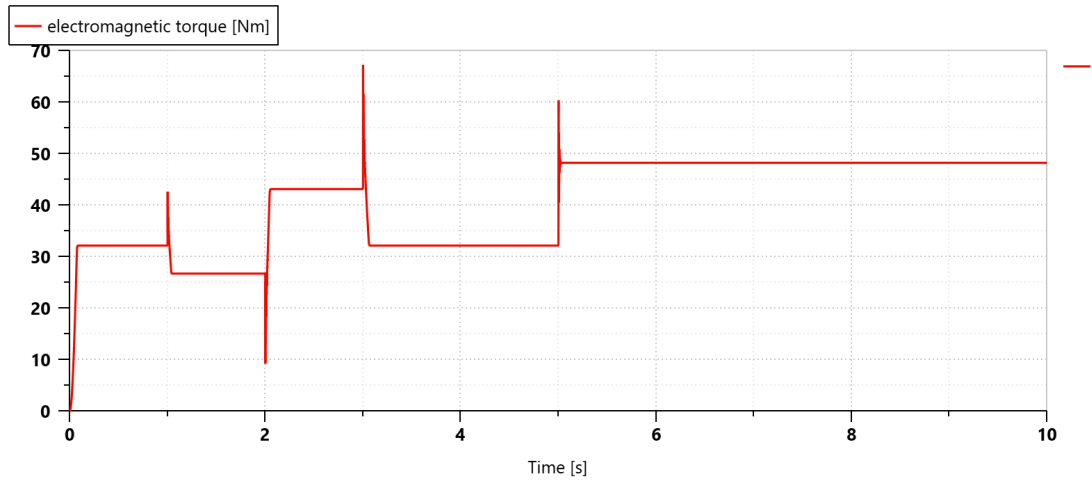


Figure 5.7: Eletromagnetic torque

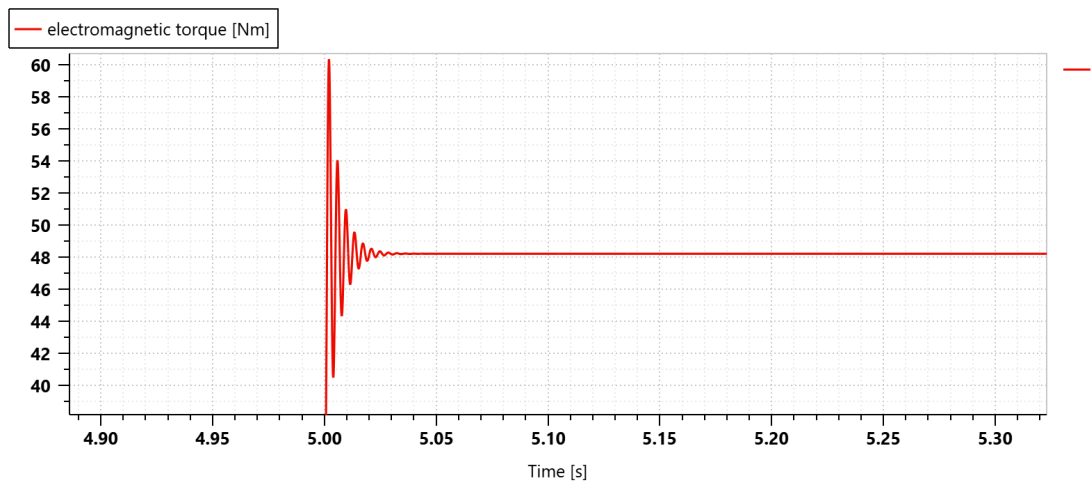


Figure 5.8: Torque transients

On the mechanical side, it's possible to observe that they're torque peaks due to load variations: the large the power demand, the larger will be the torque peak. In Figure 5.8 is reported a zoom on the torque transient in the instant when the RPM change. These mechanical transient oscillations can be responsible of vibration and cogging on the rotor shaft. The latter has to be able to absorb and damp the oscillations otherwise these can be reduce machine efficiency or lead to mechanical damage of the generator shaft.

Another purpose of this type of study is to check that the voltage fluctuations,

after the disturbances have been applied, are within the limits set by the design norms and cleared out in a reasonable time. In this case, three different simulations were carried out by increasing the resistive load by 25% (set 2) and 50% (set 3) to analyse the generator voltage trend.

time [s]	R (set 1) [Ohm]	R (set 2) [Ohm]	R (set 3) [Ohm]
0-1	1	0.75	0.5
1-2	1.25	0.9	0.6
2-3	0.75	0.5625	0.375
3-4	1	0.75	0.5

Table 5.2: Resistance profile for set 1, set 2 and set 3

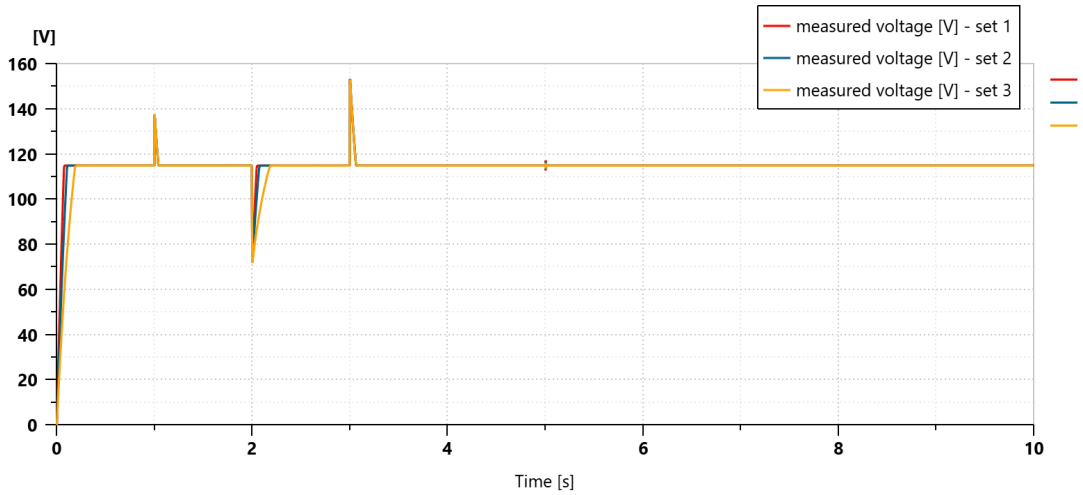


Figure 5.9: Voltage outputs

As the resistance decreases, it's notable that the voltage reaches the nominal value in a longer time than at higher resistance values. This happens because a lower resistance implies a greater current draw, which causes a greater internal voltage drop. It therefore happens that the GCU has to correct a larger error, causing the voltage to reach the nominal value in a longer time than when the load has a higher resistive value. It is also important to note that as the resistive load increases, the peak value of the voltage that is reached when there is a change in load also increases. As these values must comply with the limits imposed by the regulations, their monitoring is crucial. In this instance, the standard that is taken into consideration is MIL-STD-704 F.

MIL-STD-704F is a US military standard that defines requirements for power

supply characteristics in aircraft systems. Its main purpose is to ensure compatibility between power sources (such as generators and batteries) and electrical loads (such as avionics and on-board systems).

Taking into account the voltage variation limits imposed by the standard (Fig. 5.11), the only non-conformity occurs in the case of the load variation at $t=2s$. As shown in Table 5.3, at this instant the voltage variation assumes a value that for all 3 sets under consideration is outside the admissible range, since the minimum voltage peaks imposed by the standard is 80 V. On the other hand, with regard to the limits imposed on the time interval in which the transient must be exhausted, for each load variation the times comply with what the standard requires.

time [s]	V set 1 [V]	V set 2 [V]	V set 3 [V]
2	72.4301	72.2945	72.1654

Table 5.3: Voltage values at $t = 2s$

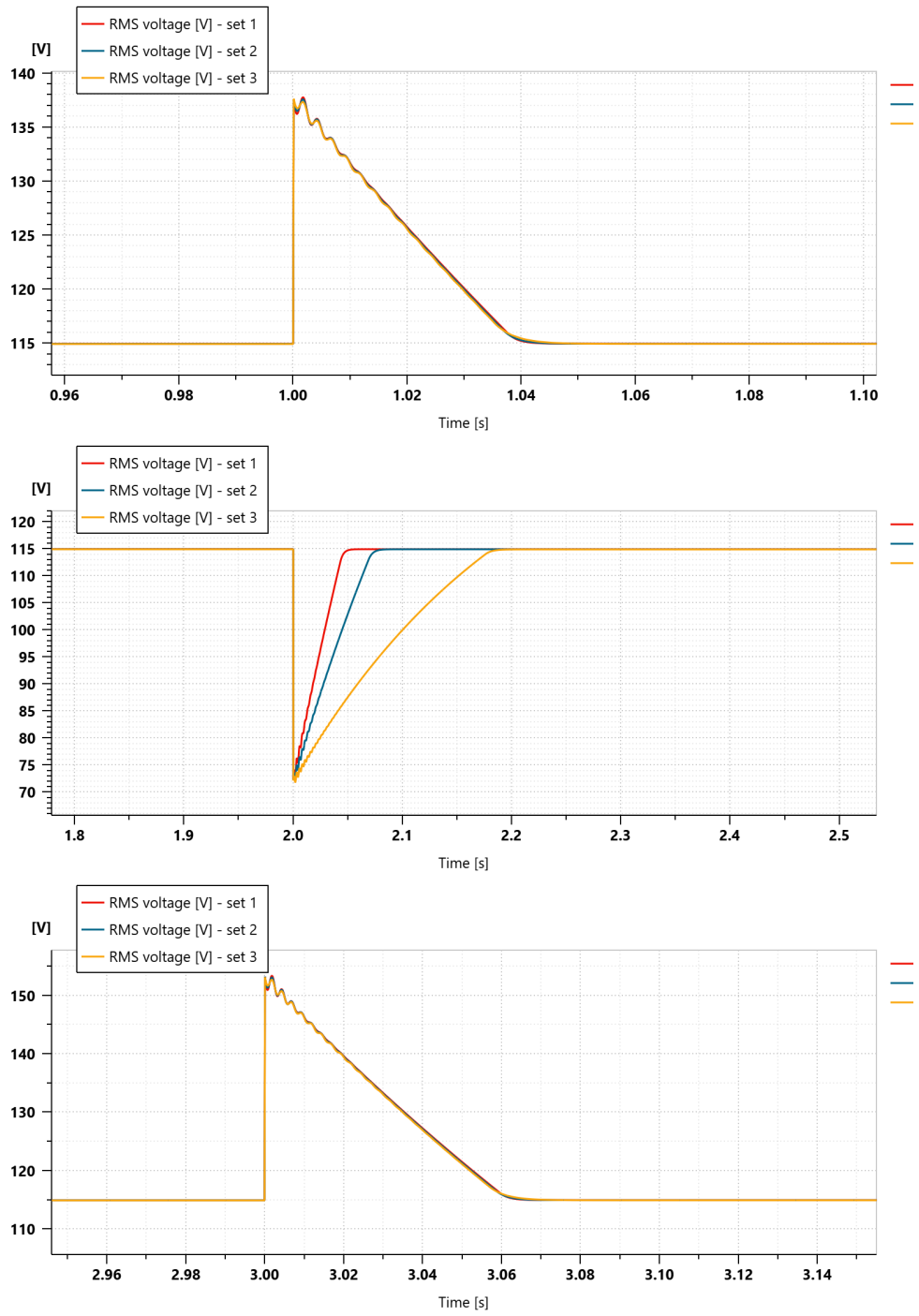


Figure 5.10: Voltage transients

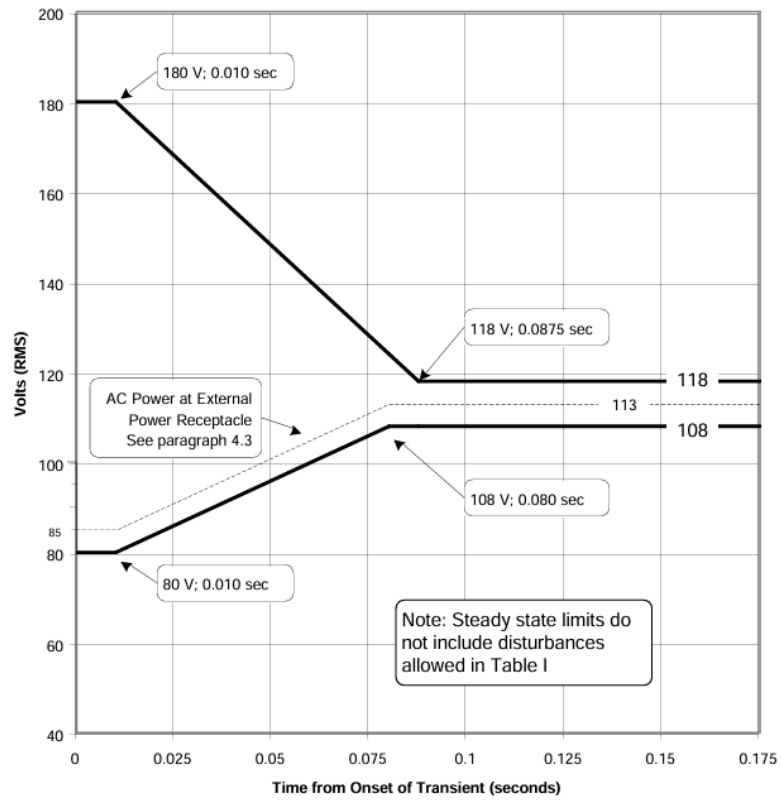


Figure 5.11: Envelope of normal 400 Hz and variable frequency AC voltage transient [42]

5.3.2 AC generation

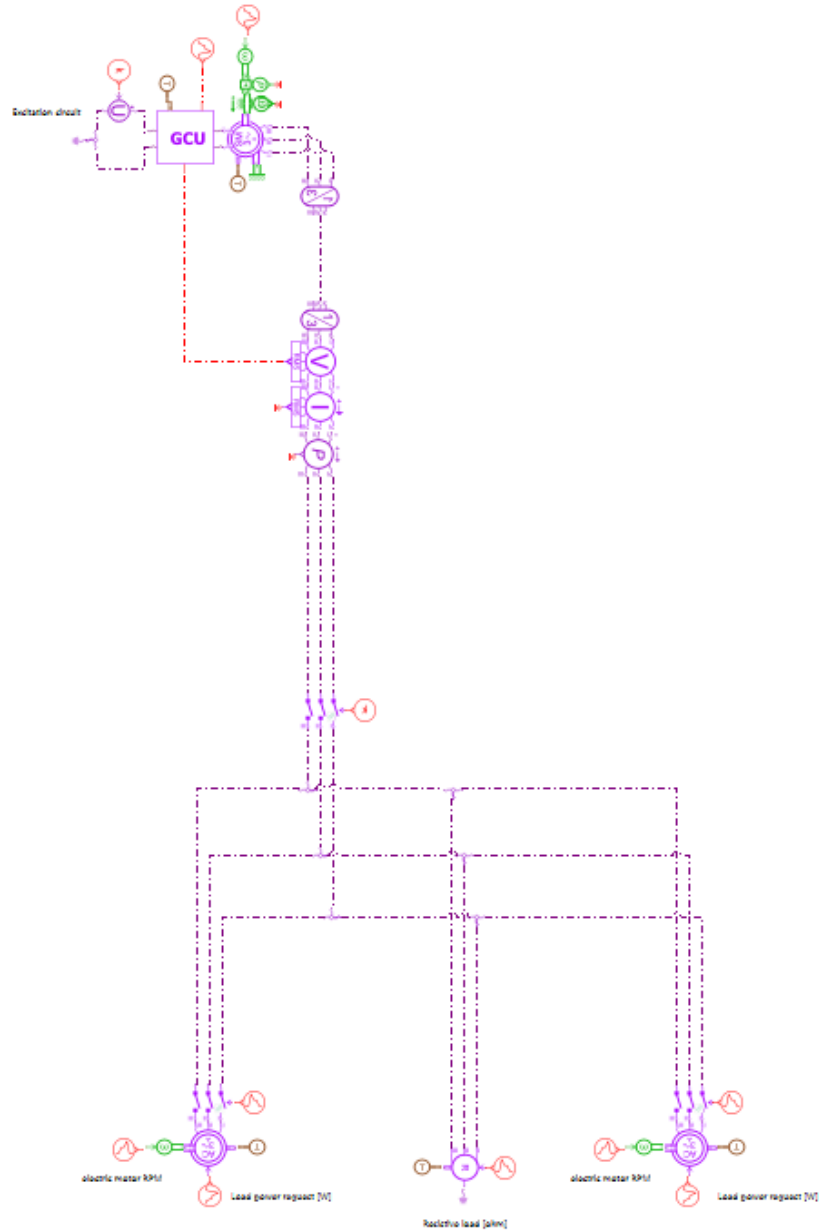


Figure 5.12: AC modelling

The next step was to construct an AC generator, starting from the diagram seen in Section 5.3.1, and considering the loads of the ATR 72.

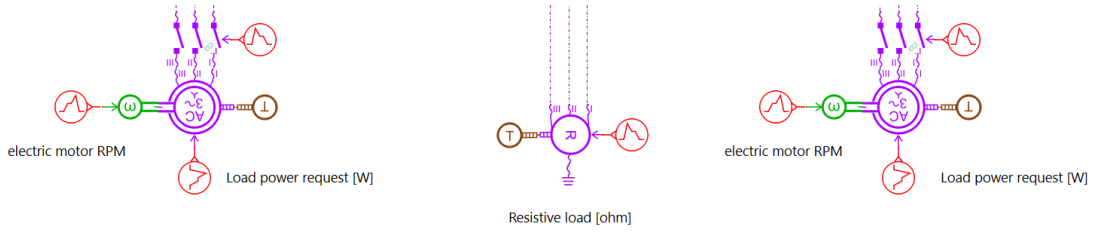


Figure 5.13: Loads modelling

The loads are placed in parallel and a distinction was made between inductive and resistive loads. The resistive loads were modelled using the ACERLOAD10 element on Amesim, which is a balanced, wye-connected resistive load. This 3-phase load can be used to represent a resistive load from current, power or resistance profile. In this case the input is a resistance profile.

On the other side, the inductive loads are modelling by an electric motor configured in a way to receive in input the load power request. The motor modelling is realized by using the submodel ACERMSMOT00 on Amesim that is a three-phase induction motor.

As far as AC generation is concerned, under cruise conditions, the loads require a power of 15.2 kW, 1/4 of which are inductive loads, the remainder resistive loads. These values refer to both AC generators, whereas in the model there is only one generator, so the inputs have been halved.

	load power request [kW]
<i>inductive</i>	3.8
<i>resistive</i>	11.4
<i>total</i>	15.2

Table 5.4: AC Loads

For resistive loads, the resistance was given as input, calculated through the law of electrical power $P = V^2/R$, knowing that the voltage is 115 V.

As for the motor parameters, a speed of 1200 RPM was entered. This derives from the fact that the AC alternator is installed on the propeller reduction gearbox, which turns at approximately 900-1200 RPM. The reduction gearbox is connected to the low pressure shaft which turns the propeller at a constant speed. These considerations are done taking into account that the reference aircraft is the ATR 72.

stage	duration of stage [s]	power [W]
1	0-0.2	0
2	0.2-0.8	1200
3	0.8-end	0

Table 5.5: First inductive load inputs

stage	duration of stage [s]	resistance [Ohm]
1	0-0.5	2.32
2	0.5-end	2.668

Table 5.6: Resistive load inputs

stage	duration of stage [s]	power [W]
1	0-0.2	0
2	0.2-end	700

Table 5.7: Second inductive load inputs

Results

As part of this simulation, the electrical output parameters of the generator were analyzed, the trends of which are shown below. The opening of the counters was set after 0.2 s to allow the generator and GCU to fully enter the desired operating regime. The simulation time is 1 second.

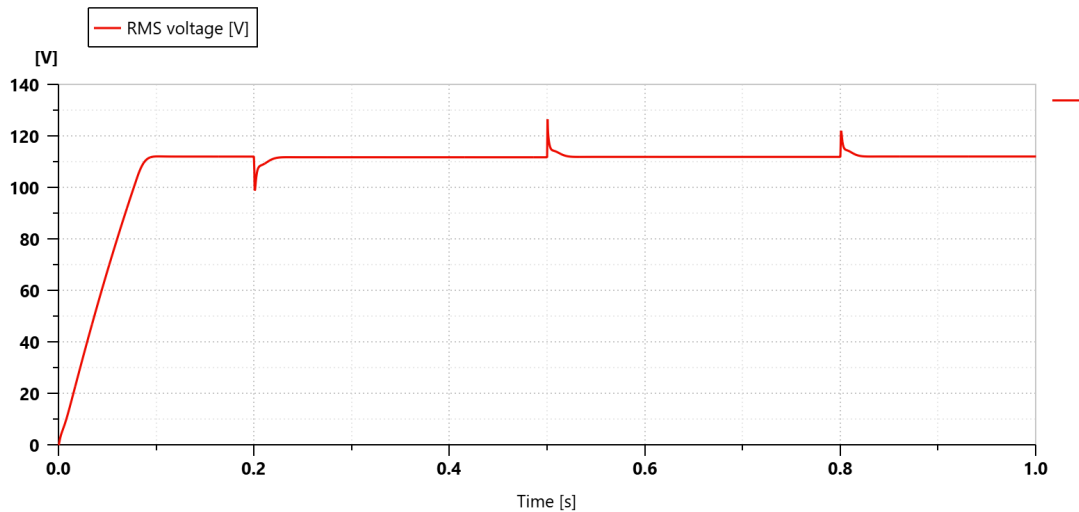


Figure 5.14: Voltage trend

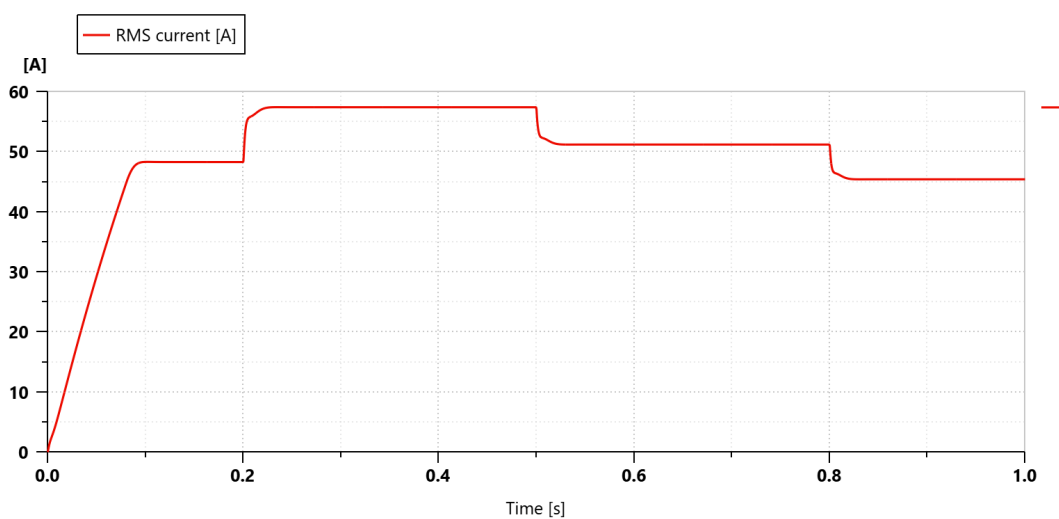


Figure 5.15: Current trend

- In the time interval between 0 and 0.2 seconds, the generator supplies the resistive load alone. Consequently, the current increases gradually until it reaches a stable value, the level of which is determined by the generator voltage and the load resistance;
- at time $t = 0.2s$, the two inductive loads are added, which in addition to absorbing active power introduce a reactive component that leads to an increase in current, as visible in Figure 5.15;
- after 0.5 seconds from the start of the simulation, the resistive load decreases, which causes the current drawn by the load to decrease. However, the effect is not very pronounced, as there are still the two inductive loads that continue to draw current;
- at $t = 0.8s$ one of the two inductive loads is switched off, causing a further current reduction.

The behaviour of the voltage follows the changes in the current, so when inductive loads are added and the current increases, the voltage undergoes a slight decrease due to the drop in the generator's internal voltage. Conversely, when the current decreases, the voltage tends to increase. In both cases, the voltage undergoes a short transient and then stabilises at the nominal value due to the action of the controller.

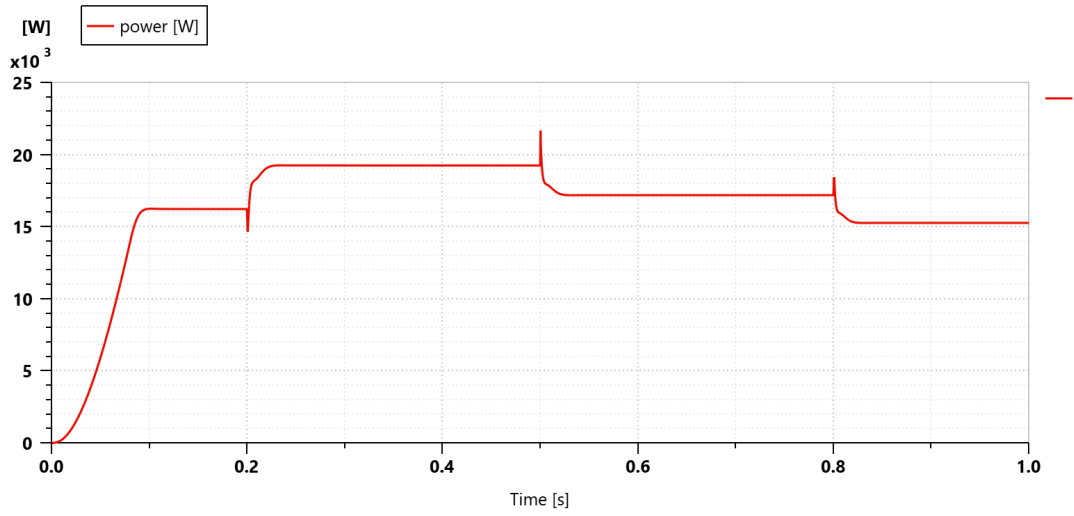


Figure 5.16: Power trend

As far as the generator power consumption trend is concerned, initially the resistive load absorbs active power, then the power increases until it stabilises. When inductive loads are connected, a small decrease in power is observed at the instant $t=0.2$ seconds, followed by a rapid increase. This is due to the fact that the inductive loads absorb both reactive (Q) and active (P) power. The former is the power associated with the phenomena of energy storage and release, while the latter is the power actually used to perform useful work. From the equation 5.2, one can see the relationship between the two powers that gives rise to the expression of apparent power, i.e. the total power transmitted from the generator to the load.

$$P = V_{\text{rms}} I_{\text{rms}} \cos \phi \quad (5.1)$$

$$S = \sqrt{P^2 + Q^2} = V_{\text{rms}} I_{\text{rms}} \quad (5.2)$$

The apparent power (S) increases as I connect inductive loads, but the active power does not increase proportionally as the loads reduce the power factor ($\cos \phi$). Therefore, it is observed that when a load varies, the power initially experiences a transient due to the voltage and then stabilises at higher or lower values, depending on the increase or decrease in current.

Once more, the voltage transients were evaluated in order to verify that they complied with MIL-STD-704 F.

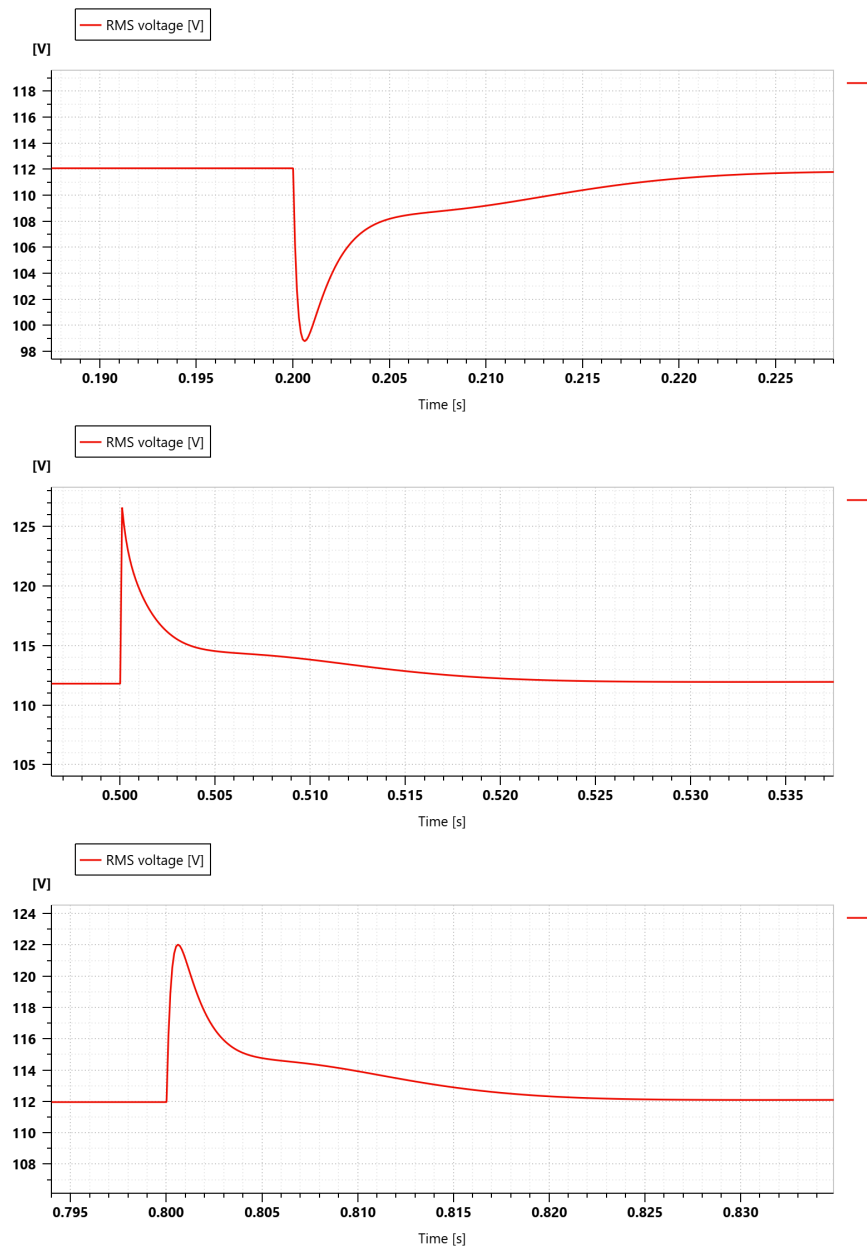


Figure 5.17: Voltage transients

The analysis of the transients shown in Figure 5.17 reveals that the peak values obtained are within the limits set by the standard for all three cases considered. As far as the transient exhaustion times are concerned, an exhaustion time of less than 0.025 seconds is observed in the three cases examined, thus being perfectly in line with the requirements of the standard.

5.4 DC generation modelling on AMESim

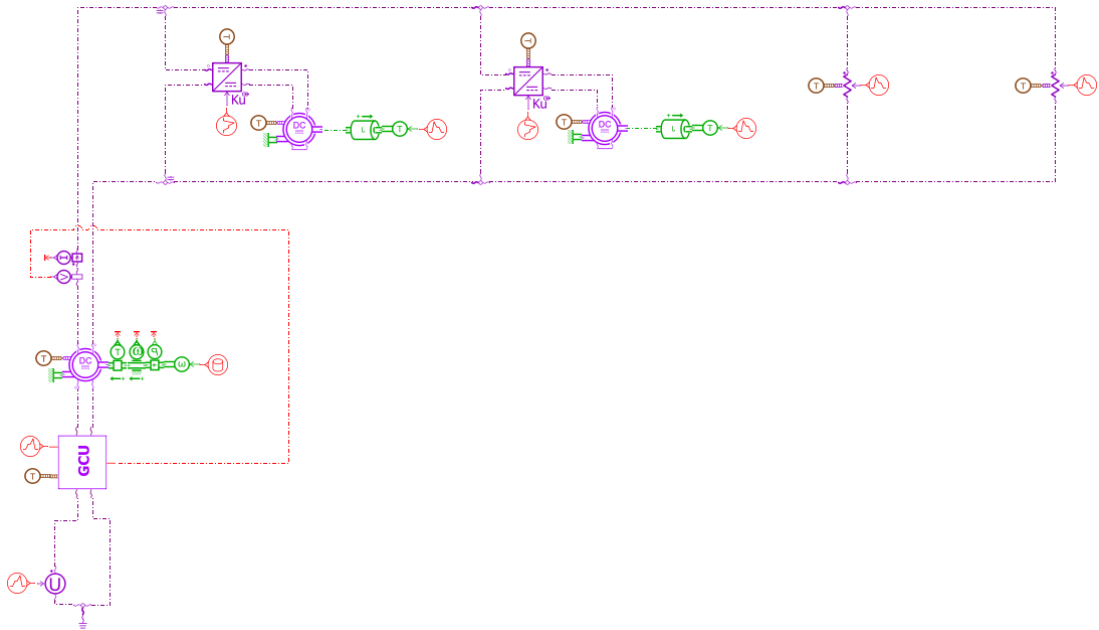


Figure 5.18: DC generation

Following the modeling of the AC loads, the focus shifted to the DC part. The motor was modelling using the element EMDSEDC01 in Amesim which is a separately excited DC machine. The machine is reversible, it can work as a motor or as a generator. Using the motor convention, the rotor relative speed can be measured with W as an output speed at the mechanical port and the electromagnetic torque can be measured with T as an output torque at the mechanical port. When W and T are of same sign, the machine is working as a motor and the output mechanical power P is positive. When W and T are of opposite sign, the machine is working as a generator and the output mechanical power P is negative.

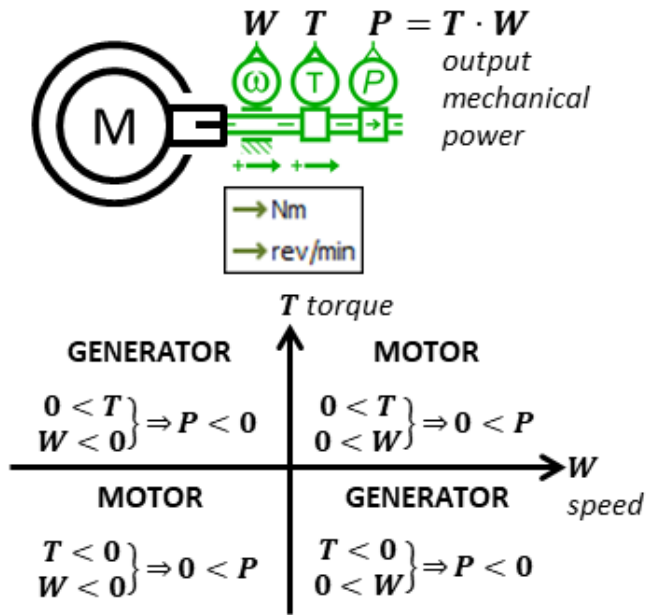


Figure 5.19: DC motor

For the DC generator, a speed of 8000 RPM was given as input, taking into account that on each motor has a starter generator, installed on the accessory gearbox, driven by the high pressure shaft. Furthermore, a dynamic lock was included as an input to the generator motor to prevent a start at rated speed without a gradual transient, which has been identified as a potential cause of excessive overvoltages when the generator is activated. The nominal RPMs are reached after three seconds after the generator is activated. The dynamic lock is modelled by SIGUDA01 element on Amesim, which reads a 1D or XY table and interpolates data as functions of time $u(t)$. The interpolation can be linear, cubic or constant. The utilisation of this submodel allows for the construction of a time-dependent signal $u(t)$.

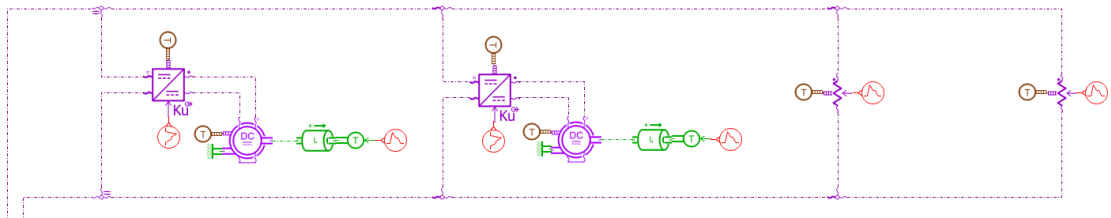


Figure 5.20: DC loads modelling

In this case the resistive loads were modelling using the EBRVT01 element in Amesim which is a variable electrical resistance, while the inductive loads are modelling by a DC electric motor configured in a way to receive in input a certain torque. The latter is calculated from the knowledge of the power developed by the inductive loads and the rotational speed of the motor, through the following relationship:

$$P = T \cdot \omega \quad (5.3)$$

The ESCSDCDCU11 element which is a functional model of DC/DC converter was inserted before the motor. This is used as a switch: the electric motor is activated as a utility only when it actually starts running so as to avoid interactions between the electric motor and generator. For electric motors of inductive loads, they are assumed to run at 1500 RPM, da cui è possibile ricavare la coppia totale generata dai carichi, tenendo conto che la potenza totale generata dai carichi induttivi (per un solo generatore) è pari a 1.05 KW:

$$T = \frac{P}{\omega} = 6.685 N \cdot m \quad (5.4)$$

La seguente coppia è stata suddivisa su due carichi induttivi.

	load power request [kW]
<i>inductive</i>	2.1
<i>resistive</i>	6.3
<i>total</i>	8.4

Table 5.8: DC Loads

As for the AC resistive loads, the resistance was given as input, calculated through the Ohm's law, knowing that the voltage is 28 V. In this case il carico resistivo è stato suddiviso su due resistenze poste in parallelo. Dunque si è calcolata la resistenza equivalente, attraverso cui si è determinato il valore delle due resistenze, secondo la seguente relazione (considering $R_1=R_2$):

$$\frac{1}{R_{eq}} = \frac{1}{R_1} + \frac{1}{R_2} \quad (5.5)$$

stage	duration of stage [s]	torque [$N \cdot m$]
1	0-4	0
2	4-end	3.3425

Table 5.9: First induction load inputs

stage	duration of stage [s]	torque [$N \cdot m$]
1	0-5	0
2	5-8	3.3425
3	8-end	0

Table 5.10: Second inductive load inputs

stage	duration of stage [s]	resistance [Ohm]
1	0-6	0.498
2	6-end	0.552

Table 5.11: First resistive load inputs

stage	duration of stage [s]	resistance [Ohm]
1	0-end	0.498

Table 5.12: Second resistive load inputs

Results

As for the AC simulation, the electrical output parameters of the generator were analyzed. The simulation time is 10 second.

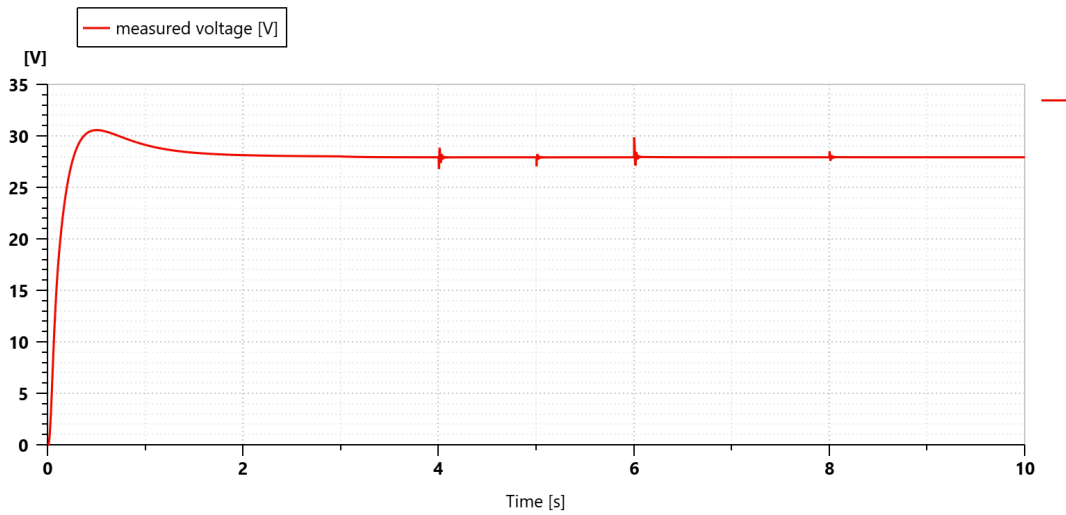


Figure 5.21: DC voltage trend

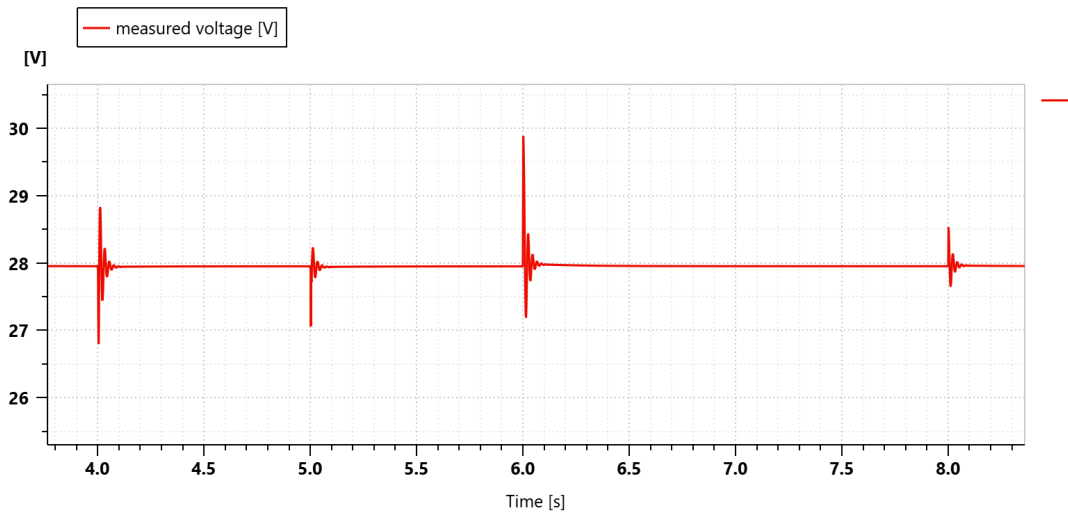


Figure 5.22: DC voltage peaks

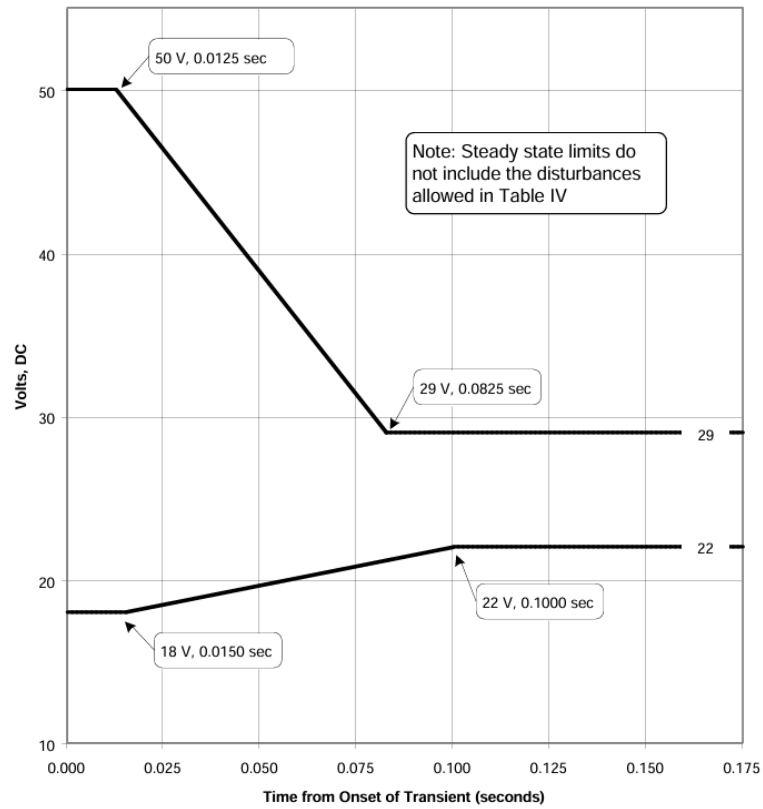


Figure 5.23: Envelope of normal voltage transients for 28 volts DC system [42]

As can be seen from the graphs, there are fluctuations in the voltage at the time when the loads change. At $t=4$ s and $t=5$ s, the voltage drops when the first and second inductive loads are connected, causing an instantaneous drop in the voltage, which is then restored to the nominal value by the GCU. For $t=6$ s and $t=8$ s, on the other hand, the voltage increases because in the first case the resistive load is reduced by 15%, thus increasing the resistance value, while in the second case the inductive load is disconnected. It should also be checked that the peaks are within the values required by the standard for a voltage of 28 VDC. As can be seen from the Figure 5.22, the transient peaks are exhausted in 0.1 seconds, thus meeting the maximum values imposed by the standard (Figure 5.23).

Regarding the current trend, there is an increase at 4 and 5 seconds due to the activation of the two inductive loads, which require more current. Thereafter, at 6 and 8 seconds there is a decrease in current due to the fact that first the resistive load decreases and then one of the two inductive loads is disconnected.

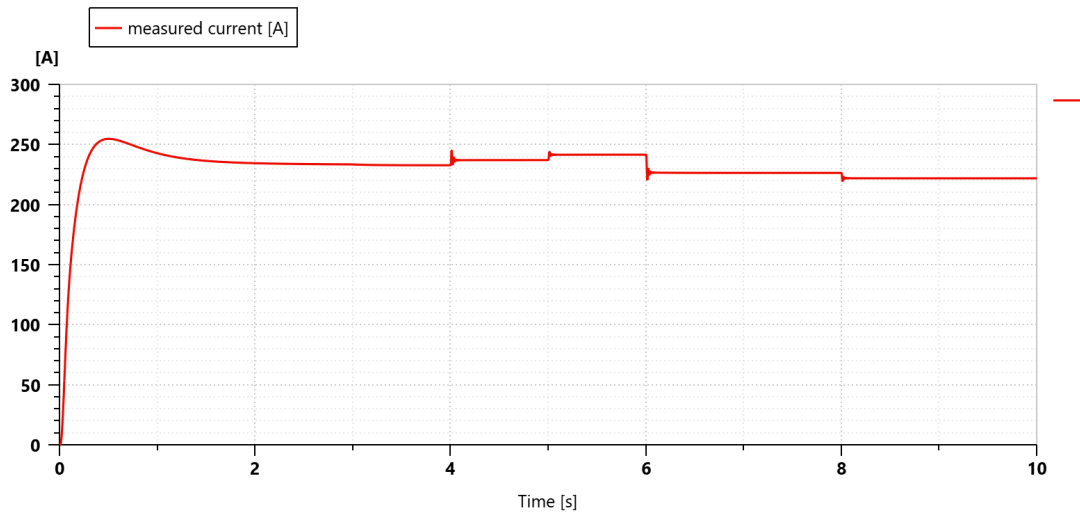


Figure 5.24: DC current trend

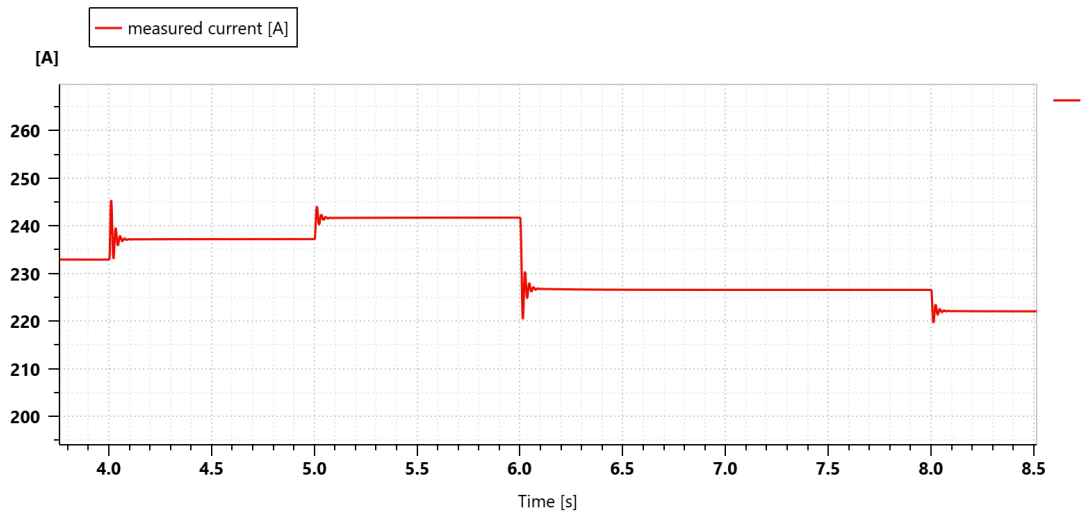


Figure 5.25: DC current peaks

Regarding the power trend, it is observed that when a load varies, the power initially experiences a transient due to the voltage and then stabilises at higher or lower values, depending on the increase or decrease in current.

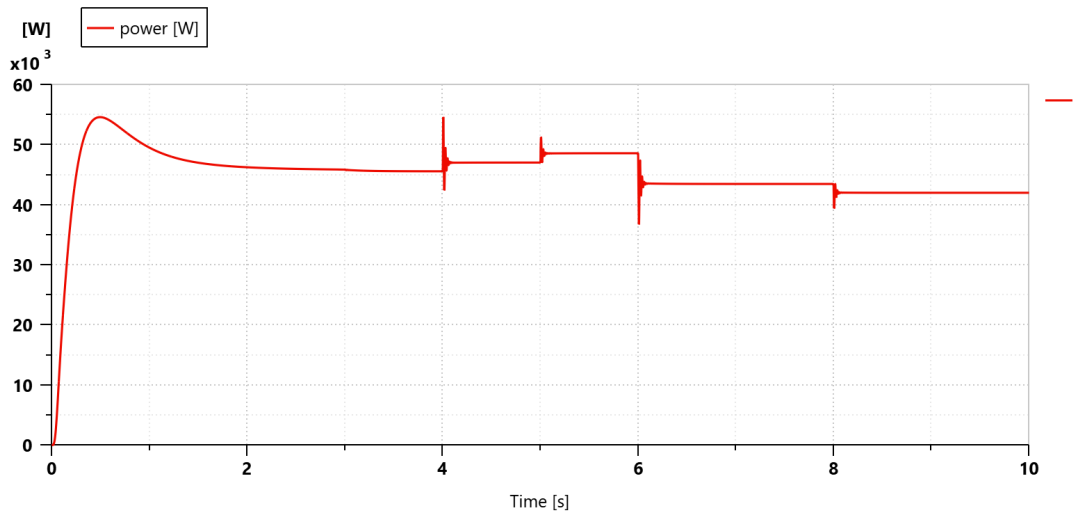


Figure 5.26: DC power trend

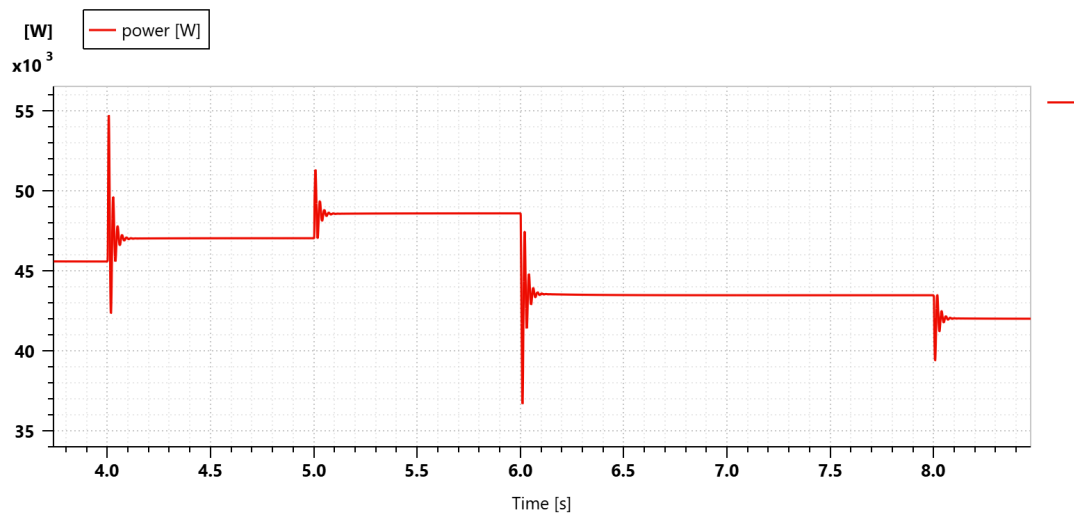


Figure 5.27: DC power peaks

Chapter 6

Battery charge

The last phase of the project consists of connecting the battery to allow it to be recharged during the cruise phase. In this case, it was decided to connect the battery to the AC circuit for reasons related to the type of devices required for voltage conversion. In order to connect the battery to the AC circuit as a load, it is necessary to insert a rectifier followed by a TRU. The former is responsible for increasing the voltage by maintaining it in an alternating current (AC) mode, while the latter is responsible for converting the voltage output by the transformer into a direct current (DC) mode. This conversion is essential since the battery operates on direct current. An alternative option would be to connect the battery to the DC circuit, which, however, operates at a lower voltage than the battery. Therefore, if this solution were chosen, a DC-DC converter would have to be introduced to raise or lower the voltage, depending on the desired purpose. In order to determine the size of the battery, it was assumed that lithium-ion cells with the following characteristics would be used:

Name	Title	Value	Unit
Upack1	High energy pack rated voltage		540 V
Epack1	High energy pack rated energy		50 kWh
Ccell1	High energy cell rated capacity		4.3 Ah
Ucell1	High energy cell rated voltage		3.8 V
Ns1	High energy pack series cell number	$\text{ceil}(\text{Upack1}/\text{Ucell1})$	null
Np1	High energy pack parallel branch number	$\text{ceil}(\text{Epack1}*1000/\text{Upack1}/\text{Ccell1})$	null

Figure 6.1: Battery pack characteristic requirement

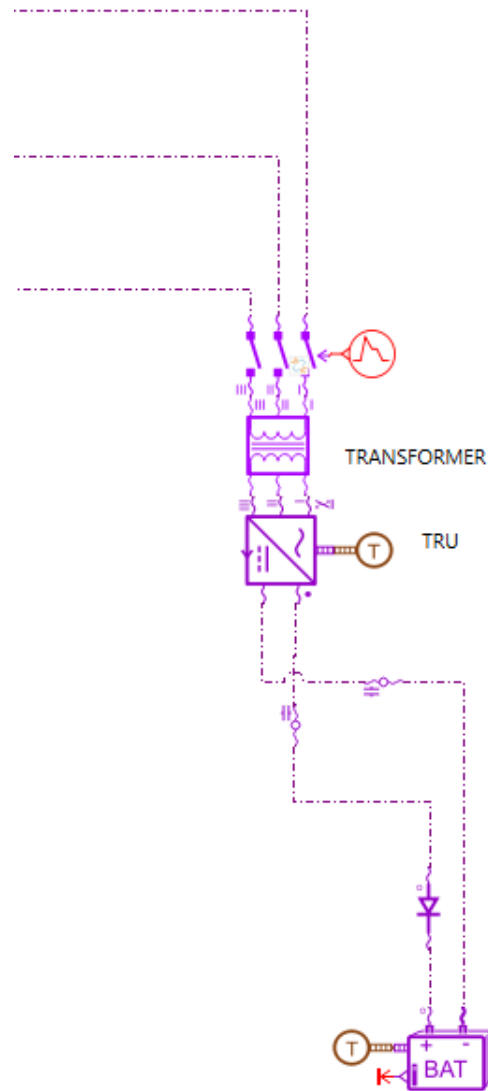


Figure 6.2: Battery modelling

The battery voltage is 540 VDC, so it was chosen to connect it to the AC circuit for charging for the following reasons:

- AC-DC converters are simpler in construction, as DC-DC converters have rather complex power electronics;
- DC-DC step-ups that have to convert from 28 V to 540 V are heavier than TRUs that have to convert from 115 VAC to 540 VDC;

- AC-DC converters for high voltages are much more common than DC-DC converters with such high step-ups, which are therefore much more expensive.

Referring to the AC circuit in Fig. 5.12, the transformer was connected followed by the rectifier to which the battery was connected, as shown in Fig. 6.2.

Capacitors were inserted into the connection lines between the battery and the rectifier to stabilize the voltage, to avoid sudden voltage jumps when the diode switches on or off. Without the use of these capacitors, the simulator cannot handle the ON/OFF transition of the diode, going into numerical instability. The diode was inserted to make the current flow in only one direction, preventing the current from flowing back from the battery to the TRU.

Results

The 50-minute simulation was set to be equivalent to the duration of a cruise for a regional aircraft. Battery charging was started four seconds after the start of the simulation.

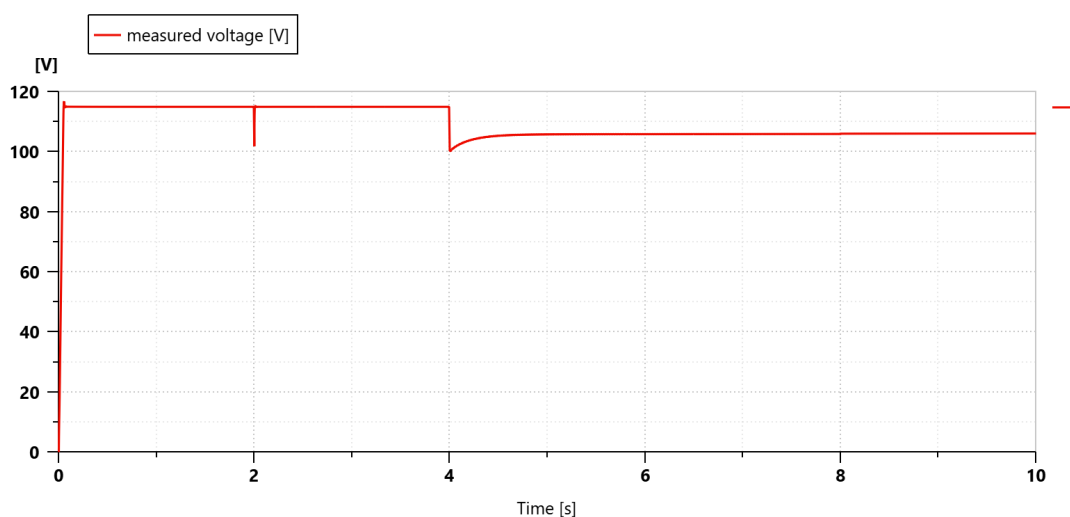


Figure 6.3: Output voltage GCU

With reference to Fig.6.3 it is observed that, at $t = 2s$, there is a decrease in voltage due to the connection of the inductive load. After 4 seconds, a further decrease is observed, attributable to the battery load. In this circumstance, the voltage decreases to a value of approximately 100 V, which is in accordance with regulatory standards. However, in contrast to the previous simulations, in this case the generator can no longer restore the nominal voltage value at the end of the transient, stabilizing at a value of 106 V.

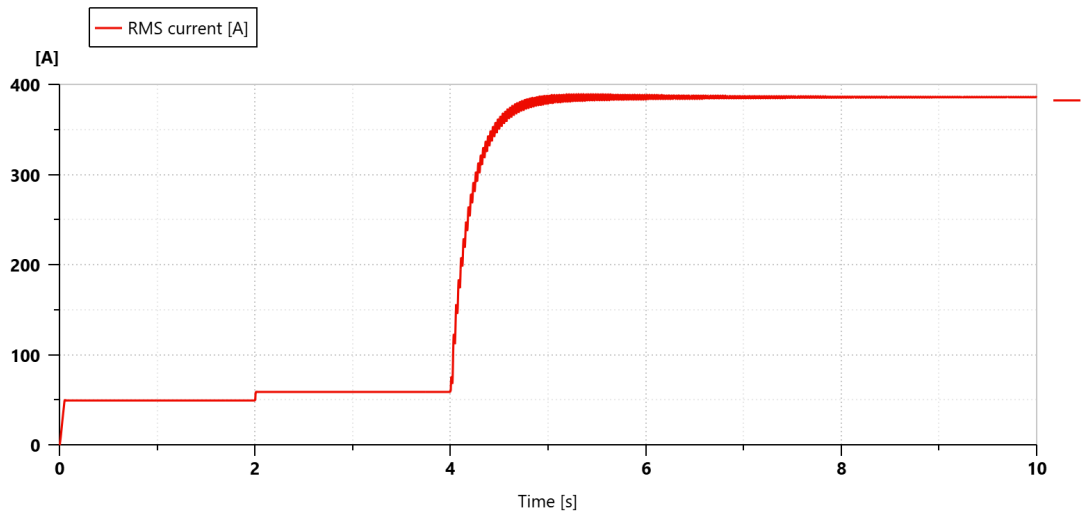


Figure 6.4: Output current GCU

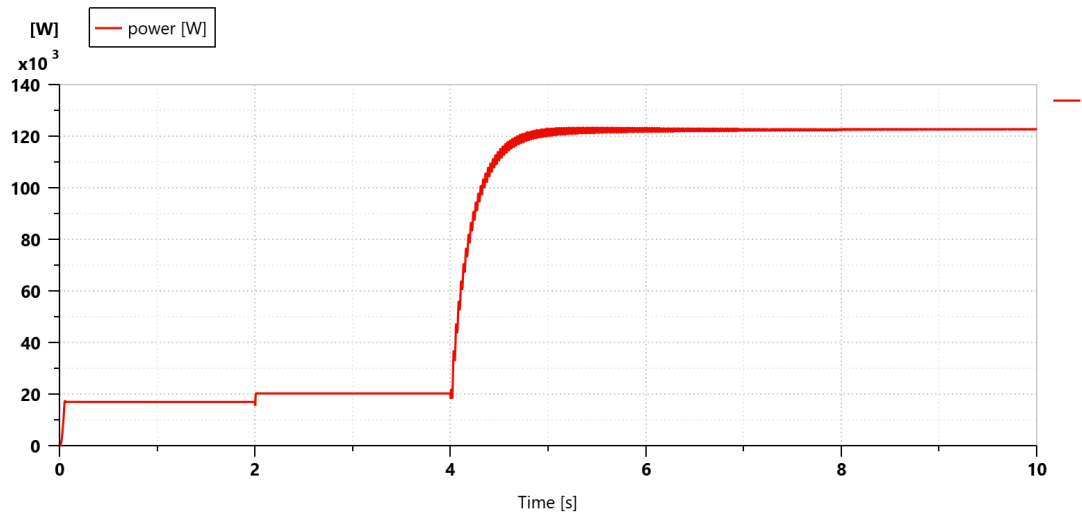


Figure 6.5: Output power GCU

Initially, during the charging phase, the battery demands a high amount of current from the generator, causing a marked increase in the generator's power output. The generator tries to compensate for this new demand, registering an increase in power from values below 20 kW up to 122 kW. The introduction of the battery causes fluctuations in current and power, due to the fact that the generator used in this model was sized according to the parameters of a generator mounted on an ATR72, which has a power of between 20 and 30 kW.

When the transformer is activated, a slight decrease in voltage is observed,

attributable to the impedance of the device (Fig.6.6). The inability of the generator to restore the nominal voltage value is reflected in the transformer, which operates from a value of approximately 106 V, with an output of 234 V.

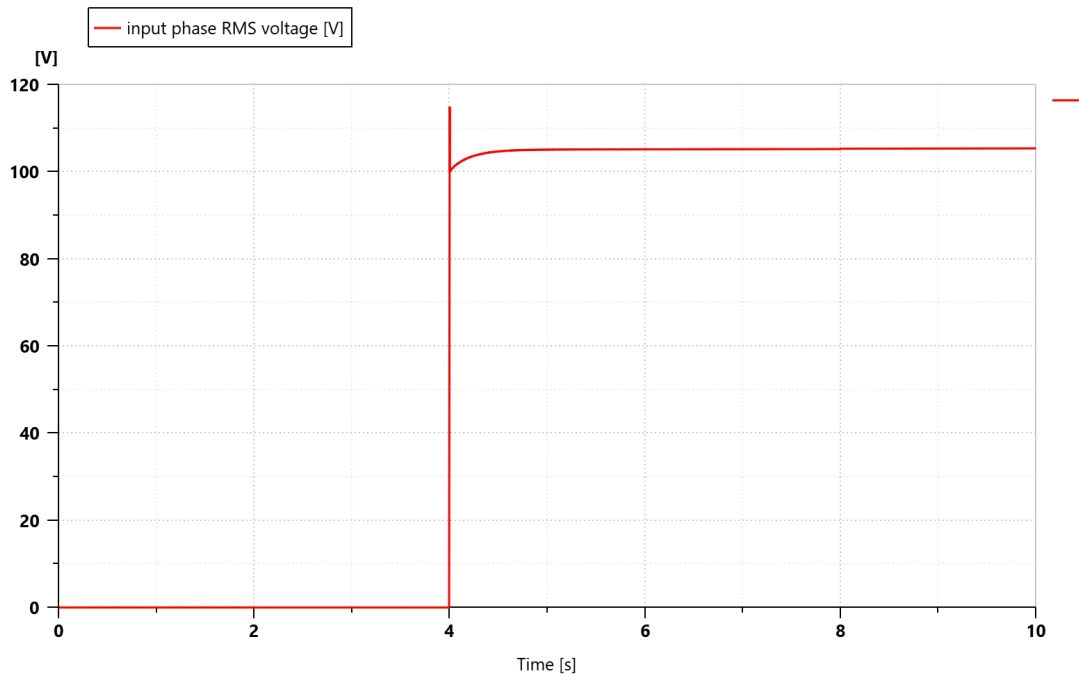


Figure 6.6: Input voltage transformer

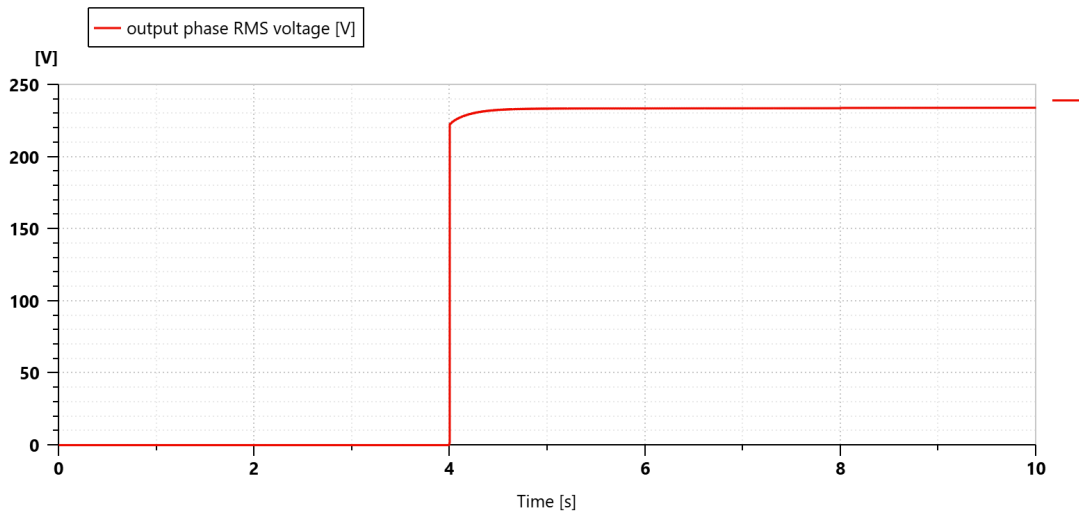


Figure 6.7: Output voltage transformer

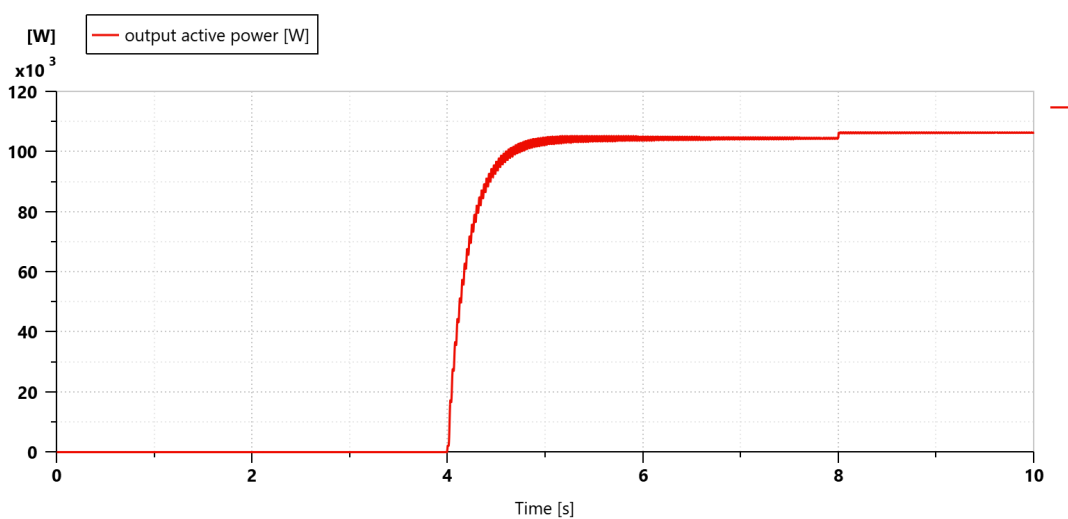


Figure 6.8: Output power transformer

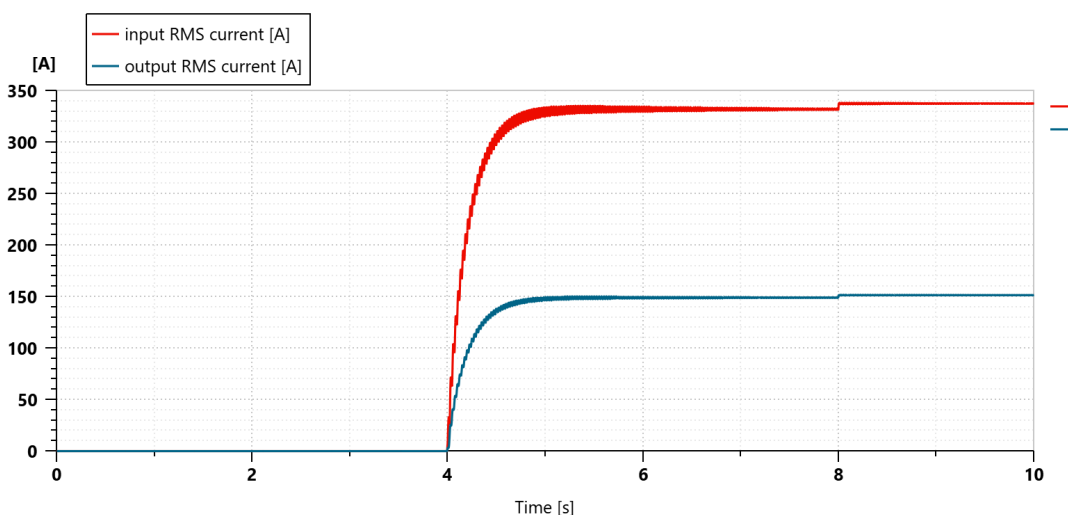


Figure 6.9: Input and output current transformer

With concerning the behaviour of the TRU, it is observed that the output voltage is different from zero already before the battery charging starts. This phenomenon is attributable to the fact that the battery is connected even in the absence of current draw. Therefore, even in the absence of power supply by the transformer, the presence of the battery imposes its voltage difference at the TRU terminals.

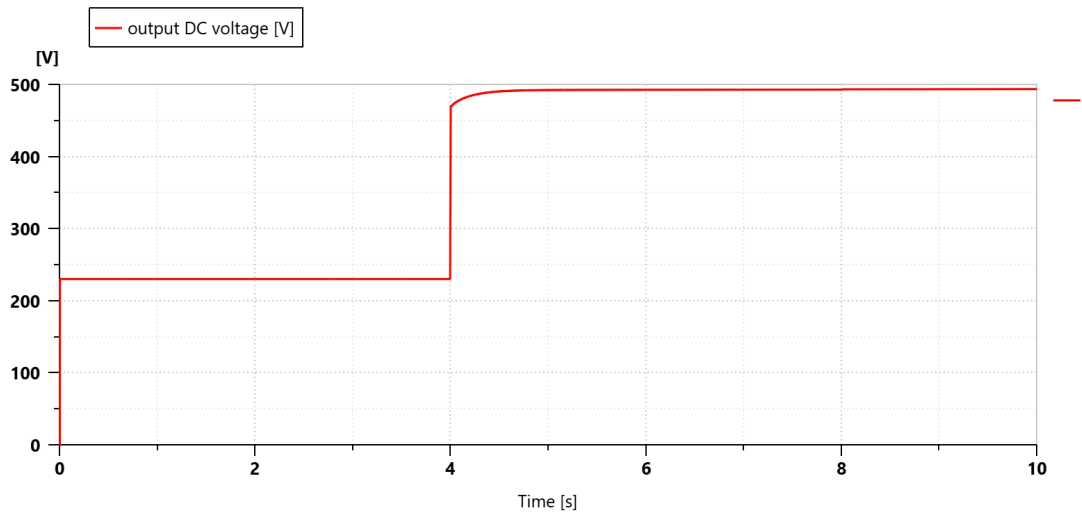


Figure 6.10: Output DC voltage

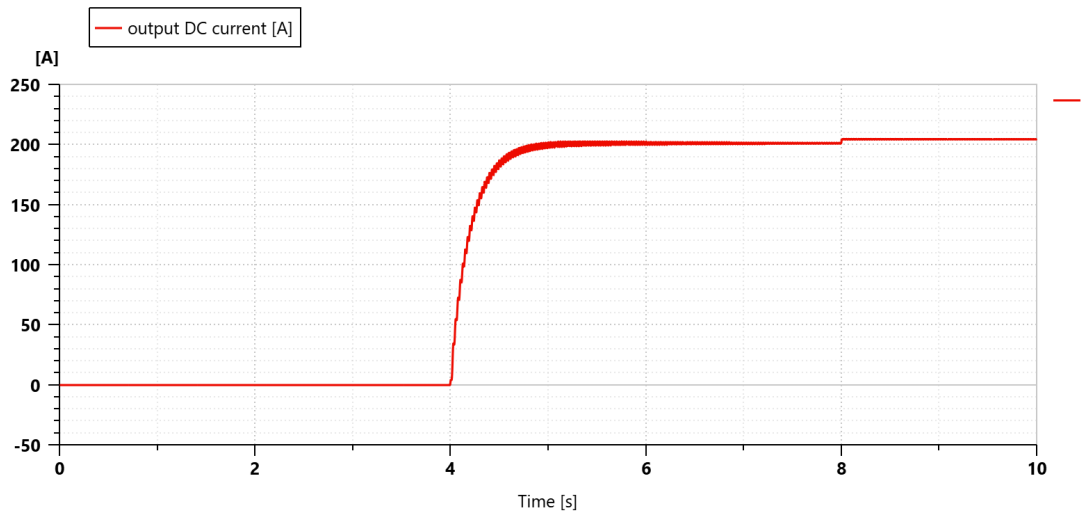


Figure 6.11: Output DC current

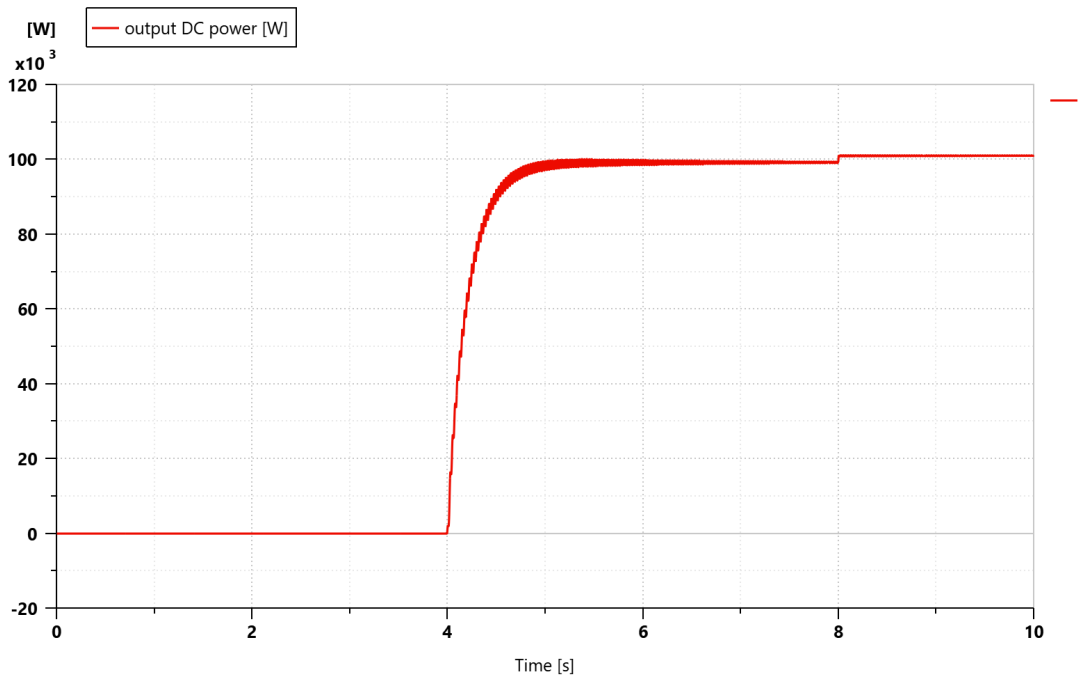


Figure 6.12: Output DC power

voltage [V]	current [A]	power [kVA]
234	151.623	106.467
493.955	204.762	101.143

Table 6.1: Output values trasformer and TRU

In Figures 6.13 and 6.14 are reported again the input voltage and current of the battery. As can be seen, at 8 seconds there is a slight increase in both voltage and current, a phenomenon that also occurs in the transformer (Fig. 6.8 and 6.9). This variation can be attributed to a voltage fluctuation at the generator level (Fig. 6.15).

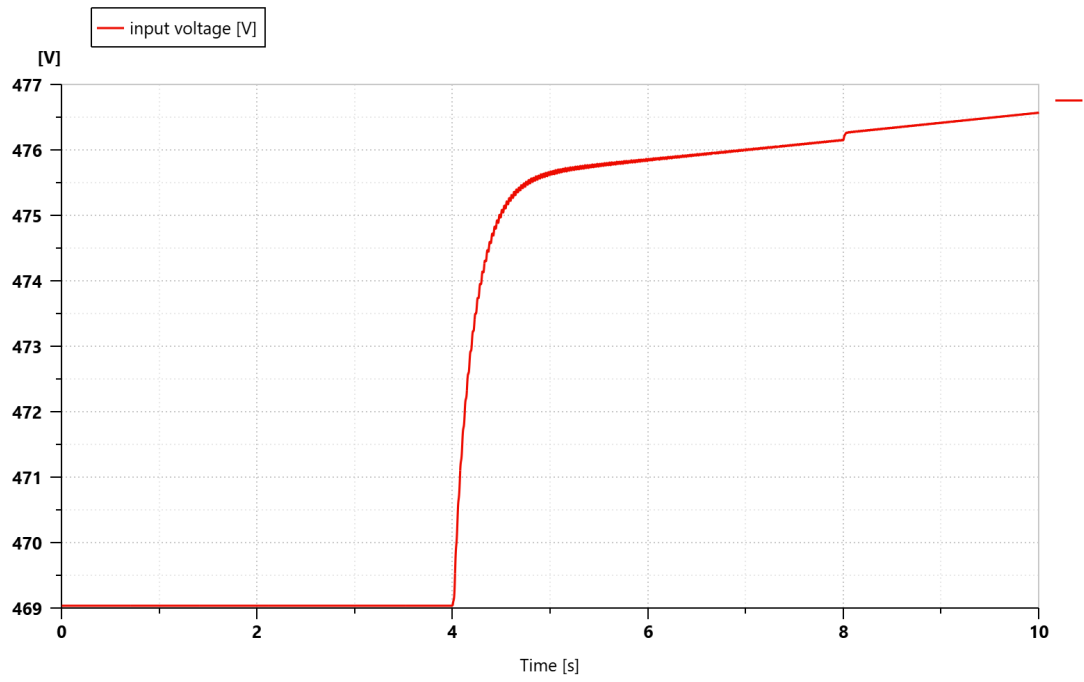


Figure 6.13: Input voltage battery

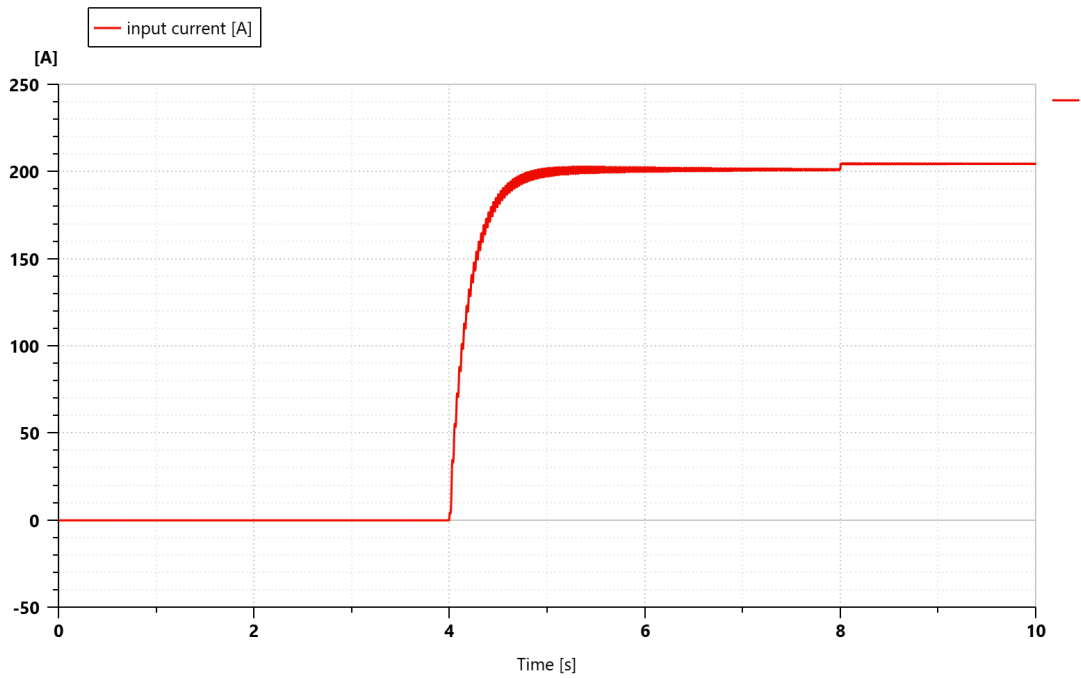


Figure 6.14: Input current battery

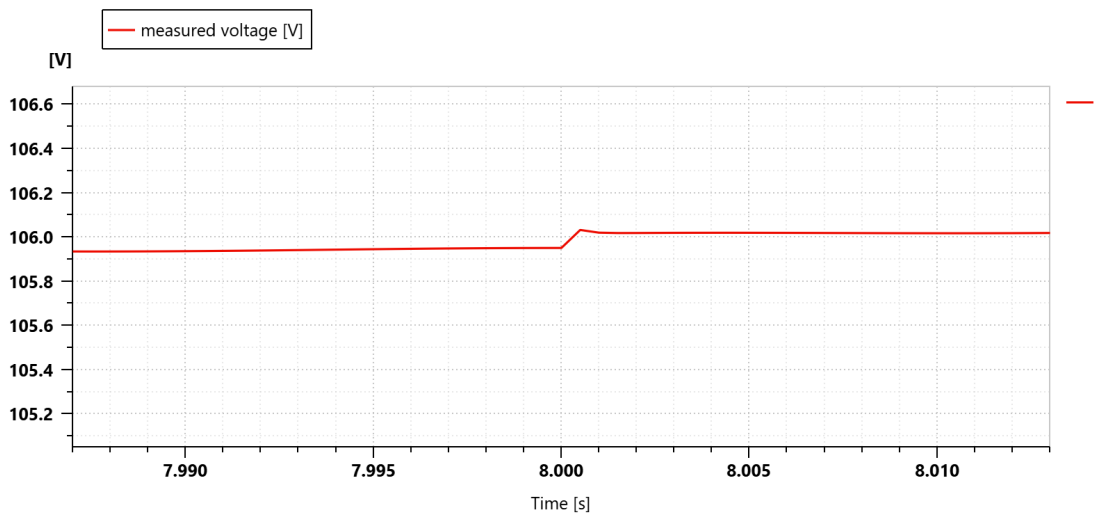


Figure 6.15: Output voltage GCU ($t=8s$)

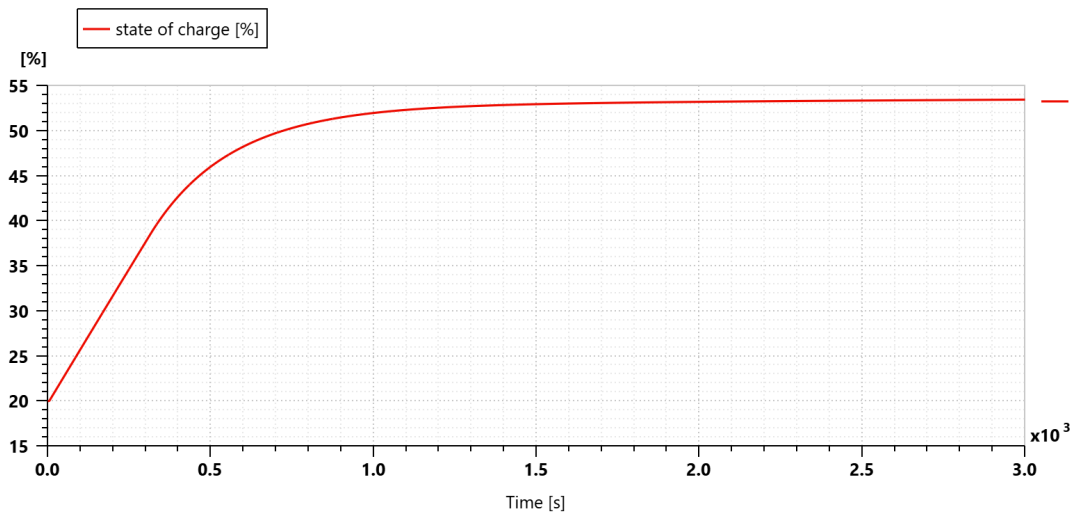


Figure 6.16: Battery state of charge

Within a time frame of 50 minutes, a significant difficulty of the system in reaching full battery charge was observed, reaching a state of charge of no more than 54%. In order to increase the battery charge level, it was necessary to increase the output voltage from the rectifier. Initially, the output voltage from the rectifier was adjusted to obtain 540V DC. However, when the battery reaches this voltage level, there is no longer enough voltage difference between the battery and the rectifier to ensure an adequate charging current for charging. In view of these observations, the rectifier was configured to generate an output voltage higher than

that of the battery, with an estimated value of 590V DC.

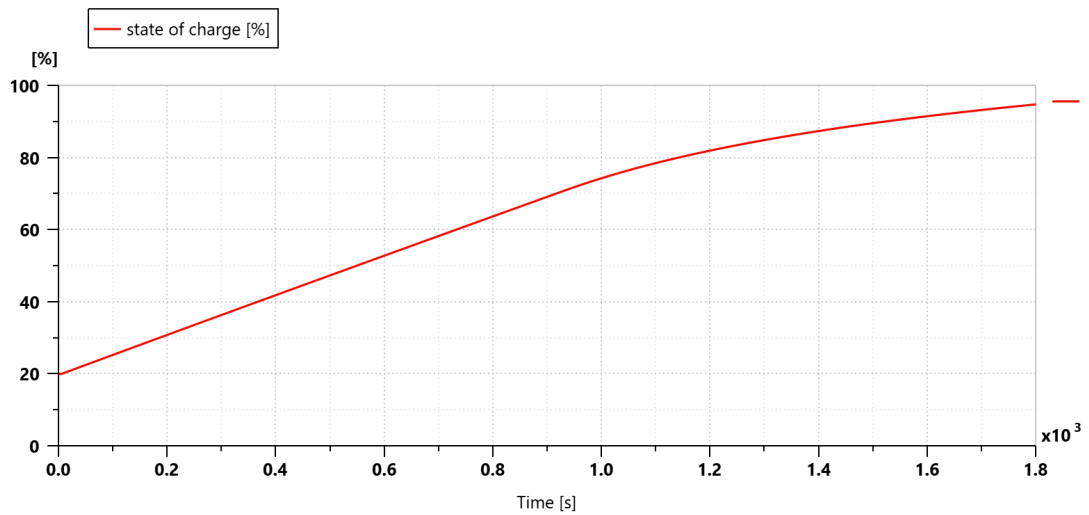


Figure 6.17: Battery state of charge

By increasing the output voltage from the rectifier, it is observed that the battery reaches 95% charge in about 30 minutes. However, this change in voltage results in a consequent change in the voltage demand on the generator.

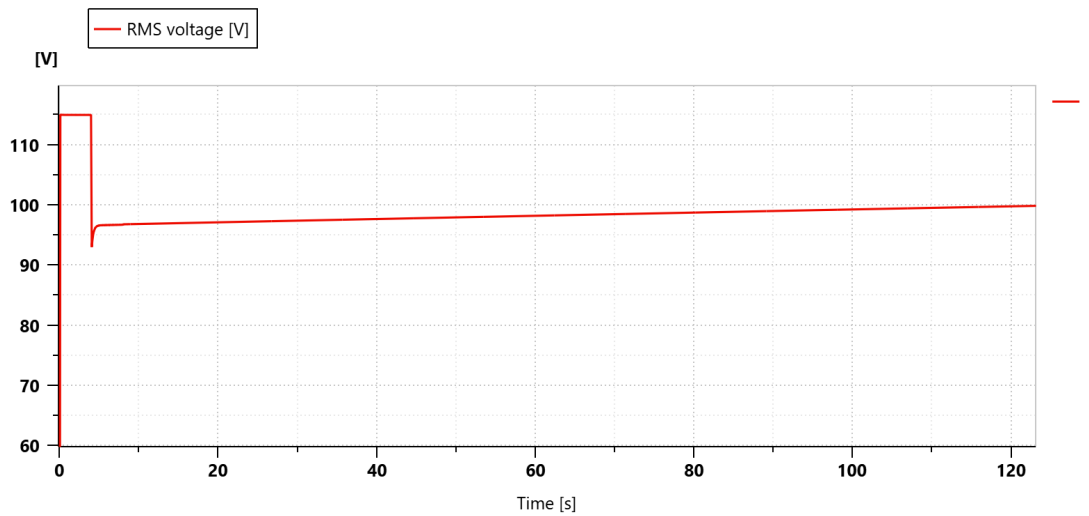


Figure 6.18: Voltage GCU (SOC=95%)

An analysis of the voltage trend in Figure 6.18 shows that, upon activation of the battery charge, the generator voltage decreases to 93 V. In addition, the transient run-out times do not comply with regulatory standards, making this

type of generator unsuitable for charging such a battery. As a result of these considerations, it was necessary to modify the capacity of the battery, reducing its value in order to ensure that the generator voltage fluctuations comply with regulatory parameters.

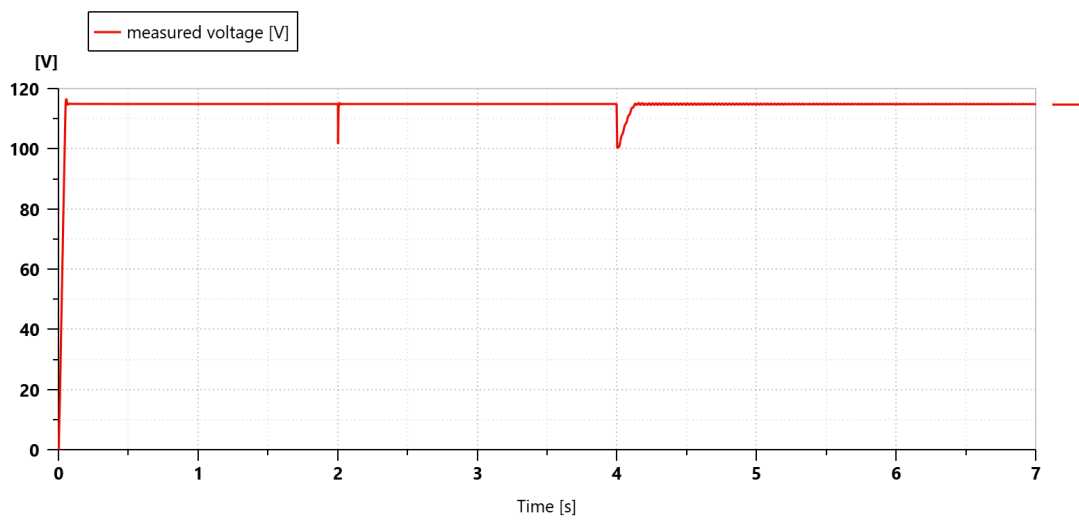


Figure 6.19: Voltage GCU (battery capacity = 2 kWh)

By reducing the capacity value to 2 kWh, it was observed that the voltage transient due to the activation of the battery charge is within the requirements of the standard. For $t = 4s$, the generator voltage drops to a value of approximately 100 V, reaching a value of 108 V in 0.06 seconds. It was also verified that by increasing the capacity of the battery to a value of 3 kWh, the voltage trend already non-compliant with the standard, as the controller only manages to bring the generator back to a voltage of 108 V after 0.10 seconds.

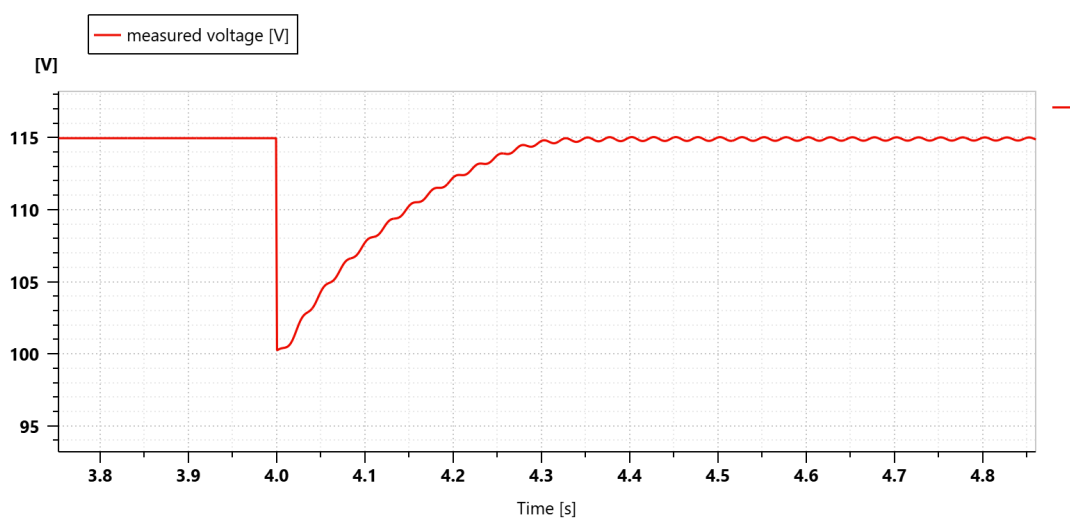


Figure 6.20: Voltage GCU (battery capacity = 3 kWh)

A further issue associated with this model concerns the current that is fed into the battery by the rectifier. As shown in Figure 6.14, it can be seen that the current entering the battery increases from 0 to 200 A. This considerable increase in current during the charging phase can have significant consequences for the battery itself. In particular, a considerable increase in current could lead to the battery overheating due to the heat generated by the Joule effect. In fact, high temperatures during the charging phase can cause degradation of the device and increase the risk of thermal fusion. In addition, high temperatures can cause the loss of active lithium and an increase in internal resistance, leading to a reduction in battery capacity. To mitigate these risks, batteries are generally equipped with battery management systems (BMS) that can monitor temperatures through current control [43]. In this circumstance, current limitation was achieved by inserting a resistor between the TRU and the battery, in order to regulate the value of current entering the battery by varying the value of the resistance.

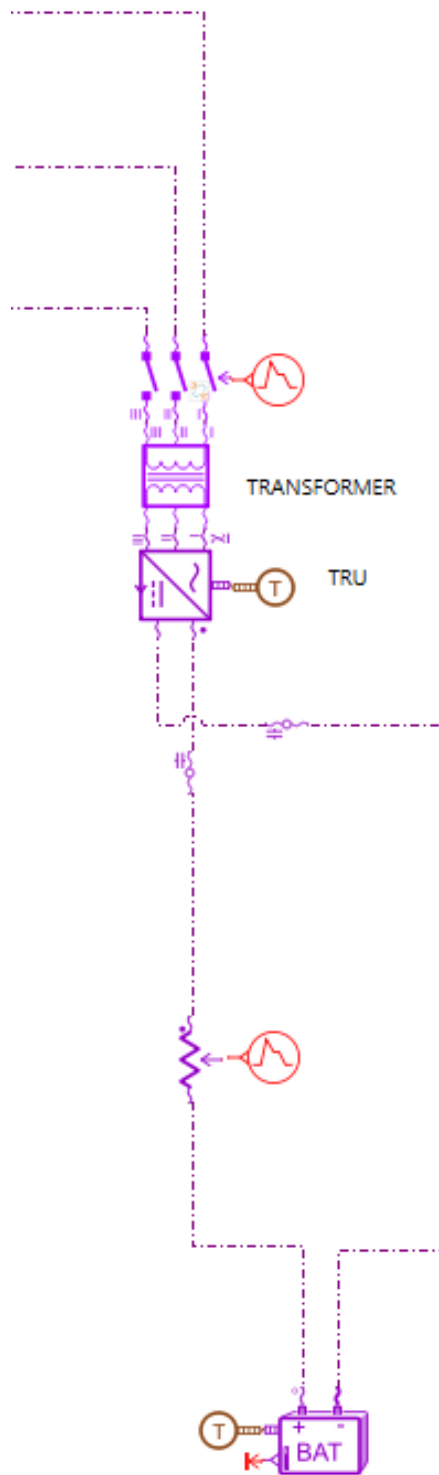


Figure 6.21: Modelling with current limitation

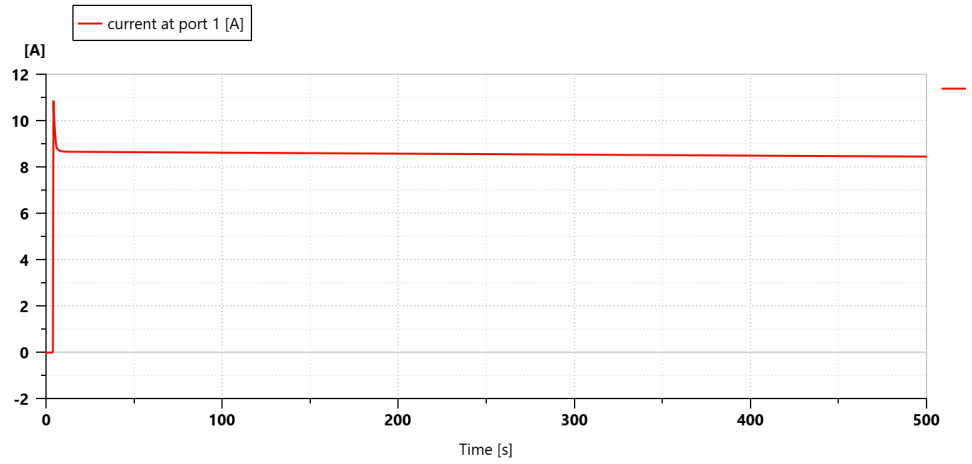


Figure 6.22: Input current battery

In order to preserve the integrity of the battery, it is recommended to apply values not exceeding 15 V. Once the resistor was inserted, the value of the battery capacity was varied to align it with the HERA design. A value of 750 kWh was assigned.

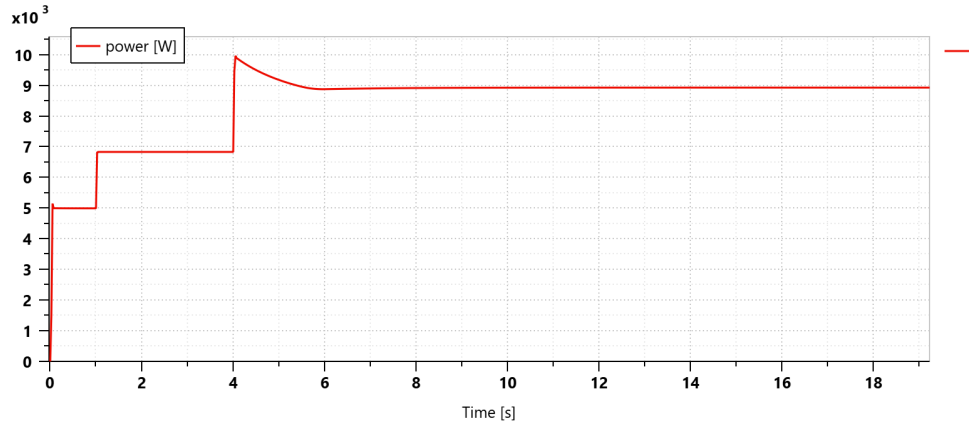


Figure 6.23: Power GCU

The Figure 6.23 clearly illustrates how the power required from the generator was significantly reduced after adjusting the input current to the battery. As a result, the power required to supply the loads respects the generator’s maximum power limit.

Regarding the voltage trend at the generator, a variation is observed at $t=4$ seconds, attributable to the start of the battery charging process, the peak value of which remains within the limits set by the standard. However, the time of transient

exhaustion does not comply with MIL STD 704F standards. In addition, no change is observed when inductive loads are activated. This phenomenon is attributable to the high value assigned to the regulator gain of GCU, which is set to prevent the occurrence of oscillations.

Translated with DeepL.com (free version)

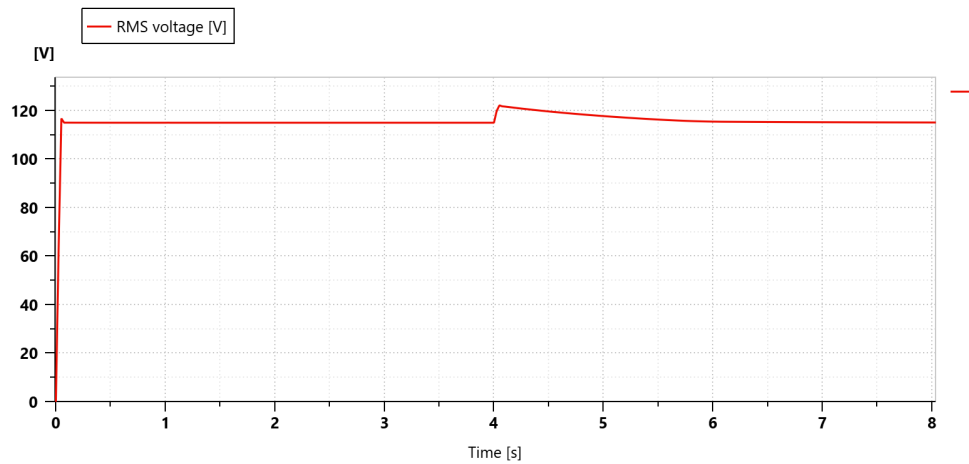


Figure 6.24: Voltage GCU

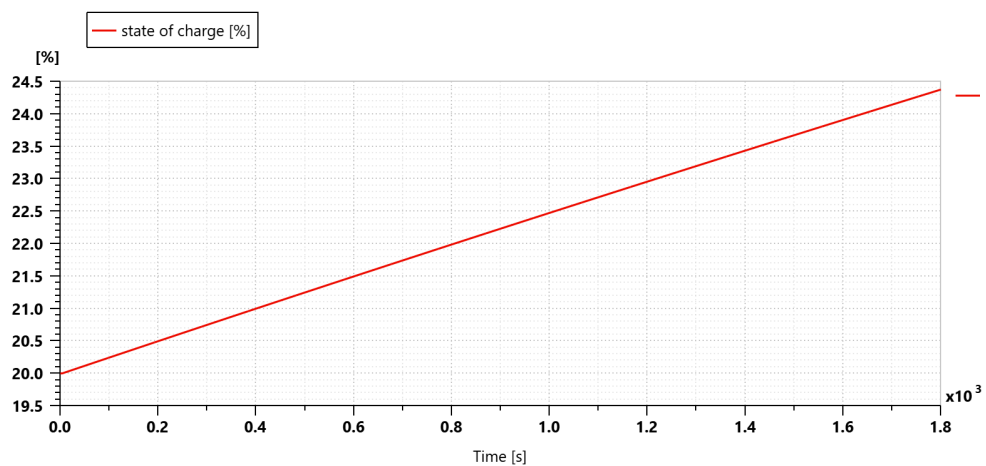


Figure 6.25: Battery SOC

However, it is important to note that the current limitation leads to a reduction in the charging speed of the battery. The Figure 6.25 illustrates how the battery reaches 24.25% of its capacity in 30 minutes of simulation.

Chapter 7

Conclusions

The aim of this thesis was to develop the load modelling of the electrical system of a hybrid-electric propulsion aircraft, taking the HERA project as a reference. The HERA project aims to study and develop an innovative configuration for regional air transport, based on existing aircraft configurations belonging to this category, such as the ATR 72, and adopting a hybrid propulsion system, with the aim of reducing the environmental impact and improving the energy efficiency of the propulsion system.

To model the system, the electrical system configuration of the ATR 72 had to be analysed and used as a reference. From this analysis, the modelling of alternating current (AC) and direct current (DC) electrical loads was carried out. Through this modelling, it was possible to define the profile of the loads and assess the behaviour of the generator adopted for the study. The tests conducted on the generator made it possible to analyse its response to load variations and to verify whether the oscillations of the electrical parameters were within the limits imposed by the MIL STD 704F aeronautical standard. The results obtained provided significant indications on the performance of the generator, highlighting its ability to adapt to load fluctuations and guarantee system stability.

Subsequently, the modelling of the battery was implemented, an element of crucial importance in this aircraft configuration, as it will be used to power the hybrid electric propulsion system. The aim of this analysis was to assess the ability of the selected generator to recharge the battery during flight. In hybrid electric aircraft, recharging the battery during the cruise phase is essential to optimise the use of available energy and improve the overall efficiency of the propulsion system. During the take-off and climb phases, the power demand from the engines is significant, making the battery contribution necessary to ensure optimal system operation. The internal combustion engine operates most efficiently under constant and optimal conditions, typical of flight at cruising speed. In the event of excessive engine power relative to propulsion requirements, this can be converted to electrical

energy in order to recharge the batteries.

The battery that is the subject of this study is a lithium-ion battery. Initially, an estimate of the battery capacity was made, assuming an initial value of 50 kWh, taking into account the fact that currently available batteries have capacities in the order of 2-3 kWh. Preliminary analysis shows that an increase in battery capacity does not automatically guarantee an adequate power supply to power all loads. In order to supply the loads and recharge the battery, the generator would have to provide a power output of approximately 120 kW, significantly exceeding the 20 kW power limit of the ATR 72 generator. A further problem is the amount of current delivered to the battery, which varies from 0 to 200 A. This variation is damaging to the battery.

To mitigate this problem, a current-limiting system was implemented by adding a resistor between the TRU and the battery. The implementation of this limitation allowed the battery capacity to be increased to 750 kWh in order to adequately reflect the expected modelling of the HERA aircraft. The current limitation produced optimal results in terms of the power required at the generator loads, which was around 8.9 kW, meeting the limit imposed by the generator itself. However, this current regulation had an impact on the battery charging speed, which was significantly lower than in the case without current limitation.

It can be concluded that the AC system examined in this study is effective for battery charging, but needs further optimisation to ensure a higher charging rate than that obtained with the current model, considering the limitations of generator power and current to be applied to the battery. The results obtained in this study represent a first step towards more advanced optimisation of the hybrid aircraft electrical system. However, several aspects can be further improved to increase the overall efficiency and reliability of the system:

- a first area of development concerns the Battery Management System (BMS), the optimisation of which would allow more efficient management of charging and battery health, reducing current fluctuations and improving the durability of the storage system;
- on the basis of the power obtained from simulations, it would be possible to proceed with the sizing of the generator, ensuring that its capacity is adequate for the aircraft's energy needs without exceeding structural and operational limits;
- a further development could concern improving the modelling of inductive and resistive loads, increasing the accuracy of the simulation of electrical system behaviour under real operating conditions and refining the prediction of system performance;

It is conclusion that for hybrid solutions to become a viable option for the future, continuous technological development is required, particularly in the field of batteries, which need to be improved in terms of specific energy and durability.

Appendix A

MIL-STD-704 F

Steady state characteristics	Limits
Steady state voltage	108.0 to 118.0 Volts, RMS
Voltage unbalance	3.0 Volts, RMS maximum
Voltage modulation	2.5 Volts, RMS maximum
Voltage phase difference	116° to 124°
Distortion factor	0.05 maximum
Distortion spectrum	Figure 7
Crest factor	1.31 to 1.51
DC component	+ 0.10 to - 0.10 Volts
Steady state frequency	393 to 407 Hz
Frequency modulation	4 Hz
Transient characteristics	Limits
Peak voltage	±271.8 Volts
Voltage transient	Figure 3
Frequency transient	Figure 5

Figure A.1: AC normal operation characteristics - 400Hz [42]

Steady state characteristics	Limits	
	28 Volt DC system	270 Volt DC system
Steady state voltage	22.0 to 29.0 Volts	250.0 to 280.0 Volts
Distortion factor	0.035 maximum	0.015 maximum
Distortion spectrum	Figure 15	Figure 18
Ripple amplitude	1.5 Volts maximum	6.0 Volts maximum
Transient characteristics	Limits	
Voltage transient	28 Volts DC system	270 Volts DC system
	Figure 13	Figure 16

Figure A.2: DC normal operation characteristics [42]

Bibliography

- [1] Qiang C., Yi-lin L., Zi-ke J., Yu W. and Ye L. «Path analysis for controlling climate change in global aviation». In: *iScience* 27.6 (2024), p. 110126 (cit. on p. 1).
- [2] Michael Kreimeier, Eike Stumpf, and Dominik Gottschalk. «Economical assessment of air mobility on demand concepts with focus on Germany». In: June 2016. DOI: 10.2514/6.2016-3304 (cit. on p. 1).
- [3] D.S. Lee et al. «The contribution of global aviation to anthropogenic climate forcing for 2000 to 2018». In: *Atmospheric Environment* 244 (2021), p. 117834. ISSN: 1352-2310. URL: <https://www.sciencedirect.com/science/article/pii/S1352231020305689> (cit. on p. 1).
- [4] *Programme overview and structure | Clean Aviation*. Last acces: 7 november 2024. URL: <https://www.clean-aviation.eu/clean-sky-2/programme-overview-and-structure> (cit. on p. 1).
- [5] URL: https://climate.ec.europa.eu/eu-action/transport/reducing-emissions-aviation_en#aviation-in-the-eu-emissions-trading-system (cit. on p. 1).
- [6] Milan Klöwer, M Allen, David Lee, S Proud, Leo Gallagher, and Agnieszka Skowron. «Quantifying aviation’s contribution to global warming». In: *Environmental Research Letters* 16 (Oct. 2021), p. 104027. DOI: 10.1088/1748-9326/ac286e (cit. on p. 2).
- [7] *HERA Project | Clean Aviation*. Last acces: 19 February 2025. URL: <https://www.clean-aviation.eu/hera> (cit. on p. 3).
- [8] *HERA Project*. Last acces: 19 February 2025. URL: <https://project-hera.eu/about/ambition> (cit. on pp. 3, 5).
- [9] G. Piscopo M. Di Giulio and V. Ascione. *HERA for AIAA Innovative Aircraft Concept and Novel Configuration vII*. Accessed: Feb 24, 2025. 2024. URL: <https://zenodo.org/records/14899287/files/HERA%20for%20AIAA%20Innovative%20Aircraft%20concept%20and%20Novel%20configuration%20vII.pdf?download=1> (cit. on pp. 4, 5).

- [10] R. Thomson. *Aircraft Electrical Propulsion - The Next Chapter of Aviation?* Tech. rep. Think, Act Roland Berger, Sept. 2017 (cit. on pp. 6–8).
- [11] Bulent Sarlioglu and Casey T. Morris. «More Electric Aircraft: Review, Challenges, and Opportunities for Commercial Transport Aircraft». In: *IEEE Transactions on Transportation Electrification* 1 (2015), pp. 54–64. URL: <https://api.semanticscholar.org/CorpusID:12815419> (cit. on pp. 6, 21, 22, 25).
- [12] Ahmet Arabul, Emre Kurt, Fatma Keskin Arabul, İbrahim Senol, Martin Schrötter, Robert Breda, and Dávid Megyesi. «Perspectives and Development of Electrical Systems in More Electric Aircraft». In: *International Journal of Aerospace Engineering* 2021 (Apr. 2021), pp. 1–14. DOI: 10.1155/2021/5519842 (cit. on pp. 7, 8, 21, 22).
- [13] Tania C. Cano, Ignacio Castro, Alberto Rodríguez, Diego G. Lamar, Yehia F. Khalil, Laura Albiol-Tendillo, and Parag Kshirsagar. «Future of Electrical Aircraft Energy Power Systems: An Architecture Review». In: *IEEE Transactions on Transportation Electrification* 7.3 (2021), pp. 1915–1929. DOI: 10.1109/TTE.2021.3052106 (cit. on p. 7).
- [14] Luigi Cardone, Giuseppe Petrone, Sergio De Rosa, Francesco Franco, and Carlo Greco. «Review of the Recent Developments About the Hybrid Propelled Aircraft». In: *Aerotecnica Missili & Spazio* 103 (Sept. 2023). DOI: 10.1007/s42496-023-00173-6 (cit. on p. 8).
- [15] Manuel Rendón, Carlos Sánchez, Josselyn Gallo Muñoz, and Alexandre Anzai. «Aircraft Hybrid-Electric Propulsion: Development Trends, Challenges and Opportunities (<https://rdcu.be/cmG4u>)». In: *Sba Controle Automação Sociedade Brasileira de Automatica* (June 2021). DOI: 10.1007/s40313-021-00740-x (cit. on pp. 8, 9).
- [16] Zirui Huang. «Electric and hybrid-electric aircraft propulsion systems: development, difficulties and opportunities». In: *Theoretical and Natural Science* 5 (May 2023), pp. 28–34. DOI: 10.54254/2753-8818/5/20230263 (cit. on p. 9).
- [17] Agata Kuśmierk, Cezary Galiński, and Wieńczysław Stalewski. «Review of the hybrid gas - electric aircraft propulsion systems versus alternative systems». In: *Progress in Aerospace Sciences* 141 (2023). Special Issue on Green Aviation, p. 100925. ISSN: 0376-0421. DOI: <https://doi.org/10.1016/j.paerosci.2023.100925>. URL: <https://www.sciencedirect.com/science/article/pii/S0376042123000416> (cit. on pp. 9, 10).

- [18] Johannes Anton and Hans-Joachim Ruff-Stahl. «Competitiveness of Hybrid Electric Aircraft on Short Range Scheduled Flights». In: *International Journal of Aviation, Aeronautics, and Aerospace* 5 (Jan. 2018). DOI: 10.15394/ijaaa.2018.1240 (cit. on p. 11).
- [19] Kevin Antcliff and Francisco Capristan. «Conceptual Design of the Parallel Electric-Gas Architecture with Synergistic Utilization Scheme (PEGASUS) Concept». In: June 2017. DOI: 10.2514/6.2017-4001 (cit. on p. 11).
- [20] URL: <https://www.atr-aircraft.com/ghh/atr-evo-concept/> (cit. on p. 12).
- [21] URL: <https://aviationweek.com/aerospace/emerging-technologies/atr-details-hybrid-electric-study-option-evo> (cit. on p. 12).
- [22] Sean Bradshaw. «Next Generation Aircraft Propulsion: A Pratt & Whitney Approach». In: *AM&P Technical Articles* 181.2 (2023), pp. 12–16 (cit. on p. 13).
- [23] Aviation Week. *Pratt & Whitney Hybrid-Electric Engine Runs At Full Power*. Access on 5th November 2024. 2024. URL: <https://aviationweek.com/shownews/farnborough-airshow/pratt-whitney-hybrid-electric-engine-runs-full-power> (cit. on p. 13).
- [24] RTX News Center. *RTX Advances Hybrid-Electric Propulsion Demonstrator with 1MW Motor Rated Power*. Accesso il 5 Novembre 2024. 2023. URL: <https://www.rtx.com/news/news-center/2023/06/19/rtx-advances-hybrid-electric-propulsion-demonstrator-with-1mw-motor-rated-power-m> (cit. on p. 13).
- [25] Committee Emissions, Aeronautics Board, Division Sciences, and National Medicine. *Commercial aircraft propulsion and energy systems research: Reducing global carbon emissions*. Sept. 2016, pp. 1–122. ISBN: 9780309440967. DOI: 10.17226/23490 (cit. on pp. 13, 14, 16, 19).
- [26] P. Wheeler, Samith Sirimanna, Serhiy Bozhko, and Kiruba Haran. «Electric/Hybrid Electric Aircraft Propulsion Systems». In: *Proceedings of the IEEE PP* (Apr. 2021), pp. 1–13. DOI: 10.1109/JPROC.2021.3073291 (cit. on p. 16).
- [27] Carlos Silva, Julius Vegh, Juan Alonso, and Tarik Orra. «Flight Path and Wing Optimization of Lithium-Air Battery Powered Passenger Aircraft». In: Feb. 2015. DOI: 10.2514/6.2015-1674 (cit. on p. 17).
- [28] Naef AA Qasem and Gubran AQ Abdulrahman. «A recent comprehensive review of fuel cells: history, types, and applications». In: *International Journal of Energy Research* 2024.1 (2024), p. 7271748 (cit. on p. 19).

- [29] Timothy Dever, Kirsten P. Duffy, Andrew Provenza, Patricia L. Loyselle, Benjamin B. Choi, Carlos R. Morrison, and Angela M. Lowe. «Assessment of Technologies for Noncryogenic Hybrid Electric Propulsion». In: 2015. URL: <https://api.semanticscholar.org/CorpusID:137586229> (cit. on p. 20).
- [30] Pat Wheeler and Sergei Bozhko. «The More Electric Aircraft: Technology and challenges». In: *IEEE Electrification Magazine* 2.4 (2014), pp. 6–12. DOI: 10.1109/MELE.2014.2360720 (cit. on pp. 22, 42).
- [31] M. Sinnett. «787 No-Bleed Systems: saving fuel and enhancing operational efficiencies». In: *Boeing Aero Magazine* (2007), pp. 6–11 (cit. on p. 23).
- [32] Michael Armstrong, Mark Blackwelder, Andrew Bollman, Christine Ross, Angela Campbell, Catherine Jones, and Pj Norman. «Architecture, Voltage, and Components for a Turboelectric Distributed Propulsion Electric Grid». In: (Jan. 2015) (cit. on p. 23).
- [33] Ian Cotton, Richard Gardner, Daniel Schweickart, Dennis Grosean, and Christopher Severns. «Design considerations for higher electrical power system voltages in aerospace vehicles». In: *2016 IEEE International Power Modulator and High Voltage Conference (IPMHVC)*. 2016, pp. 57–61. DOI: 10.1109/IPMHVC.2016.8012771 (cit. on p. 24).
- [34] Mona Ghassemi, Ashkan Barzkar, and Mohammadreza Saghafi. «All-Electric NASA N3-X Aircraft Electric Power Systems». In: *IEEE Transactions on Transportation Electrification* (Mar. 2022), pp. 1–1. DOI: 10.1109/TTE.2022.3158186 (cit. on p. 28).
- [35] Accessed: 2025-01-23. URL: <https://www.atr-aircraft.com/aircraft-services/aircraft-family/atr-72-600/> (cit. on pp. 30, 31).
- [36] Accessed: 2025-01-24. URL: https://www.fzt.haw-hamburg.de/pers/Scholz/transfer/Brochure-ATR-600-Series_2014.pdf (cit. on pp. 31, 32).
- [37] ATR Aircraft. *ATR 72 Flight Crew Operating Manual (FCOM)*. July 1999 (cit. on pp. 34, 36, 38).
- [38] Pilotbrary. *ATR 72-600 Electrical System*. Accessed: 2024-09-18. 2023. URL: <https://youtu.be/OHVM57UTMfk?feature=shared> (cit. on pp. 37, 41).
- [39] BJ Schiltgen and JL Freeman. «SAE AIR 6326: Aircraft Electrical Power Systems Modeling and Simulation Definitions». In: *SAE International* (2015) (cit. on pp. 42, 43).
- [40] *AMESim 4.0 User Manual*. IMAGINE, 2004. URL: <https://www.yumpu.com/en/document/view/42813746/amesim-40-user-manual-nupet> (cit. on p. 44).

BIBLIOGRAPHY

- [41] Simcenter Amesim 2310. *Aircraft Electrics Library User's guide*. Available in the programme help documentation. 2023 (cit. on p. 44).
- [42] Accessed: 2025-01-24. URL: <https://iee.li/pdf/standards-handbooks/MIL-STD-704F.pdf> (cit. on pp. 52, 63, 86).
- [43] Todd Bandhauer, Srinivas Garimella, and Thomas Fuller. «A Critical Review of Thermal Issues in Lithium-Ion Batteries». In: *Journal of The Electrochemical Society* 158 (Jan. 2011), R1. DOI: 10.1149/1.3515880 (cit. on p. 79).